J. Fluid Mech. (2013), *vol.* 720, *pp.* 15–65. © Cambridge University Press 2013
doi:10.1017/jfm.2012.633

Wall effects on pressure fluctuations in turbulent channel flow

G. A. Gerolymos, D. Sénéchal and I. Vallet†

Institut d'Alembert, Université Pierre et Marie Curie (UPMC), 4 place Jussieu, 75005 Paris, France

(Received 17 February 2012; revised 28 September 2012; accepted 16 December 2012;
first published online 27 February 2013)

The purpose of the present paper is to study the influence of wall echo on pressure fluctuations p', and on statistical correlations containing p', namely, redistribution ϕ_{ij}, pressure diffusion $d_{ij}^{(p)}$ and velocity pressure-gradient Π_{ij}. We extend the usual analysis of turbulent correlations containing pressure fluctuations in wall-bounded direct numerical simulations (Kim, *J. Fluid Mech.*, vol. 205, 1989, pp. 421–451), separating p' not only into rapid $p'_{(r)}$ and slow $p'_{(s)}$ parts (Chou, *Q. Appl. Maths*, vol. 3, 1945, pp. 38–54), but also further into volume ($p'_{(r;\mathfrak{V})}$ and $p'_{(s;\mathfrak{V})}$) and surface (wall echo, $p'_{(r;w)}$ and $p'_{(s;w)}$) terms. An algorithm, based on a Green's function approach, is developed to compute the above splittings for various correlations containing pressure fluctuations (redistribution, pressure diffusion, velocity pressure-gradient), in fully developed turbulent plane channel flow. This exact analysis confirms previous results based on a method-of-images approximation (Manceau, Wang & Laurence, *J. Fluid Mech.*, vol. 438, 2001, pp. 307–338) showing that, at the wall, $p'_{(\mathfrak{V})}$ and $p'_{(w)}$ are usually of the same sign and approximately equal. The above results are then used to study the contribution of each mechanism to the pressure correlations in low-Reynolds-number plane channel flow, and to discuss standard second-moment-closure modelling practices.

Key words: turbulence simulation, turbulent boundary layers, turbulent flows

1. Introduction

Understanding the physics of turbulent fluctuations of pressure p' is of major importance, not only because of their direct implication in noise (Hu, Morfey & Sandham 2002, 2006) and excitation of immersed solid surfaces (Corcos 1964), but also because they appear in correlations present in the transport equations for the Reynolds stresses and the dissipation tensor (Pope 2000; Jovanović 2004). Traditionally, the analysis of p' is based on the Poisson equation for the fluctuating pressure (Chou 1945), which, at the incompressible flow limit ($\rho \approxeq \text{const.} = \bar{\rho}, \forall\, t, x$, and $\mu \approxeq \text{const.} = \bar{\mu}, \forall\, t, x$), in a non-rotating frame of reference, reads

$$\nabla^2 p' = \nabla^2(p'_r + p'_s) = \underbrace{-2\rho \frac{\partial u'_k}{\partial x_\ell}\frac{\partial \bar{u}_\ell}{\partial x_k}}_{rapid} \underbrace{-\rho \frac{\partial^2}{\partial x_\ell \partial x_k}(u'_k u'_\ell - \overline{u'_k u'_\ell})}_{slow}. \tag{1.1}$$

† Email address for correspondence: isabelle.vallet@upmc.fr

https://doi.org/10.1017/jfm.2012.633 Published online by Cambridge University Press

The incompressible flow Poisson equation (1.1) suggests (Chou 1945) that solenoidal (Hamba 1999) pressure fluctuations, associated with the fluctuating velocity field, are generated by two separate mechanisms (Rotta 1951*a*,*b*; Lumley 1978; Piquet 1999; Pope 2000; Jovanović 2004):

(*a*) the interaction of velocity fluctuations with mean velocity gradients, called mean flow–turbulence interaction terms (also termed rapid pressure fluctuations, because they interact immediately with an imposed mean velocity gradient, or linear pressure fluctuations, because the corresponding source term in (1.1) is linear in velocity fluctuations), and

(*b*) the turbulence–turbulence interaction (also termed slow pressure fluctuations, because they react much more slowly than the rapid ones, which are directly driven by mean velocity gradients, or nonlinear pressure fluctuations, because the corresponding source term in (1.1) is quadratic in velocity fluctuations).

This idea of distinguishing between pressure fluctuations associated with mean flow gradients ($p'_{(r)}$) and pressure fluctuations associated with turbulence–turbulence interactions only ($p'_{(s)}$) can be applied in general to all correlations that contain the fluctuating pressure (Rotta 1951*a*,*b*; Lumley 1978; Hanjalić 1994; Piquet 1999; Pope 2000; Jovanović 2004).

Chou (1945) pointed out that, because of the linearity in p' of the incompressible flow Poisson equation (1.1), separate solutions can be obtained for each of the two source terms, based on the free-space Green's function for the Poisson equation (Katz & Plotkin 1991)

$$p'_{(r)}(\boldsymbol{x},t)=\underbrace{\frac{1}{2\pi}\iiint_{\mathfrak{V}}\left(\rho\frac{\partial\overline{\mathrm{u}}_\ell}{\partial\mathfrak{x}_k}\frac{\partial\mathrm{u}'_k}{\partial\mathfrak{x}_\ell}\right)\frac{\mathrm{d}\mathfrak{v}(\boldsymbol{\mathfrak{x}},t)}{|\boldsymbol{\mathfrak{x}}-\boldsymbol{x}|}}_{p'_{(r;\mathfrak{V})}(\boldsymbol{x},t)}+\underbrace{\frac{1}{4\pi}\iint_{\partial\mathfrak{V}}\left(\frac{1}{|\boldsymbol{\mathfrak{x}}-\boldsymbol{x}|}\frac{\partial\mathfrak{p}'_r}{\partial\mathfrak{n}}-\mathfrak{p}'_r\frac{\partial}{\partial\mathfrak{n}}\left[\frac{1}{|\boldsymbol{\mathfrak{x}}-\boldsymbol{x}|}\right]\right)\mathrm{d}\mathfrak{S}(\boldsymbol{\mathfrak{x}},t)}_{p'_{(r;w)}(\boldsymbol{x},t)},\tag{1.2a}$$

$$p'_{(s)}(\boldsymbol{x},t)=\underbrace{\frac{1}{4\pi}\iiint_{\mathfrak{V}}\left(\rho\frac{\partial^2\mathrm{u}'_k\mathrm{u}'_\ell}{\partial\mathfrak{x}_\ell\partial\mathfrak{x}_k}-\rho\frac{\partial^2\overline{\mathrm{u}'_k\mathrm{u}'_\ell}}{\partial\mathfrak{x}_\ell\partial\mathfrak{x}_k}\right)\frac{\mathrm{d}\mathfrak{v}(\boldsymbol{\mathfrak{x}},t)}{|\boldsymbol{\mathfrak{x}}-\boldsymbol{x}|}}_{p'_{(s;\mathfrak{V})}(\boldsymbol{x},t)}+\underbrace{\frac{1}{4\pi}\iint_{\partial\mathfrak{V}}\left(\frac{1}{|\boldsymbol{\mathfrak{x}}-\boldsymbol{x}|}\frac{\partial\mathfrak{p}'_s}{\partial\mathfrak{n}}-\mathfrak{p}'_s\frac{\partial}{\partial\mathfrak{n}}\left[\frac{1}{|\boldsymbol{\mathfrak{x}}-\boldsymbol{x}|}\right]\right)\mathrm{d}\mathfrak{S}(\boldsymbol{\mathfrak{x}},t)}_{p'_{(s;w)}(\boldsymbol{x},t)},\tag{1.2b}$$

where $p(\boldsymbol{x},t)$ and $\boldsymbol{u}(\boldsymbol{x},t)$ are the pressure and velocity at point $\boldsymbol{x}$, and the volume $\mathrm{d}\mathfrak{v}(\boldsymbol{\mathfrak{x}},t)$ and surface $\mathrm{d}\mathfrak{S}(\boldsymbol{\mathfrak{x}},t)$ integrals are taken over all other points $\boldsymbol{\mathfrak{x}}$ where the pressure and velocity are $\mathfrak{p}(\boldsymbol{\mathfrak{x}},t)$ and $\mathbf{u}(\boldsymbol{\mathfrak{x}},t)$. Note that, if equations (1.2) are multiplied by a function of $\boldsymbol{x}$, this function can be entered into the integrals that are over $\boldsymbol{\mathfrak{x}}$. In the case of unbounded flow, where $\partial\mathfrak{V}$ is very far (at infinity), only the volume integrals remain. On the other hand, for flow near solid boundaries, the surface integrals indicate that the unsteady pressure field reacts to the presence of the wall (surface integral; $\mathfrak{n}$ is the wall-normal coordinate, directed outwards from the fluid volume $\mathfrak{V}$). Terms related to the surface integrals are usually called wall-echo terms

https://doi.org/10.1017/jfm.2012.633 Published online by Cambridge University Press

(Hanjalić 1994), since for an isolated infinite plane solid boundary they can be related to reflection from the wall, using the method of images (Shir 1973; Launder, Reece & Rodi 1975; Gibson & Launder 1978; Piquet 1999; Pope 2000; Jovanović 2004). Wall-echo terms, as defined by the surface integrals in (1.2), contain the entire effect of the wall on the pressure fluctuations produced by the inhomogeneous velocity field (already influenced by the wall), and cannot distinguish between different mechanisms by which the presence of the wall affects turbulence (Hunt & Graham 1978), whose precise identification would require further specific decomposition (projection) of the velocity field computed by direct numerical simulation (DNS) (Marmanis 1998; Perot 1999).

Starting from the seminal paper of Chou (1945), all models (Rotta 1951*a*,*b*; Lumley 1978; Piquet 1999; Pope 2000; Jovanović 2004) for the redistribution tensor ϕ_{ij}, the velocity pressure-gradient tensor Π_{ij} or the pressure transport $\overline{p'u_i'}$ appearing in the pressure–diffusion tensor $d_{ij}^{(p)}$ are traditionally composed of four parts corresponding to the splitting (1.2), $p' = p'_{(r;\mathfrak{V})} + p'_{(r;w)} + p'_{(s;\mathfrak{V})} + p'_{(s;w)}$. At present there is no possibility of measuring $p'_{(r;\mathfrak{V})}$, $p'_{(r;w)}$, $p'_{(s;\mathfrak{V})}$ and $p'_{(s;w)}$ separately, and, despite advances in experimental techniques for the measurement of p' (Tsuji & Ishihara 2003; Tsuji *et al.* 2007), the simultaneous measurement of p' and $\partial_{x_j} u_i'$ in the vicinity of the wall is a difficult challenge (Naka *et al.* 2006). DNS offers the possibility of computing the different terms directly, experimental uncertainty being replaced by the eventual influence of the finite size of the computational box and of convergence of statistics.

In the context of pseudospectral DNS of incompressible plane channel flow (Kim, Moin & Moser 1987; Moser, Kim & Mansour 1999), Kim (1989) used a Green's function approach (Ince 1926; Courant & Hilbert 1953; Bender & Orszag 1978; Ockendon *et al.* 2003; Zauderer 2006; Myint-U & Debnath 2007) to solve, as a function of y (wall-normal coordinate), the incompressible flow Poisson equation (1.1) for p', for each wall-parallel wavenumber κ_x and κ_z. Throughout this paper x denotes the streamwise coordinate with corresponding velocity component u, y denotes the wall-normal coordinate with corresponding velocity component v, and z denotes the spanwise coordinate with corresponding velocity component w. Finally, $y = 0$ at the channel centreline, and the non-dimensional distance from the wall is defined as $y^+ := (y - y_w)\bar{u}_\tau \nu^{-1}$, where u_τ is the friction velocity and ν the kinematic viscosity. The separate solution for each source term (1.1) permits the separation of slow $p'_{(s)}$ and rapid $p'_{(r)}$ parts. In this way (Kim 1989; Chang, Piomelli & Blake 1999), the slow and rapid contributions to ϕ_{ij} were computed (Mansour, Kim & Moin 1988). This procedure (Kim 1989) is now used in a standard way in incompressible plane channel flow DNS, at least as far as $\overline{p'^2_{(s)}}$, $\overline{p'^2_{(r)}}$ and $\overline{p'^2_{(\tau)}}$ are concerned, and has also been extended to compressible flow studies (Foysi, Sarkar & Friedrich 2004). The term $\overline{p'^2_{(\tau)}}$, usually called Stokes pressure (Mansour *et al.* 1988; Chang *et al.* 1999), corresponds to the separately computed contribution of the wall boundary condition (Pope 2000, (11.173), p. 439) $[\partial_y p']_w = [\mu \partial^2_{yy} v']_w$, y being the wall-normal direction. Note that this boundary condition is associated with the source term $\partial^2_{x_i x_j}[\tau'_{ij}]$ in the Poisson equation for p', which is equal to 0 in the incompressible flow limit (Kim *et al.* 1987; Moser *et al.* 1999; Hu & Sandham 2001; Hoyas & Jiménez 2006). This procedure was used by Chang *et al.* (1999) to study the detailed contributions from different locations in the flow field to wall-pressure wavenumber–frequency spectra.

Manceau, Wang & Laurence (2001) have studied the wall-echo problem from the specific point of view of the so-called elliptic relaxation approach of Durbin (1993),

https://doi.org/10.1017/jfm.2012.633 Published online by Cambridge University Press

which lumps together all wall-echo effects (both on pressure correlations and on dissipation rate) into a single tensor. These authors (Manceau *et al.* 2001) used two-point correlations (in physical space) from the DNS data of Moser *et al.* (1999), at wall-friction Reynolds number $Re_{\tau_w} = 590$. The method used, which is related to classic work on wall-pressure spectra (Panton & Linebarger 1974) in that it uses two-point correlations in physical space, introduces wall echo by an approximate method of images, one image channel for the upper wall and another for the lower wall. Furthermore, Manceau *et al.* (2001) neglect the Stokes pressure. When analysed under a formal Green's function framework, the approximation in the method of images used in Manceau *et al.* (2001) is equivalent to using an approximate Green's function, instead of the exact one. By comparison with the exact solution obtained in the present work, it is possible to quantify the approximation error of the method of images.

All known second-moment closures (SMCs) for wall-bounded flows treat pressure correlations appearing in Reynolds stress transport equations by separating them into a quasi-homogeneous part and a second part accounting for inhomogeneity and/or wall echo. Concerning the quasi-homogeneous part of the redistribution term, general tensorial representations are available (Ristorcelli, Lumley & Abid 1995; Craft & Launder 1996; Jakirlić & Hanjalić 2002; Gerolymos, Lo & Vallet 2012*a*), which, in order to satisfy the two-component limit (TCL) realizability constraint (i.e. turbulence tends to the TCL as the wall is approached because of the strong damping of velocity fluctuations normal to the wall (Shih & Lumley 1993)), should use representation coefficients that are function of the Reynolds stress anisotropy tensor invariants (Lumley 1978). The early closures (Rotta 1951*a*; Launder *et al.* 1975; Speziale, Sarkar & Gatski 1991), which use constant coefficients, do not satisfy the two-component realizability constraint (Shih & Lumley 1993; Hanjalić 1994; Schwarz & Bradshaw 1994).

Concerning inhomogeneity and wall echo, these two mechanisms are not necessarily identical. Wall echo, which is related to the surface integrals in (1.2), diminishes with distance from the wall, whereas turbulence inhomogeneity effects may be active away from the wall, and even in the absence of walls. Indeed, comparison of models including inhomogeneity-based correction (Craft & Launder 1996; Gerolymos & Vallet 2001; Suga 2004) and models using wall-topology-based echo terms suggests that inhomogeneity-based terms are active at the edge of the boundary layer and improve the prediction of boundary layer entrainment. According to the way in which wall proximity is handled, SMCs can be classified into three categories.

(*a*) Models that use wall-topology-based (e.g. distance from the wall or geometric normal to the wall) corrections of the quasi-homogeneous closures, which tend to the homogeneous limit away from the wall ($y^+ \gtrapprox 30$). Note that elliptic blending models (Manceau & Hanjalić 2002) use the same family of tensorial representations for the redistribution ϕ_{ij}, the velocity pressure-gradient correlation Π_{ij} or the dissipation ε_{ij} terms, and introduce the knowledge of wall topology via the boundary conditions of the scalar Helmholtz equation used to define the scalar blending parameter. Therefore, it can be argued that elliptic blending models belong to this category.

(*b*) Models free from any wall-topology parameters, which use terms based on gradients of local turbulence quantities in the tensorial representations for ϕ_{ij}, Π_{ij} or ε_{ij}, and are active both near to and away from the wall. These models include wall-normal-free models based on a unit vector in the direction of inhomogeneity $\boldsymbol{e}_I$ (Gerolymos & Vallet 2001; Gerolymos *et al.* 2004), the proposal of Launder

https://doi.org/10.1017/jfm.2012.633 Published online by Cambridge University Press

& Li (1994) to Taylor-expand the mean velocity gradient in (1.2*a*) leading to terms containing $\partial^2_{x_j x_k}\bar{u}_i$ in the tensorial representation for ϕ_{ij}, and the work of Cormack (1975) who suggested the use of extended tensorial representations including gradients of $\overline{u_i' u_j'}$ and of ε_{ij}. This last proposal (Cormack 1975) has not yet been applied to the development of a working model, and recent work (Gerolymos *et al.* 2012*b*) suggests that further terms can be profitably added to Cormack's basis.

(*c*) The full (tensorial) elliptic relaxation approach of Durbin (1993), where all wall-affected terms (both inhomogeneous and wall echo) are lumped together into a correction of the homogeneous closures, which is obtained by the solution of six Helmholtz equations, one for each component of the Reynolds stress tensor $\overline{u_i' u_j'}$. This approach is fundamentally different from elliptic blending in that it postulates no particular tensorial representation for the near-wall corrections but, instead, determines these via appropriately chosen wall boundary conditions for the Helmholtz equations. Unfortunately, very few applications of this approach are available in the literature, where, for complex flows, a simplified three-equation closure version is used instead (Durbin 1995). On the other hand, despite statements to the contrary, this approach uses turbulent Reynolds number near-wall dampings. Indeed, the Kolmogorov-scale clippings of the elliptic relaxation length scale L_{ER} (Durbin 1993, (9), p. 469) and time scale T_{ER} (Durbin 1993, (6), p. 468) can be rewritten as

$$T_{ER} := \max\left[\frac{k}{\varepsilon}, C_{T_{ER}}\sqrt{\frac{\nu}{\varepsilon}}\right] = \max\left[1, C_{T_{ER}} Re_T^{-1/2}\right]\frac{k}{\varepsilon}, \tag{1.3a}$$

$$L_{ER} := C_{L_{ER}} \max\left[\frac{k^{3/2}}{\varepsilon}, C_{\eta ER}\left(\frac{\nu^3}{\varepsilon}\right)^{1/4}\right] = C_{L_{ER}} \max\left[1, C_{\eta ER} Re_T^{-3/4}\right]\frac{k^{3/2}}{\varepsilon}. \tag{1.3b}$$

Hence the switches in L_{ER} and T_{ER} used in elliptic relaxation are in essence Re_T dampings (where $Re_T := k^2\varepsilon^{-1}\nu^{-1}$ is the turbulence Reynolds number, k is the turbulence kinetic energy, ε is its dissipation rate, and ν is the kinematic viscosity), as expected, since the ratios of large to Kolmogorov scales are invariably equal to some power of Re_T (Davidson 2004, p. 20).

None of the above three approaches is perfectly consistent with flow physics, which, ideally, would require an inhomogeneous (including gradients of the Reynolds stresses) tensorial representation coupled to a wall-echo correction.

In the present work we are interested in determining the wall effects on correlations containing the fluctuating pressure. We aim both to develop a methodology for creating databases of the contribution of each mechanism to ϕ_{ij}, Π_{ij} and $\overline{p' u_i'}$, and to highlight the differences between volume ($\mathfrak{V}$), wall (w), homogeneous (H) and inhomogeneous (I) contributions. The first two contributions are extracted from the DNS computations, while the latter two are used in modelling. Homogeneous terms are not volume terms. They would correspond to hypothetical values of the pressure correlations of a series of independent homogeneous flows, each corresponding to the local values of anisotropy, length scale and mean velocity gradients. These homogeneous terms are approximately equal to the volume terms away from the wall. Whether such hypothetical homogeneous flows are obtainable for the anisotropy observed near the wall, in pure shear, is an open question.

https://doi.org/10.1017/jfm.2012.633 Published online by Cambridge University Press

In § 2, after a brief description of the present DNS calculations (§ 2.1 and appendix A), we revisit the Green's function (§ 2.2) approach (Kim 1989) applied to DNS computations of incompressible plane channel flow (§ 2.1), and we develop a procedure for separately evaluating (§ 2.2.3) the volume ($p'_{(r;\mathfrak{V})}$ and $p'_{(s;\mathfrak{V})}$) and the wall-echo ($p'_{(r;w)}$ and $p'_{(s;w)}$) terms in (1.2). By comparison with these exact results, we also quantify the error of the approximate method of images of Manceau *et al.* (2001), as a function of the wavenumber (§ 2.2.4), showing that this method is a high-wavenumber approximation. Analytical details on the Green's functions, with particular emphasis on the singular problem of xz constant pressure fluctuations ($\kappa = 0$), are given in appendix B. In § 3 we apply the algorithm (§ 2.2) for computing the p' splitting (1.2) to low-Reynolds-number plane channel flow and study the contributions of different terms to correlations containing p'.

2. DNS computations and p' splitting

The DNS computations used to obtain the results analysed in the present paper are discussed in § 2.1, and the p' splitting methodology is described in § 2.2.

2.1. *Plane channel flow configuration and computational method*

In the particular case of plane channel flow, the boundary surface consists of the upper and lower walls ($\mathfrak{W}_l$ at $y = -L_y/2 = -\delta$, and $\mathfrak{W}_u$ at $y = +L_y/2 = +\delta$, respectively), and the periodic boundaries at $x = \pm L_x/2$ and $z = \pm L_z/2$. The methodology described in the present paper is independent of the particular DNS solver used. The DNS database was generated for $Re_{\tau_w} := \bar{u}_\tau \delta \nu^{-1} = 180$ (where $2\delta = L_y$ is the channel height, $u_\tau := \sqrt{\bar{\tau}_w \rho^{-1}}$ is the friction velocity and ν is the kinematic viscosity) using the DNS solver described and validated in Gerolymos, Sénéchal & Vallet (2010), which solves the flow equations in physical space, with $O(\Delta x^{17})$ discretization of the convective terms (Gerolymos, Sénéchal & Vallet 2009). The flow is modelled by the compressible Navier–Stokes equations with air as working medium, but, for the quasi-incompressible $\bar{M}_{CL} \approxeq 0.34$ Mach number considered in the present work, mean density $\bar{\rho}$ variations do not exceed 1.5 %, and density fluctuations are negligibly small ($\rho'_{rms} \lessapprox 0.25\,\%\,\bar{\rho}$). For this reason the turbulent correlations obtained can be considered as incompressible. This has been verified by systematic comparison with standard incompressible pseudospectral DNS data (Kim *et al.* 1987; Moser *et al.* 1999; del Álamo & Jiménez 2003; del Álamo *et al.* 2004; Hoyas & Jiménez 2006, 2008), both for single-point statistics (Gerolymos *et al.* 2010: all second-order moments ($\overline{u'_i u'_j}$, figure 7, p. 797; $\overline{p' u'_i}$, figure 8, p. 798; $\phi_{ij} := 2\overline{p' S'_{ij}}$, figure 10, p. 800; $\varepsilon^{(\mu)}_{ij} := 2\nu \overline{\partial_{x_\ell} u'_i \partial_{x_\ell} u'_j}$, figure 11, p. 801) and third-order moments ($\overline{u'_i u'_j u'_k}$, figure 9, p. 799) appearing in the Reynolds stress budgets) and for spectra of velocity fluctuations in the homogeneous streamwise and spanwise directions (Gerolymos *et al.* 2010, figures 12–15, pp. 802–805). This very good agreement with pseudospectral incompressible DNS (Kim *et al.* 1987; Hoyas & Jiménez 2008) is also valid for two-point correlations

$$R_{a'b'}(\boldsymbol{x}, \boldsymbol{r}) := \overline{a'(\boldsymbol{x}, t) b'(\boldsymbol{x} + \boldsymbol{r}, t)} \tag{2.1}$$

containing the fluctuating pressure p', namely, $[R^{(x,z)}_{p'p'}]^+$, $[R^{(x,z)}_{p'u'}]^+$ and $[R^{(x,z)}_{p'v'}]^+$ (figure 1) and fluctuating pressure spectra $[E^{(x)}_{p'p'}]^+$ and $[E^{(z)}_{p'p'}]^+$ (figure 2). Note that the spectra given by Moser *et al.* (1999) are twice the discrete Fourier transform (DFT) of $R^+_{p'p'}$ (in wall units), and have to be appropriately rescaled (Briggs & Henson 1995)

https://doi.org/10.1017/jfm.2012.633 Published online by Cambridge University Press

Re_{τ_w}	$\bar{M}_{CL}$	$N_x \times N_y \times N_z$	L_x	L_y	L_z	Δx^+	Δy_w^+	$N_{y^+\leqslant 10}$	Δy_{CL}^+	Δz^+	Δt^+	$t^+_{obs_{R_2}}$	$\Delta t^+_{s_{R_2}}$
179	0.34	$193 \times 129 \times 169$	$4\pi\delta$	2δ	$4\pi\delta/3$	11.7	0.22	20	4.9	4.4	6.47×10^{-3}	2329	6.47×10^{-1}
178	0.00	$128 \times 129 \times 128$	$4\pi\delta$	2δ	$4\pi\delta/3$	17.7	0.05	14	4.4	5.9	Moser *et al.* (1999)		

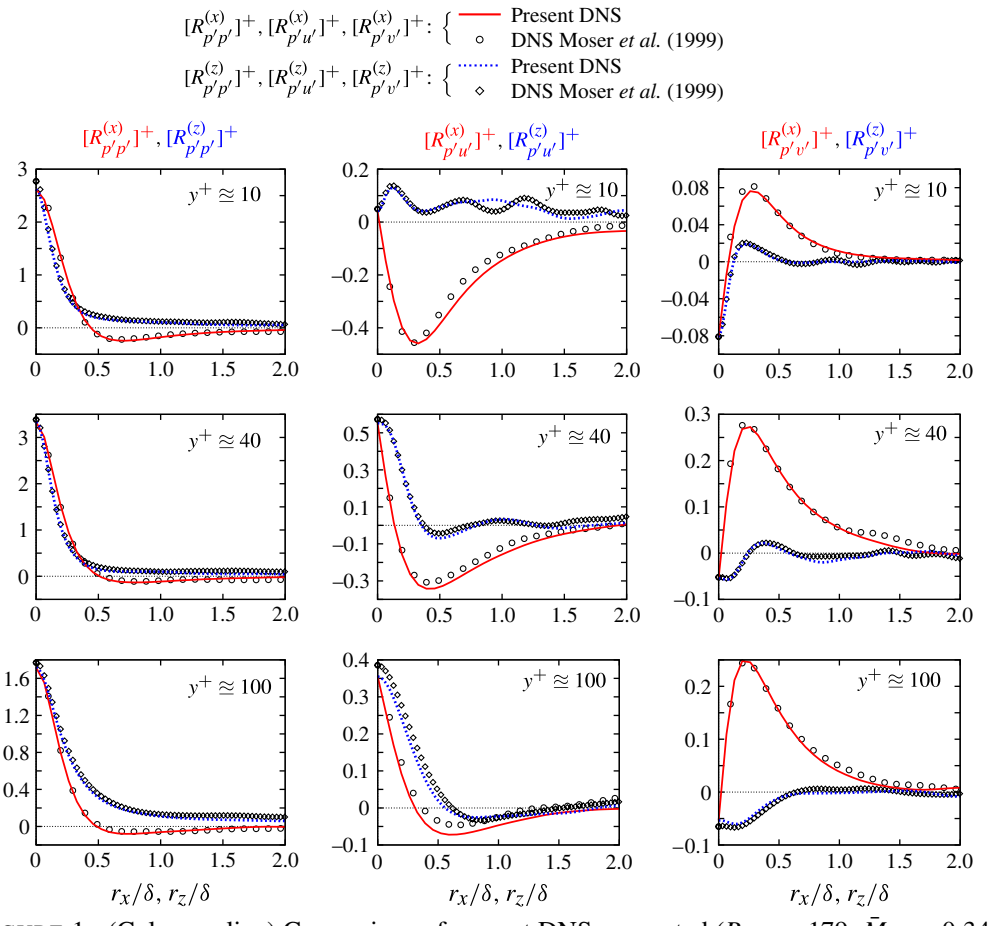


FIGURE 1. (Colour online) Comparison of present DNS-computed ($Re_{\tau_w} = 179$; $\bar{M}_{CL} = 0.34$; $193 \times 129 \times 169$ grid; table 1) two-point correlations (2.1) containing the fluctuating pressure in wall scaling ($[R^{(x)}_{p'p'}]^+$, $[R^{(x)}_{p'u'}]^+$ and $[R^{(x)}_{p'v'}]^+$ in the homogeneous streamwise (x) direction; $[R^{(z)}_{p'p'}]^+$, $[R^{(z)}_{p'u'}]^+$ and $[R^{(z)}_{p'v'}]^+$ in the homogeneous spanwise (z) direction), as a function of distance in outer scaling ($\delta^{-1}r_x$ and $\delta^{-1}r_z$), with reference results of incompressible pseudospectral (Kim *et al.* 1987) DNS computations (Moser *et al.* 1999; $Re_{\tau_w} = 178$, $M_{CL} = 0$).

by $(2\pi)^{-1}L_x^+$ or $(2\pi)^{-1}L_z^+$ to get actual one-dimensional spectra $E^+_{u_iu_j}$ (Pope 2000, (6.206), p. 225), as those given by del Álamo *et al.* (2004).

In order to evaluate more precisely how the small compressibility in the DNS computations affects the fluctuating pressure field, an order-of-magnitude analysis of the complete compressible flow equation for $\nabla^2 p'$ (A 1*e*) was performed (appendix A), indicating that the additional compressible terms in (A 1*e*) scale with density fluctuations and gradients (A 8), and may be reasonably neglected for the present flow conditions (figure 14). The main effect of compressibility in the present computations,

https://doi.org/10.1017/jfm.2012.633 Published online by Cambridge University Press

Re_{τ_w}	$\bar{M}_{CL}$	$N_x \times N_y \times N_z$	L_x	L_y	L_z	Δx^+	Δy^+_w	$N_{y^+\leqslant 10}$	Δy^+_{CL}	Δz^+	Δt^+	$t^+_{obs_{R_2}}$	$\Delta t^+_{s_{R_2}}$
179	0.34	$193\times129\times169$	$4\pi\delta$	2δ	$4\pi\delta/3$	11.7	0.22	20	4.9	4.4	6.47×10^{-3}	2329	6.47×10^{-1}
178	0.00	$128\times129\times128$	$4\pi\delta$	2δ	$4\pi\delta/3$	17.7	0.05	14	4.4	5.9	Moser *et al.* (1999)		

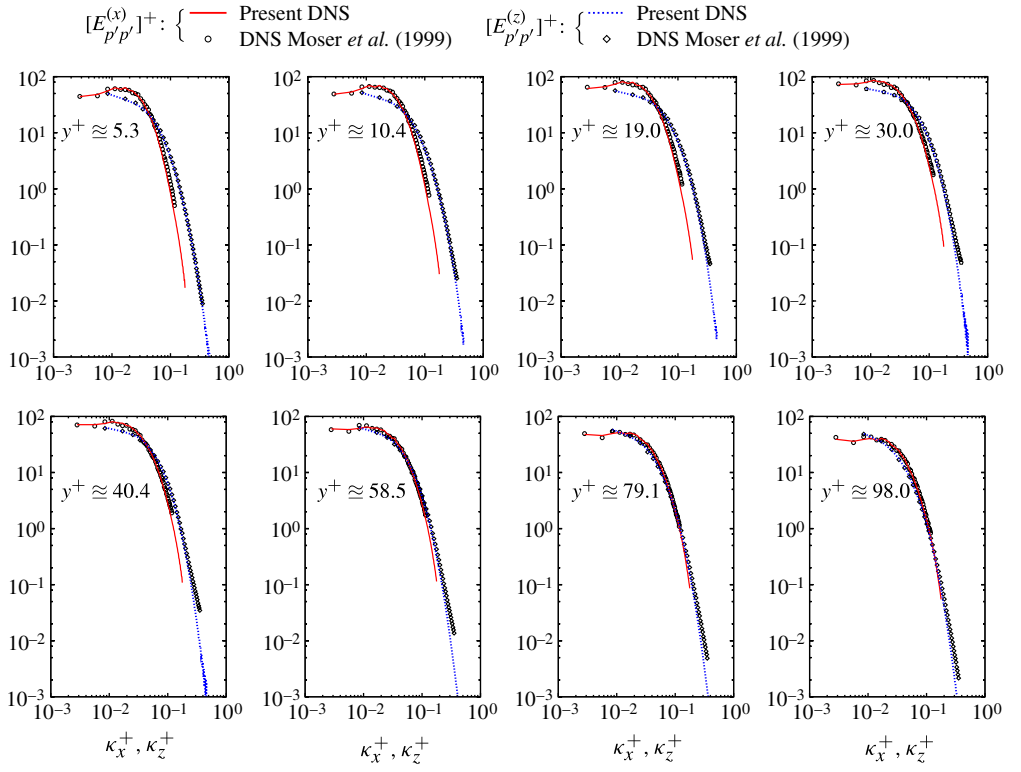


FIGURE 2. (Colour online) Comparison of present DNS-computed ($Re_{\tau_w} = 179$; $\bar{M}_{CL} = 0.34$; $193 \times 129 \times 169$ grid; table 1) one-dimensional pressure spectra in wall scaling ($[E^{(x)}_{p'p'}]^+$ and $[E^{(z)}_{p'p'}]^+$ in the homogeneous streamwise (x) and spanwise (z) directions), as a function of wavenumber in wall units (κ_x^+ and κ_z^+), with reference results of incompressible pseudospectral (Kim *et al.* 1987) DNS computations (Moser *et al.* 1999, $Re_{\tau_w} = 178$, $\bar{M}_{CL} = 0$).

as far as p' splitting is concerned, comes from the variations of mean density $\bar{\rho}$ ($\lessapprox 1.5$ %), which appears in the source terms $Q'_{(s)} + Q'_{(r)}$ ((1.1) and (A 1*e*)), in line with Morkovin's hypothesis (So, Gatski & Sommer 1998).

The influence of the Reynolds number needs consideration, especially as the data used in the present computations correspond to a rather low $Re_{\tau_w} \approxeq 180$. It is well known that wall-pressure fluctuations, in wall units, $[p'_w]^+_{rms}$, show a marked influence on Reynolds number (Goody 2004; Hu *et al.* 2006; Tsuji *et al.* 2007), although alternative scalings exhibit a less pronounced dependence (Tsuji *et al.* 2007, figure 14, p. 21). However, the ratio of slow to rapid pressure fluctuations $[p'_{(r)}]^{-1}_{rms}\,[p'_{(s)}]_{rms}$ (figure 3) shows little dependence on Re_{τ_w} for $y^+ \lessapprox 100$, ranging from $\sim$0.9 at the wall to $\sim$1.6 at $y^+ \approxeq 50$, and is approximately constant at $\sim$1.6 in the region $\frac{2}{10}\delta \lessapprox y - y_w \lessapprox \frac{7}{10}\delta$ (figure 3). At and near the centreline $y = \delta$, there is some scatter between different Re_{τ_w}, but no clear trend is discernible (figure 3). These results, based on the DNS data of Hoyas & Jiménez (2008), suggest that, although p'

https://doi.org/10.1017/jfm.2012.633 Published online by Cambridge University Press

Re_{τ_w}	$\bar{M}_{CL}$	$N_x \times N_y \times N_z$	L_x	L_y	L_z	Δx^+	Δy_w^+	$N_{y^+\leqslant 10}$	Δy_{CL}^+	Δz^+	t_{obs}^+	Δt_s^+
186	0.00	$768 \times 97 \times 340$	$12\pi\delta$	2δ	$4\pi\delta$	8.9	0.10	11	6.1	6.7	11 740	110
547	0.00	$1536 \times 257 \times 1536$	$8\pi\delta$	2δ	$4\pi\delta$	8.9	0.04	16	6.7	4.5	12 034	81
934	0.00	$3072 \times 385 \times 2304$	$8\pi\delta$	2δ	$3\pi\delta$	9.2	0.03	18	7.6	3.8	11 208	151
2003	0.00	$6144 \times 633 \times 4608$	$8\pi\delta$	2δ	$3\pi\delta$	8.2	0.32	12	8.9	4.1	22 033	97

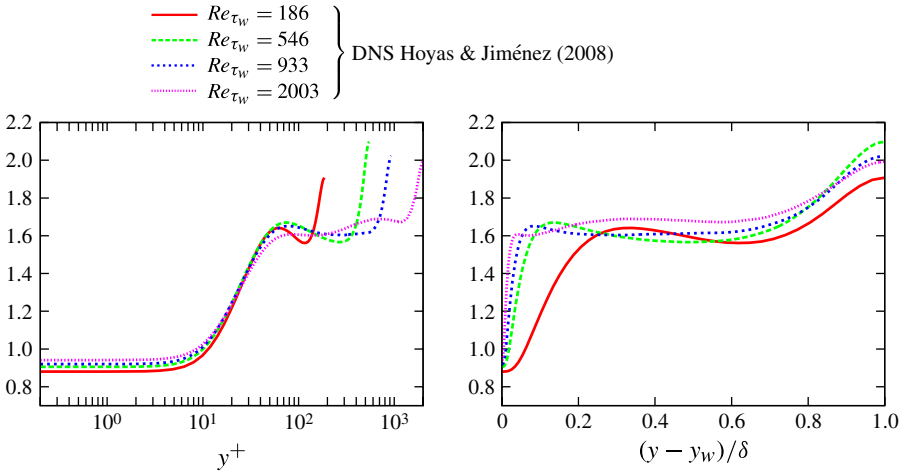


FIGURE 3. (Colour online) Ratio of slow to rapid pressure fluctuations $[p'_{(r)}]^{-1}_{rms}\,[p'_{(s)}]_{rms}$ (1.1), from the incompressible DNS database of Hoyas & Jiménez (2006, 2008), for different Reynolds numbers ($Re_{\tau_w} \in \{186, 547, 934, 2003\}$), plotted against the non-dimensional distance from the wall in inner (y^+) and outer ($\delta^{-1}(y - y_w)$) scaling.

exhibits a strong dependence on Re_{τ_w}, the relative importance of the slow and rapid mechanisms in the creation of p' does not. Therefore, despite the low $Re_{\tau_w} \approxeq 180$ of the present DNS computations, it is believed that the obtained p' splitting results provide useful information on the relative importance of different mechanisms in the correlations containing p'. Nevertheless, DNS data on volume ($p'_{(r;\mathfrak{V})}$ and $p'_{(s;\mathfrak{V})}$) and wall-echo ($p'_{(r;w)}$ and $p'_{(s;w)}$) terms at higher Re_{τ_w} are required to substantiate this.

2.2. *Green's function solution of the Poisson equations*

For fully developed (x-wise invariant in the mean) turbulent plane channel flow, the Poisson equation (1.1) for p' can be simplified to a system of independent ordinary differential equations (ODEs), one for each Fourier component of p', which can be efficiently solved by a Green's function approach (Kim 1989). In § 2.2.1, we formalize the problem, in relation to previous work. Using mathematical tools and solutions detailed in appendix B, we discuss, in § 2.2.2, the standard decomposition $p' = p'_{(r)} + p'_{(s)} + p'_{(\tau)}$ (2.2), with special emphasis on the singular case of the xz-averaged component $\overline{p'}^{xz}(y, t)$ (2.6*d*). In § 2.2.3, we present the new methodology for the identification of volume and wall-echo terms in the decomposition $p' = p'_{(r;\mathfrak{V})} + p'_{(r;w)} + p'_{(s;\mathfrak{V})} + p'_{(s;w)} + p'_{(\tau)}$ of (2.11). In § 2.2.4, we show how the method-of-images approach applied to fully developed turbulent plane channel flow can be represented by an appropriate Green's function. Finally, in § 2.2.5, we show that the approximation made in the method of images consists of neglecting the interaction of wall echo between the two walls, and demonstrate by comparison of the exact and approximate Green's functions that this is a high-wavenumber approximation.

https://doi.org/10.1017/jfm.2012.633 Published online by Cambridge University Press

2.2.1. *ODEs for the Fourier transforms*

The solution to (1.1), with Neumann boundary conditions at the walls (Pope 2000, p. 439) and periodic boundary conditions in the homogeneous directions, can only be obtained up to an additive function of time t (Ince 1926; Courant & Hilbert 1953; Myint-U & Debnath 2007). We split the fluctuating pressure field as (Kim 1989)

$$p'(x,y,z,t) = p'_{(r)}(x,y,z,t) + p'_{(s)}(x,y,z,t) + p'_{(\tau)}(x,y,z,t), \tag{2.2}$$

where the rapid $p'_{(r)}$, slow $p'_{(s)}$ and Stokes $p'_{(\tau)}$ pressure fluctuations are solutions (Kim 1989; Chang *et al.* 1999; recall that, for strictly incompressible flow, the continuity equation for the fluctuating velocity field, $\partial_{x_\ell} u'_\ell = 0$, implies that $\partial^2_{x_\ell x_k}(u'_k u'_\ell) = \partial_{x_\ell} u'_k \partial_{x_k} u'_\ell$) of

$$\nabla^2 \begin{bmatrix} p'_{(r)} \\ p'_{(s)} \\ p'_{(\tau)} \end{bmatrix} = \begin{bmatrix} Q'_{(r)} \\ Q'_{(s)} \\ Q'_{(\tau)} \end{bmatrix} := \begin{bmatrix} -2\rho \partial_{x_\ell} u'_k \partial_{x_k} \bar{u}_\ell \\ -\rho(\partial_{x_\ell} u'_k \partial_{x_k} u'_\ell - \overline{\partial_{x_\ell} u'_k \partial_{x_k} u'_\ell}) \\ 0 \end{bmatrix}, \tag{2.3a}$$

with boundary conditions (Pope 2000, pp. 390–392, 439–442)

$$\frac{\partial}{\partial y} \begin{bmatrix} p'_{(r)} \\ p'_{(s)} \\ p'_{(\tau)} \end{bmatrix} (x, y = \pm \tfrac{1}{2} L_y, z, t) = \begin{bmatrix} 0 \\ 0 \\ B'_{(\tau)_\pm} \end{bmatrix} := \begin{bmatrix} 0 \\ 0 \\ \mu \partial^2_{yy} v' \end{bmatrix}. \tag{2.3b}$$

Since (2.3) is linear in $p'_{(m)}$ ($m \in \{r, s, \tau\}$), the three problems can be solved independently to compute the three fields in (2.2). The last field in the superposition (2.2) is introduced to satisfy the wall boundary conditions associated with the wall-normal (y) momentum equation

$$\left.\frac{\partial p'}{\partial y}\right|_{y=\pm L_y/2} = \left.\frac{\partial \tau'_{y\ell}}{\partial x_\ell}\right|_{y=\pm L_y/2} = \mu \nabla^2 v'|_{y=\pm L_y/2} = \mu \left.\frac{\partial^2 v'}{\partial y^2}\right|_{y=\pm L_y/2} \tag{2.4}$$

because of the no-slip wall boundary condition $u'_i(x, y = \pm L_y/2, z, t) = 0$ for all x, z, t. By (2.4) the field $p'_{(\tau)}$ is obviously related to the fluctuating wall shear stress, and is usually called the Stokes pressure (Mansour *et al.* 1988; Kim 1989; Chang *et al.* 1999), although Pope (2000, p. 439) suggests the alternative term harmonic pressure, because in incompressible flow $\nabla^2 p'_\tau = 0$. This is, however, no longer true in the compressible flow case (Foysi *et al.* 2004).

The directions x and z being homogeneous (periodic in the computational model), following Kim (1989), we replace the xz Fourier transforms (the Fourier transforms $\hat{p}'_{(m)}, \hat{Q}'_{(m)}, \hat{B}'_{(m)_\pm} \in \mathbb{C}$ are computed using standard DFT techniques (Briggs & Henson 1995) in the periodic directions x and z, with maximum computable wavenumbers $\kappa_{x_{max}} = \pi\,(\Delta x)^{-1}$ and $\kappa_{z_{max}} = \pi\,(\Delta z)^{-1}$) of $p'_{(m)}$, $Q'_{(m)}$ ($m \in \{r, s, \tau\}$) and $B'_{(\tau)_\pm}$,

$$p'_{(m)}(x,y,z,t) = \int_{-\infty}^{+\infty}\int_{-\infty}^{+\infty} \hat{p}'_{(m)}(\kappa_x, y, \kappa_z, t) \mathrm{e}^{\mathrm{i}\kappa_x x + \mathrm{i}\kappa_z z}\, \mathrm{d}\kappa_x\, \mathrm{d}\kappa_z, \tag{2.5a}$$

$$Q'_{(m)}(x,y,z,t) = \int_{-\infty}^{+\infty}\int_{-\infty}^{+\infty} \hat{Q}'_{(m)}(\kappa_x, y, \kappa_z, t) \mathrm{e}^{\mathrm{i}\kappa_x x + \mathrm{i}\kappa_z z}\, \mathrm{d}\kappa_x\, \mathrm{d}\kappa_z, \tag{2.5b}$$

$$B'_{(\tau)_\pm}(x,z,t) = \int_{-\infty}^{+\infty}\int_{-\infty}^{+\infty} \hat{B}'_{(\tau)_\pm}(\kappa_x, \kappa_z, t) \mathrm{e}^{\mathrm{i}\kappa_x x + \mathrm{i}\kappa_z z}\, \mathrm{d}\kappa_x\, \mathrm{d}\kappa_z, \tag{2.5c}$$

https://doi.org/10.1017/jfm.2012.633 Published online by Cambridge University Press

in the partial differential equations (PDEs) (2.3) to obtain the ODEs

$$\left[\frac{\partial^2}{\partial y^2} - \kappa^2\right] \begin{bmatrix} \hat{p}'_{(r)} \\ \hat{p}'_{(s)} \\ \hat{p}'_{(\tau)} \end{bmatrix} (\kappa_x, y, \kappa_z, t) = \begin{bmatrix} \hat{Q}'_{(r)} \\ \hat{Q}'_{(s)} \\ \hat{0} \end{bmatrix} (\kappa_x, y, \kappa_z, t), \tag{2.6a}$$

$$\frac{\partial \hat{p}'_{(m)}}{\partial y}(\kappa_x, y = \pm\tfrac{1}{2}L_y, \kappa_z, t) = \begin{bmatrix} 0 \\ 0 \\ \hat{B}'_{(\tau)_\pm}(\kappa_x, \kappa_z, t) \end{bmatrix}, \tag{2.6b}$$

$$\kappa := \sqrt{\kappa_x^2 + \kappa_z^2} \in \mathbb{R}_{\geqslant 0}. \tag{2.6c}$$

The classic solution of (2.6) by Kim (1989), using a Green's function approach, provides detailed information on the structure of the rapid and slow fields, and was extended by Chang *et al.* (1999) to study the detailed influence of the sources, in both type (slow and rapid) and y location in the channel. In the present work we extend this analysis by identifying and studying the wall-echo influence. Note that, by (2.5),

$$\hat{p}'(\kappa_x = 0, y, \kappa_z = 0, t) \overset{(2.5a)}{=} \overline{p'(x, y, z, t)}^{xz} \in \mathbb{R}, \tag{2.6d}$$

the case $\kappa = 0$ corresponds to the time fluctuation of the xz-averaged pressure at each y location, while

$$p'_B(t) := \overline{p'(x, y, z, t)}^{xyz} \overset{(2.5a),\ (2.6d)}{=} \frac{1}{L_y}\int_{-L_y/2}^{+L_y/2} \hat{p}'(\kappa_x = 0, y, \kappa_z = 0, t)\,\mathrm{d}y \tag{2.6e}$$

is the time fluctuation of the bulk (volume-averaged) pressure.

2.2.2. *Exact solution of (2.6)*

The exact solution to (2.6*a*) with boundary conditions (2.6*b*), for the xz Fourier components (2.5*a*) of the slow $p'_{(s)}$ and rapid $p'_{(r)}$ fields, is given in Kim (1989), and has been widely used (Mansour *et al.* 1988; Chang *et al.* 1999; Foysi *et al.* 2004). Following the analysis in § B.2.1 for $\kappa \neq 0$ (B 10*b*) and in § B.3.1 for $\kappa = 0$ (B 29), it reads

$$\begin{bmatrix} \hat{p}'_{(r)} \\ \hat{p}'_{(s)} \end{bmatrix} (\kappa_x, y, \kappa_z, t) = \int_{-L_y/2}^{+L_y/2} G_{Kim}(y, Y; \kappa) \begin{bmatrix} \hat{Q}'_{(r)} \\ \hat{Q}'_{(s)} \end{bmatrix} (\kappa_x, Y, \kappa_z, t)\,\mathrm{d}Y, \tag{2.7a}$$

where the Green's function

$$G_{Kim}(y, Y; \kappa) \overset{(\mathrm{B}\,10b),\ (\mathrm{B}\,29)}{=} \begin{cases} -\dfrac{\cosh[\kappa(L_y - |y - Y|)] + \cosh[\kappa(y + Y)]}{2\kappa \sinh \kappa L_y}, & \kappa \neq 0, \\ \dfrac{1}{2}|y - Y|, & \kappa = 0, \end{cases} \tag{2.7b}$$

and satisfies the correct homogeneous Neumann boundary conditions on both walls (figure 4). The exact solution to (2.6*a*) for the xz Fourier components (2.5*a*) of the Stokes (harmonic) pressure with boundary conditions (2.6*b*) was given in Chang *et al.* (1999), and following the analysis in § B.2.2 for $\kappa \neq 0$ (B 12) and in § B.3.2

https://doi.org/10.1017/jfm.2012.633 Published online by Cambridge University Press

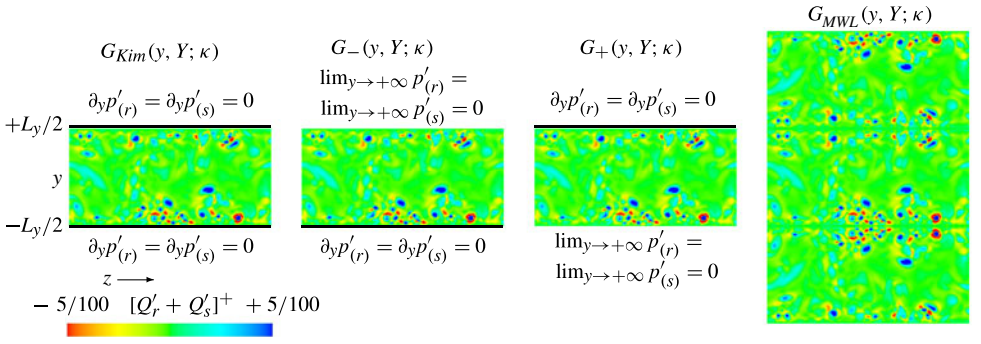


FIGURE 4. Instantaneous pressure fluctuation sources (sum $[Q'_{(r)} + Q'_{(s)}]^+$ of rapid and slow sources in wall units) at $x = 0$ (DNS; $Re_{\tau_w} = 179$; $\bar{M}_{CL} = 0.34$; $193 \times 129 \times 169$ grid; table 1), and boundary conditions for the exact problem (2.6) whose solution (Kim 1989) is given by $G_{Kim}(y, Y; \kappa)$ (B 10*b*), and for the two virtual half-space problems with only one wall present defining $G_\pm(y, Y; \kappa)$ (B 18), which define the local wall corrections appearing in the high-wavenumber approximation of the method of images (Manceau *et al.* 2001), corresponding to the approximate Green's function $G_{MWL}(y, Y; \kappa)$ (B 43*c*).

for $\kappa = 0$ (B 33) reads

$$\hat{p}'_{(\tau)}(\kappa_x, y, \kappa_z, t) \overset{\text{(B 12), (B 33)}}{=} \begin{cases} \dfrac{\hat{B}'_{(\tau)_+}(\kappa_x, \kappa_z, t)\cosh[\kappa(\frac{1}{2}L_y + y)] - \hat{B}'_{(\tau)_-}(\kappa_x, \kappa_z, t)\cosh[\kappa(\frac{1}{2}L_y - y)]}{\kappa \sinh \kappa L_y}, \\ \quad \kappa \neq 0, \\ \dfrac{1}{2}\hat{B}'_{(\tau)_-}(\kappa_x, \kappa_z, t)y + \dfrac{1}{2}\hat{B}'_{(\tau)_+}(\kappa_x, \kappa_z, t)y + p'_{BC_0}(t), \quad \kappa = 0, \end{cases} \tag{2.8}$$

where the choice of the additive constant $p'_{BC_0} \in \mathbb{R}$, up to which the harmonic pressure can be defined (§ B.3.2), was chosen to satisfy the constraint $p'_B(t) := \overline{p'}^{xyz}(t) = 0$ (i.e. constant bulk pressure).

As discussed in § B.3, the case $\kappa = 0$ is singular, and a solution exists if and only if the compatibility conditions (B 32) and (B 25)

$$L_y \begin{bmatrix} \overline{Q'_{(r)}}^{xyz} \\ \overline{Q'_{(s)}}^{xyz} \end{bmatrix}(t) = \int_{-L_y/2}^{+L_y/2} \begin{bmatrix} \hat{Q}'_{(r)} \\ \hat{Q}'_{(s)} \end{bmatrix}(\kappa_x = 0, Y, \kappa_z = 0, t)\,\mathrm{d}Y = \begin{bmatrix} 0 \\ 0 \end{bmatrix}, \tag{2.9a}$$

$$\hat{B}'_{(\tau)_+}(\kappa_x = 0, \kappa_z = 0, t) = \hat{B}'_{(\tau)_-}(\kappa_x = 0, \kappa_z = 0, t) \iff \overline{B'_{(\tau)_+}}^{xz}(t) = \overline{B'_{(\tau)_-}}^{xz}(t) \tag{2.9b}$$

hold, where $\overline{(\cdot)}^{xyz}$ denotes the volume average (bulk average) and $\overline{(\cdot)}^{xz}$ is the surface average in the homogeneous directions x and z, defined by

$$\overline{(\cdot)}^{xyz} := \frac{1}{L_x L_y L_z}\int_{-L_x/2}^{+L_x/2}\int_{-L_y/2}^{+L_y/2}\int_{-L_z/2}^{+L_z/2}(\cdot)\,\mathrm{d}x\,\mathrm{d}y\,\mathrm{d}z, \tag{2.10a}$$

$$\overline{(\cdot)}^{xz} := \frac{1}{L_x L_z}\int_{-L_x/2}^{+L_x/2}\int_{-L_z/2}^{+L_z/2}(\cdot)\,\mathrm{d}x\,\mathrm{d}z. \tag{2.10b}$$

https://doi.org/10.1017/jfm.2012.633 Published online by Cambridge University Press

If the computational box is large enough in the homogeneous directions for the ergodic hypothesis (Monin & Yaglom 1971, pp. 243–256) to hold, conditions (2.9) are satisfied, at least approximately. In practice, the compatibility condition (2.9*a*) was enforced numerically when computing the Fourier transforms (2.5*b*). The form (B 33) of $q_{BC}(y;\kappa=0,B_\pm)$ automatically enforces the compatibility condition, by taking the average gradient $(B_- + B_+)/2$. In practice $\hat{B}'_{(\tau)_-}(\kappa_x=0,\kappa_z=0,t) \approxeq \hat{B}'_{(\tau)_+}(\kappa_x=0,\kappa_z=0,t) \approxeq 0$ in (2.9*b*), especially with increasing box size, so that taking the average is a good choice. Of course, (1.1) with Neumann boundary conditions at the walls (Pope 2000, p. 439) can only be solved up to an additive constant, which is fixed by the choice of p'_{BC_0} in the Stokes field $p'_{(\tau)}$ (2.8) (i.e. constant bulk pressure).

2.2.3. *Volume and wall-echo terms*

The main purpose of the present algorithm is to distinguish in (1.2) the contributions of the volume integral (volume terms denoted by $(\cdot)_{\mathfrak{V}}$) from the contributions of the surface integral (wall-echo terms denoted by $(\cdot)_w$), i.e. to extend (2.2) as

$$p'(x,y,z,t) = \underbrace{p'_{(r;\mathfrak{V})}(x,y,z,t) + p'_{(r;w)}(x,y,z,t)}_{p'_{(r)}(x,y,z,t)} + \underbrace{p'_{(s;\mathfrak{V})}(x,y,z,t) + p'_{(s;w)}(x,y,z,t)}_{p'_{(s)}(x,y,z,t)} + p'_{(\tau)}(x,y,z,t), \tag{2.11}$$

where $p'_{(r;\mathfrak{V})}$ corresponds to the contribution of the volume integral in (1.2*a*), $p'_{(r;w)}$ corresponds to the contribution of the surface integral in (1.2*a*), $p'_{(s;\mathfrak{V})}$ corresponds to the contribution of the volume integral in (1.2*b*), and $p'_{(s;w)}$ corresponds to the contribution of the surface integral in (1.2*b*).

Working directly with the surface integrals in (1.2) would have been a complex task, because they are implicit, i.e. they contain the value of the corresponding field at the wall. On the other hand, it is straightforward to evaluate the volume integrals in (1.2), which contain only the sources and the three-dimensional free-space Green's function, which satisfies $\lim_{|\mathfrak{x}-\boldsymbol{x}|\to\infty} |\mathfrak{x}-\boldsymbol{x}|^{-1} = 0$. Therefore the xz Fourier components of the volume terms should satisfy (2.6*a*), corresponding to the same distribution of sources as the complete physical problem, for $y \in [-L_y/2, +L_y/2]$,

$$\left[\frac{\partial^2}{\partial y^2} - \kappa^2\right] \begin{bmatrix} \hat{p}'_{(r;\mathfrak{V})} \\ \hat{p}'_{(s;\mathfrak{V})} \end{bmatrix} (\kappa_x, y, \kappa_z, t) = \begin{bmatrix} \hat{Q}'_{(r)} \\ \hat{Q}'_{(s)} \end{bmatrix} (\kappa_x, y, \kappa_z, t), \tag{2.12a}$$

but not the homogeneous Neumann wall boundary conditions (2.6*b*), which are directly related to the surface integrals in (1.2). They are required instead to decay as $|y| \to \infty$,

$$\lim_{|y|\to\infty} \begin{bmatrix} \hat{p}'_{(r;\mathfrak{V})} \\ \hat{p}'_{(s;\mathfrak{V})} \end{bmatrix} (\kappa_x, y, \kappa_z, t) = 0, \tag{2.12b}$$

i.e. they correspond to the solution of the hypothetical problem where p' is generated by the same distribution of sources in $y \in [-L_y/2, +L_y/2]$ with the walls absent. Following the analysis in § B.2.3 for $\kappa \neq 0$ (B 14) and in § B.3.3 for $\kappa = 0$ (B 35), the solution of (2.12) reads

$$\begin{bmatrix} \hat{p}'_{(r;\mathfrak{V})} \\ \hat{p}'_{(s;\mathfrak{V})} \end{bmatrix} (\kappa_x, y, \kappa_z, t) = \int_{-L_y/2}^{+L_y/2} G_{\mathfrak{V}}(y, Y; \kappa) \begin{bmatrix} \hat{Q}'_{(r)} \\ \hat{Q}'_{(s)} \end{bmatrix} (\kappa_x, Y, \kappa_z, t)\, \mathrm{d}Y, \tag{2.13a}$$

https://doi.org/10.1017/jfm.2012.633 Published online by Cambridge University Press

where the free-space Green's function

$$G_{\mathfrak{V}}(y,Y;\kappa) \overset{\text{(B 14), (B 35)}}{=} \begin{cases} -\dfrac{\mathrm{e}^{-\kappa|y-Y|}}{2\kappa}, & \kappa\neq 0, \\ \dfrac{1}{2}|y-Y|, & \kappa=0, \end{cases} \tag{2.13b}$$

ensures boundedness at infinity. The same compatibility relation for the distribution of sources, as for the complete problem (2.9*a*), is required for the case $\kappa=0$ (§B.3.3).

Because of the linearity of (1.1) and (1.2), the splitting (2.11) readily implies that

$$\begin{bmatrix}\hat{p}'_{(r;w)}\\ \hat{p}'_{(s;w)}\end{bmatrix}(\kappa_x,y,\kappa_z,t) = \begin{bmatrix}\hat{p}'_{(r)}\\ \hat{p}'_{(s)}\end{bmatrix}(\kappa_x,y,\kappa_z,t) - \begin{bmatrix}\hat{p}'_{(r;\mathfrak{V})}\\ \hat{p}'_{(s;\mathfrak{V})}\end{bmatrix}(\kappa_x,y,\kappa_z,t). \tag{2.14}$$

Combining (2.7), (2.13) and (2.14) we may define the wall-echo Green's function

$$G_w(y,Y;\kappa) := G_{Kim}(y,Y;\kappa) - G_{\mathfrak{V}}(y,Y;\kappa) \tag{2.15}$$

corresponding to the surface integrals (wall echo) in (1.2), which satisfies

$$\begin{bmatrix}\hat{p}'_{(r;w)}\\ \hat{p}'_{(s;w)}\end{bmatrix}(\kappa_x,y,\kappa_z,t) = \int_{-L_y/2}^{+L_y/2} G_w(y,Y;\kappa)\begin{bmatrix}\hat{Q}'_{(r)}\\ \hat{Q}'_{(s)}\end{bmatrix}(\kappa_x,Y,\kappa_z,t)\,\mathrm{d}Y. \tag{2.16}$$

Note that, since, for $\kappa=0$, $G_{Kim}(y,Y;\kappa=0)=G_{\mathfrak{V}}(y,Y;\kappa=0)$ (B 36), we have $G_w(y,Y;\kappa=0)=0$, i.e. wall echo applies only on fields varying in at least one of the homogeneous directions x or z ($\kappa\neq 0$).

2.2.4. *The approximate method of images*

With the above developments we can directly evaluate the wall-echo terms for the slow and rapid parts in each of the correlations containing p' (§ 3). By comparison with the exact solution obtained in the present work, it is possible to evaluate the approximation error of the method of images of Manceau *et al.* (2001).

The approximate method of images (Manceau *et al.* 2001) simply adds two mirror images of the channel, one above the upper wall and another below the lower wall (figure 4) to account for the presence of the walls, postulating that an approximation to the solution is obtained by using the free-space Green's function $G_{\mathfrak{V}}(y,Y;\kappa)$ in the extended domain $y\in[-\frac{3}{2}L_y,+\frac{3}{2}L_y]$. Taking into account the mirror symmetry of the ghost channels with respect to the corresponding wall (figure 4), this is equivalent (§ B.4) to using an appropriate Green's function $G_{MWL}(y,Y;\kappa)$ (B 43*c*) on the actual sources between the channel walls, i.e. for $y\in[-L_y/2,+L_y/2]$

$$\begin{bmatrix}\hat{p}'_{(r;MWL)}\\ \hat{p}'_{(s;MWL)}\end{bmatrix}(\kappa_x,y,\kappa_z,t) = \int_{-L_y/2}^{+L_y/2} G_{MWL}(y,Y;\kappa)\begin{bmatrix}\hat{Q}'_{(r)}\\ \hat{Q}'_{(s)}\end{bmatrix}(\kappa_x,Y,\kappa_z,t)\,\mathrm{d}Y. \tag{2.17}$$

By (B 43*c*),

$$G_{MWL}(y,Y;\kappa) = G_{\mathfrak{V}}(y,Y;\kappa) + G_{w_-}(y,Y;\kappa) + G_{w_+}(y,Y;\kappa), \tag{2.18}$$

where $G_{w_\pm}(y,Y;\kappa)$ (B 19) are the wall-echo Green's functions corresponding to the virtual half-space problems with only one of the walls present (figure 4). Note that the half-space problems are solved exactly (§§ B.2.4 and B.3.4). Inherently, this is tantamount to assuming that there is no interaction between the echo effects of the upper and lower walls, since in the case of an isolated wall (half-space problem; figure 4) the method of images yields the exact solution (Pope 2000, pp. 439–442).

https://doi.org/10.1017/jfm.2012.633 Published online by Cambridge University Press

The approximation error of the method of images comes from the fact that the direct influence of the upper wall, approximated by the half-space problem $G_{w_+}(y, Y; \kappa)$ (figure 4), induces a non-zero gradient $\partial_y\,[\hat{p}'_{(r;+)}, \hat{p}'_{(s;+)}]^{\mathrm{T}}(\kappa_x, y = -L_y/2, \kappa_z, t) \neq 0$ at the lower wall, and that there is no feedback from the lower wall to correct this (and vice versa). The non-dimensional approximation error can be evaluated (§ B.4) by comparison with the exact solution (B 10*b*) of Kim (1989), and is a function of the non-dimensional wavenumber $\kappa L_y = 2\kappa\delta$ (B 46). For large non-dimensional wavenumbers κL_y, i.e. structures with small streamwise and spanwise extent compared to the channel height, this error is small, and rapidly decreases with increasing wavenumber (figure 5).

Let $\ell_\kappa := 2\pi\kappa^{-1}$ be the representative size (wavelength) in the xz plane of structures corresponding to $\kappa := \sqrt{\kappa_x^2 + \kappa_z^2}$ (2.6*c*). For $\kappa L_y \gtrapprox 3 \iff \ell_\kappa \lessapprox 4\delta$, the approximation of $G_{Kim}(y, Y; \kappa)$ (B 10*b*) by $G_{MWL}(y, Y; \kappa)$ (B 43*c*) is satisfactory (figure 5), the non-dimensional error being $\lessapprox 1\,\%$. For the present case with $Re_{\tau_w} \approxeq 180$, this corresponds roughly to $\kappa^+ \gtrapprox 1/100$, which includes the wavenumbers where most of the energy of the p' spectra is contained (figure 2), implying that the method of images is a satisfactory engineering approximation. However, for larger structures, for example, $\kappa L_y \approxeq 3/2 \iff \ell_\kappa \approxeq 8\delta$, such as the superstructures observed in higher-Re_{τ_w} wall turbulence (Balakumar & Adrian 2007; Hutchins & Marusic 2007), the approximation error is roughly 10 %, and then grows exponentially with increasing size.

2.2.5. *Interaction of wall echo between walls*

Since the free-space Green's function $G_{\mathfrak{V}}(y, Y; \kappa)$ ((B 14) and (B 36)) is the same for all problems (figure 4), the differences (figure 5) between the exact solution $G_{Kim}(y, Y; \kappa)$ (B 10*b*) and the method-of-images approximation $G_{MWL}(y, Y; \kappa)$ (B 43) correspond to increasingly strong interaction between the two walls with decreasing non-dimensional wavenumber $\kappa L_y = 2\kappa\delta$, leading to amplification of the echo effect. To further explain this phenomenon note that the identity

$$\begin{aligned} G_{\mathfrak{V}}(y = -\tfrac{1}{2}L_y, Y; \kappa \neq 0) &\overset{\text{(B 14)}}{=} -\frac{\mathrm{e}^{\kappa(Y+L_y/2)}}{2\kappa} \\ &\overset{\text{(B 18}a\text{)}}{=} G_-(y = -\tfrac{1}{2}L_y, Y; \kappa \neq 0) \\ &\quad - G_{\mathfrak{V}}(y = -\tfrac{1}{2}L_y, Y; \kappa \neq 0) \\ &\overset{\text{(B 43}c\text{)}}{=:} G_{w_-}(y = -\tfrac{1}{2}L_y, Y; \kappa \neq 0) \\ \forall\ Y \in (-\tfrac{1}{2}L_y, +\tfrac{1}{2}L_y), & \end{aligned} \tag{2.19}$$

which implies by (B 3) that for the half-space problems (§ B.2.4) the wall echo, at the wall ($y = -L_y/2$), exactly equals the volume term at the wall:

$$p'_{(s;w_-)}(x, y = -\tfrac{1}{2}L_y, z, t) \overset{(2.19),\ (B\,3)}{=} p'_{(s;\mathfrak{V})}(x, y = -\tfrac{1}{2}L_y, z, t), \tag{2.20a}$$

$$p'_{(r;w_-)}(x, y = -\tfrac{1}{2}L_y, z, t) \overset{(2.19),\ (B\,3)}{=} p'_{(r;\mathfrak{V})}(x, y = -\tfrac{1}{2}L_y, z, t). \tag{2.20b}$$

This result (2.20) following from the equality of the corresponding Green's functions (2.19) is valid independently of the particular sources $\hat{Q}(y; \kappa)$ (2.6*a*).

At high non-dimensional wavenumbers κL_y, the exact wall-echo Green's function $G_w(y = -L_y/2, Y; \kappa)$ (2.18), for the computation of p'_w at the lower wall ($y = -L_y/2$), is approximately equal ($\kappa L_y = 3$; figure 6) to the wall-echo Green's function $G_{w_-}(y = -L_y/2, Y; \kappa)$ (B 43) of the half-space problem with only the lower wall present (figure 4), except at the upper part of the channel $Y \in [L_y/4, L_y/2]$, where

https://doi.org/10.1017/jfm.2012.633 Published online by Cambridge University Press

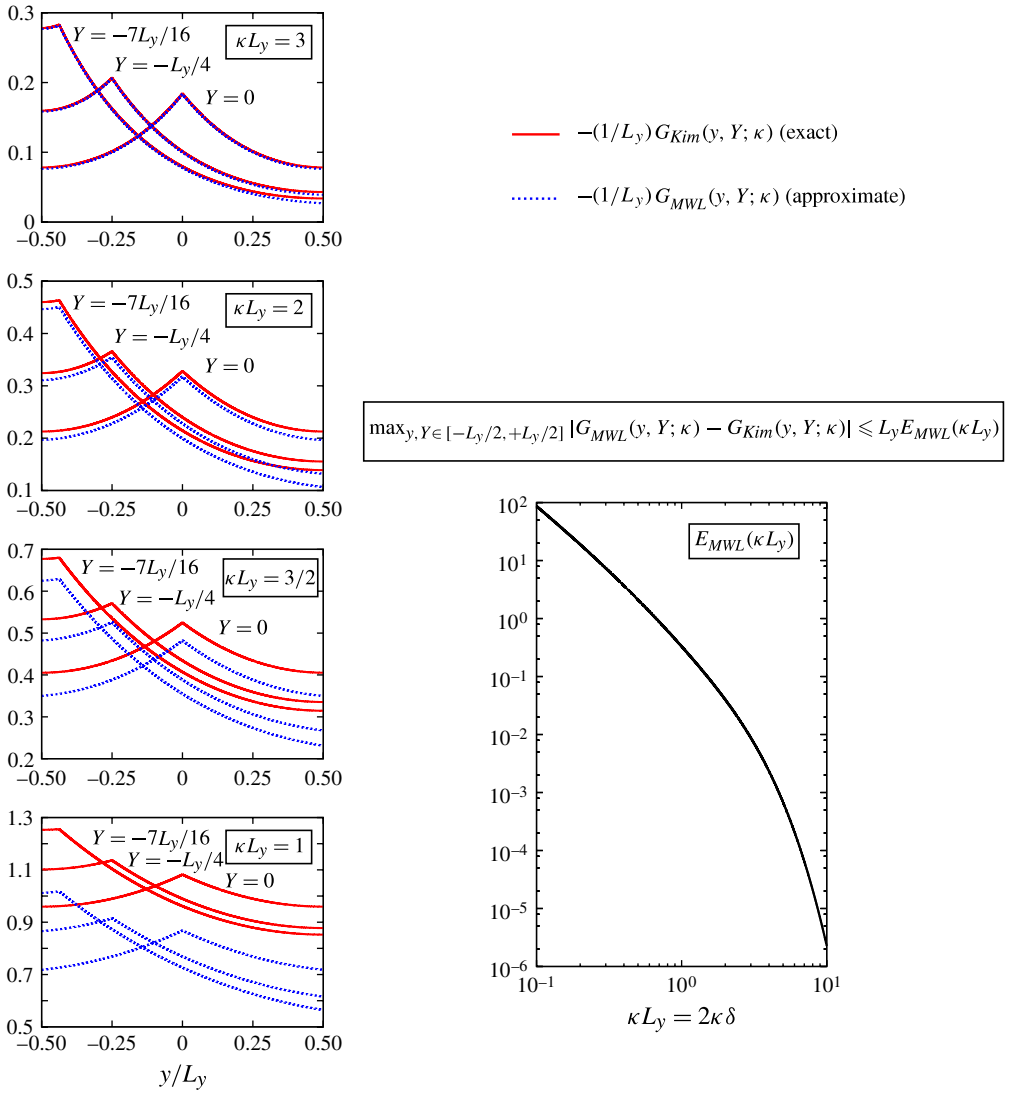


FIGURE 5. (Colour online) Comparison of the exact Green's function (B 10*b*), $G_{Kim}(y, Y; \kappa)$ (Kim 1989), with the method-of-images approximation (B 43), $G_{MWL}(y, Y; \kappa)$ (Manceau *et al.* 2001), for $Y \in \{-7L_y/16, -L_y/4, 0\}$ and $\kappa L_y \in \{1, 3/2, 2, 3\}$, plotted as a function of yL_y^{-1}, and log plot of the upper bound estimate of the error made by the method-of-images approximation (B 46) as a function of the non-dimensional wavenumber $\kappa L_y = 2\kappa\delta$ ($L_y = 2\delta$ is the channel height).

the influence of the upper wall on the Green's function used for the computation of p'_w at the lower wall ($y = -L_y/2$) is felt. As the non-dimensional wavenumber κL_y further decreases (i.e. the corresponding structure size $\ell_\kappa \delta^{-1} := 2\pi\kappa^{-1}\delta^{-1}$ increases), the influence of the upper wall is felt further down (figure 4). Of course, there is an analogous effect concerning the influence of the lower wall on the upper wall. As the non-dimensional wavenumber κL_y decreases, this mutual interaction between the two

https://doi.org/10.1017/jfm.2012.633 Published online by Cambridge University Press

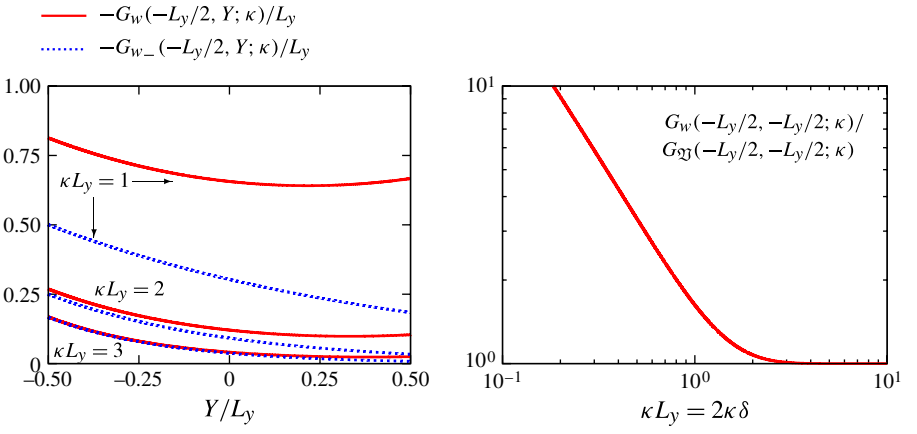


FIGURE 6. (Colour online) Comparison of the exact wall-echo Green's function $G_w(y = -L_y/2, Y; \kappa)$ (2.18), for the computation of the solution at the lower wall $y = -L_y/2$, with the wall-echo Green's function $G_{w_}(y = -L_y/2, Y; \kappa)$ (B 43), of the corresponding half-space problem with only the lower wall present (figure 4), for $\kappa L_y \in \{1, 2, 3\}$, plotted as a function of YL_y^{-1}, and log-plot of the ratio at the wall ($y = Y = -L_y/2$) of the exact wall-echo Green's function $G_w(y = -L_y/2, Y = -L_y/2; \kappa)$ (2.18) on the corresponding free-space Green's function $G_{\mathfrak{V}}(y = -L_y/2, Y = -L_y/2; \kappa)$ (B 14) plotted against the non-dimensional wavenumber $\kappa L_y = 2\kappa\delta$ ($L_y = 2\delta$ is the channel height).

walls amplifies the echo effect, the amplification growing exponentially with structure size (figure 4).

3. Analysis of pressure correlations

The algorithm (§ 2.2.3) for separating the rapid and slow contributions to p' (§ 2.2.2) into weakly inhomogeneous volume ($p'_{(r;\mathfrak{V})}$ and $p'_{(s;\mathfrak{V})}$) and strongly inhomogeneous wall-echo terms ($p'_{(r;w)}$ and $p'_{(s;w)}$) was applied to a low-Reynolds-number ($Re_{\tau_w} \approxeq 180$) well-resolved DNS (grid $193 \times 129 \times 169$; table 1). The simulation was started at $t = t_0$ by interpolation of a well-converged simulation on a coarser grid (grid $129 \times 129 \times 129$; table 1), and continued for $t^+_{GF_0} - t^+_0 = 681$. During this interval $t^+ \in [t^+_0, t^+_{GF_0}]$, the statistics for $\bar{u}_i$ and $\overline{u'_i u'_j}$ necessary for the computation of the source terms in (2.3*a*) were computed with sampling at every iteration ($\Delta t^+_s = \Delta t^+ \approxeq 6.47 \times 10^{-3} \iff f^+_s \approxeq 154$). Then the Green's function algorithm for p' splitting (2.11) was applied, and the statistics of pressure correlations were computed for an observation time $t^+_{obs_{GF}} = 1648$, with sampling every 10 iterations ($\Delta t^+_{s_{GF}} = 10\Delta t^+ \approxeq 6.47 \times 10^{-2} \iff f^+_{s_{GF}} \approxeq 15.4$).

3.1. *Fluctuating pressure field*

The instantaneous fluctuating pressure p' field reconstructed by the Green's function approach of (2.7) and (2.8) according to the splitting (2.2) agrees quite well (figure 7) with the instantaneous p' field directly computed (without making use of Green's functions) by the compressible DNS solver (Gerolymos *et al.* 2010).

Both the directly computed p'_{rms} and the r.m.s. values ($[p'_{(r)}]_{rms}$, $[p'_{(s)}]_{rms}$, $[p'_{(\tau)}]_{rms}$) of the p' splitting (2.2) compare globally satisfactorily (figure 8) with standard results

https://doi.org/10.1017/jfm.2012.633 Published online by Cambridge University Press

https://doi.org/10.1017/jfm.2012.633 Published online by Cambridge University Press

Re_{τ_w}	$\bar{M}_{CL}$	$N_x \times N_y \times N_z$	L_x	L_y	L_z	Δx^+	Δy^+_w	$N_{y^+\leqslant 10}$	Δy^+_{CL}	Δz^+	Δt^+	t^+_{obs}	Δt^+_s	$\Delta t^+_{s_{R_2}}$
179	0.34	$193\times129\times169$	$4\pi\delta$	2δ	$\frac{4}{3}\pi\delta$	11.7	0.22	20	4.9	4.4	6.47×10^{-3}	2329	6.47×10^{-3}	6.47×10^{-1}
180	0.34	$257\times129\times385$	$8\pi\delta$	2δ	$4\pi\delta$	17.6	0.23	20	5.0	5.9	6.56×10^{-3}	289	6.57×10^{-3}	6.57×10^{-1}
180	0.34	$129\times129\times129$	$4\pi\delta$	2δ	$\frac{4}{3}\pi\delta$	17.7	0.23	20	5.0	5.9	6.56×10^{-3}	1539	6.56×10^{-3}	6.56×10^{-1}
184	0.34	$121\times161\times\ 81$	$4\pi\delta$	2δ	$\frac{4}{3}\pi\delta$	19.3	0.19	25	4.4	9.6	5.50×10^{-3}	1014	5.50×10^{-3}	5.50×10^{-1}

TABLE 1. Parameters of the DNS computations: L_x, L_y, L_z (N_x, N_y, N_z) are the dimensions (number of grid points) of the computational domain (x = homogeneous streamwise, y = wall normal, z = homogeneous spanwise directions); δ is the channel half-height; Δx^+, Δy^+_w, Δy^+_{CL}, Δz^+ are the mesh sizes in wall units; $(\cdot)_w$ denotes wall and $(\cdot)_{CL}$ centreline values; $N_{y^+\leqslant 10}$ is the number of grid points between the wall and $y^+ = 10$; $Re_{\tau_w} := \bar{u}_\tau \delta \bar{\nu}_w^{-1}$; $\bar{u}_\tau$ is the friction velocity; δ is the channel half-height; $\bar{\nu}_w$ is the kinematic viscosity at the wall; $\bar{M}_{CL}$ is the centreline Mach number; Δt^+ is the computational time step in wall units; t^+_{obs} is the observation period in wall units over which statistics were computed; Δt^+_s is the sampling time step for the single-point statistics in wall units; and $\Delta t^+_{s_{R_2}}$ is the sampling time step for the two-point statistics in wall units.

Re_{τ_w}	$\bar{M}_{CL}$	$N_x \times N_y \times N_z$	L_x	L_y	L_z	Δx^+	Δy_w^+	$N_{y^+\leqslant 10}$	Δy_{CL}^+	Δz^+	Δt^+	$t^+_{obs_{GF}}$	$\Delta t^+_{s_{GF}}$
179	0.34	$193 \times 129 \times 169$	$4\pi\delta$	2δ	$4\pi\delta/3$	11.7	0.22	20	4.9	4.4	6.47×10^{-3}	1648	6.47×10^{-2}

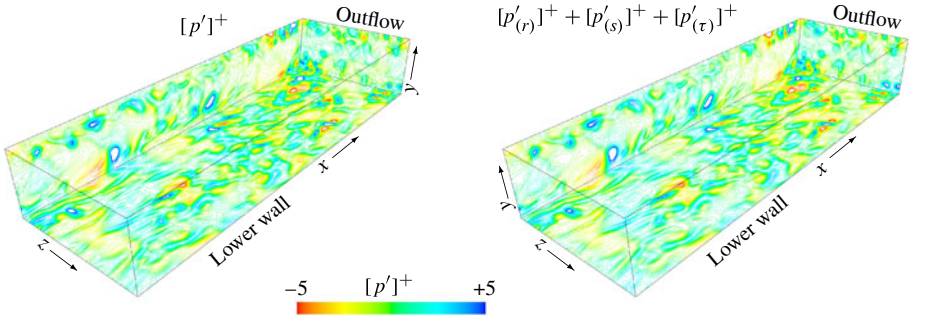


FIGURE 7. Instantaneous fluctuating pressure in wall units $[p']^+$ obtained directly ($Re_{\tau_w} = 179$; $\bar{M}_{CL} = 0.34$; $193 \times 129 \times 169$ grid; table 1) by the compressible DNS solver (Gerolymos *et al.* 2010) compared to the superposition of the three fields, rapid $[p'_{(r)}]^+$ and slow $[p'_{(s)}]^+$ obtained by the Green's function solution (2.7), and Stokes field $[p'_{(\tau)}]^+$ (2.8), in wall units (50 contours in the range $[-5, +5]$ on the lower wall, the outflow x periodic interface, and the z periodic interface).

Re_{τ_w}	$\bar{M}_{CL}$	$N_x \times N_y \times N_z$	L_x	L_y	L_z	Δx^+	Δy_w^+	$N_{y^+\leqslant 10}$	Δy_{CL}^+	Δz^+	Δt^+	$t^+_{obs_{GF}}$	$\Delta t^+_{s_{GF}}$
179	0.34	$193 \times 129 \times 169$	$4\pi\delta$	2δ	$4\pi\delta/3$	11.7	0.22	20	4.9	4.4	6.47×10^{-3}	1648	6.47×10^{-2}
178	0.00	$128 \times 129 \times 128$	$4\pi\delta$	2δ	$4\pi\delta/3$	17.7	0.05	14	4.4	5.9	Moser *et al.* (1999)		
186	0.00	$768 \times 97 \times 340$	$12\pi\delta$	2δ	$4\pi\delta$	8.9	0.10	11	6.1	6.7	Hoyas & Jiménez (2008)		

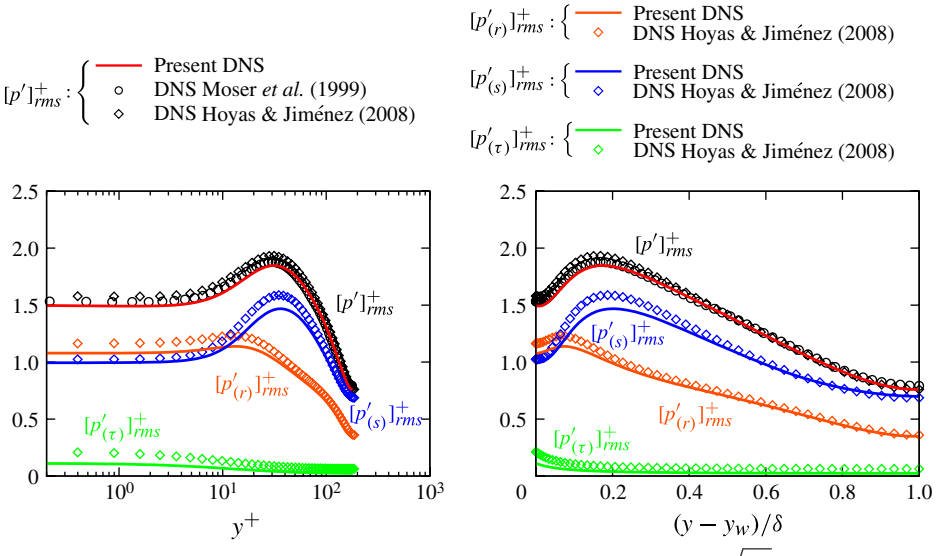


FIGURE 8. (Colour online) Comparison of r.m.s. values $p'_{rms} := \sqrt{\overline{p'^2}}$ of the fluctuating pressure p' and of the fields $p'_{(r)} + p'_{(s)} + p'_{(\tau)} = p'$ (2.2), from the present DNS computations ($Re_{\tau_w} = 179$; $\bar{M}_{CL} = 0.34$; $193 \times 129 \times 169$ grid; table 1) with reference results of incompressible pseudospectral (Kim *et al.* 1987) DNS computations of Hoyas & Jiménez (2008, $Re_{\tau_w} = 186$, $M_{CL} = 0$) and of Moser *et al.* (1999, $Re_{\tau_w} = 178$, $M_{CL} = 0$), in wall units, plotted against the non-dimensional distance from the wall in inner (y^+) and outer ($\delta^{-1}(y - y_w)$) scaling.

https://doi.org/10.1017/jfm.2012.633 Published online by Cambridge University Press

from incompressible DNS computations (Kim *et al.* 1987; Hoyas & Jiménez 2008), in both the wall and the outer regions (figure 8). Computed p'_{rms} corresponds, for the present DNS results (figure 8), to the fluctuation of the actual thermodynamic pressure, obtained from the equation of state (Gerolymos *et al.* 2010). There is quite good agreement between the present results for p'_{rms} and the incompressible DNS of Kim *et al.* (1987), obtained with similar resolution on the same computational box (figure 8), the present data being marginally lower, because of the small mean density variation effect ($\lessapprox 1.5\,\%$; § 2.1). The incompressible DNS data of Hoyas & Jiménez (2008), with similar resolution but a larger computational box, indicate slightly higher $[p']^+_{rms}$ (figure 8). This is attributed to the higher $Re_{\tau_w}=186$ in the simulations of Hoyas & Jiménez (2008), compared to $Re_{\tau_w}=178$ in Kim *et al.* (1987) and $Re_{\tau_w}=179$ for the present simulations. The variation of $[p'_w]^+_{rms}$ with Re_{τ_w} (Hu *et al.* 2006; Tsuji *et al.* 2007) indicates a $\sim 2\,\%$ increase in $[p'_w]^+_{rms}$ from $Re_{\tau_w}=178$ to $Re_{\tau_w}=186$. Incompressible DNS data of the different fields ($[p'_{(r)}]_{rms}$, $[p'_{(s)}]_{rms}$, $[p'_{(\tau)}]_{rms}$) were available only for the simulation of Hoyas & Jiménez (2008), and are, as expected, a little higher than those of the present computations (figure 8), consistent with the difference in $[p']^+_{rms}$. Note also that $\overline{p'^2}=\overline{(p'_{(r)}+p'_{(s)}+p'_{(\tau)})^2}\neq\overline{p'^2_{(r)}}+\overline{p'^2_{(s)}}+\overline{p'^2_{(\tau)}}$. There is, nonetheless, a difference in the level of Stokes pressure $[p'_{(\tau)}]_{rms}$ near the wall (figure 8), which should be further investigated, but this term is quite small compared to the others.

The new results (figure 9) in the present work concern the further splitting ($p'=p'_{(r;\mathfrak{V})}+p'_{(r;w)}+p'_{(s;\mathfrak{V})}+p'_{(s;w)}+p'_{(\tau)}$) into volume and wall-echo terms (2.11). The r.m.s. levels of wall echo ($[p'_{(r;w)}]_{rms}$, $[p'_{(s;w)}]_{rms}$) at the wall ($y=0$; figure 9) are approximately equal to the corresponding volume terms ($[p'_{(r;\mathfrak{V})}]_{rms}$, $[p'_{(s;\mathfrak{V})}]_{rms}$). This implies (§ 2.2.5) that the dominant contributions to the spectra (2.5*b*) of the source terms $\hat{Q}'_{(r)}(\kappa_x,y,\kappa_z,t)$ and $\hat{Q}'_{(s)}(\kappa_x,y,\kappa_z,t)$ (2.6*a*) occur at sufficiently high non-dimensional wavenumbers $\kappa L_y=2\kappa\delta$ (figure 6) for the interaction between the wall echo from the upper wall and the wall echo from the lower wall to be negligibly small. This approximate equality of wall-echo and volume terms holds up to $y^+\lessapprox 2$ (figure 9). Further away from the wall, both wall-echo terms ($[p'_{(r;w)}]_{rms}$, $[p'_{(s;w)}]_{rms}$) decay with increasing distance from the wall, always remaining much higher than the Stokes pressure $[p'_{(\tau)}]_{rms}$ (figure 9). In the buffer and outer regions ($y-y_w\gtrapprox(5/100)\delta\overset{Re_{\tau_w}\approx 180}{\Longleftrightarrow}y^+\gtrapprox 10$), the well-known predominance of the slow volume term $[p'_{(s;\mathfrak{V})}]_{rms}$ over the rapid volume term $[p'_{(r;\mathfrak{V})}]_{rms}$ (Kim 1989; Chang *et al.* 1999) is evident (figure 9). Nonetheless, it is essential, from the point of view of near-wall modelling, to note that, for $y^+\lessapprox 10$, $[p'_{(r;\mathfrak{V})}]_{rms}\approxeq[p'_{(s;\mathfrak{V})}]_{rms}\approxeq[p'_{(r;w)}]_{rms}\approxeq[p'_{(s;w)}]_{rms}>[p'_{(\tau)}]_{rms}$ (figure 9). Since all of the terms are of the same order of magnitude near the wall, but may have different phases, and hence different correlation coefficients with the fluctuating velocity field, they all require accurate modelling. Despite the fact that, further away from the wall ($y^+\gtrapprox 50$), homogeneous models are reasonably accurate (Gerolymos *et al.* 2012*a*, figure 2, p. 9), the global predictive performance of models in actual flows is dominated by the quality of near-wall modelling (Durbin 1993; Hanjalić 1994).

The above quantitative results (figure 9) are also observed qualitatively in the instantaneous levels (figure 10) of the five terms in the p' splitting (2.11). Comparison of instantaneous levels of the slow ($p'_{(s)}$) and rapid ($p'_{(r)}$) terms (figure 10) clearly

https://doi.org/10.1017/jfm.2012.633 Published online by Cambridge University Press

Re_{τ_w}	$\bar{M}_{CL}$	$N_x \times N_y \times N_z$	L_x	L_y	L_z	Δx^+	Δy^+_w	$N_{y^+\leqslant 10}$	Δy^+_{CL}	Δz^+	Δt^+	$t^+_{obs_{GF}}$	$\Delta t^+_{s_{GF}}$
179	0.34	$193 \times 129 \times 169$	$4\pi\delta$	2δ	$4\pi\delta/3$	11.7	0.22	20	4.9	4.4	6.47×10^{-3}	1648	6.47×10^{-2}
178	0.00	$128 \times 129 \times 128$	$4\pi\delta$	2δ	$4\pi\delta/3$	17.7	0.05	14	4.4	5.9	Moser *et al.* (1999)		
186	0.00	$768 \times 97 \times 340$	$12\pi\delta$	2δ	$4\pi\delta$	8.9	0.10	11	6.1	6.7	Hoyas & Jiménez (2008)		

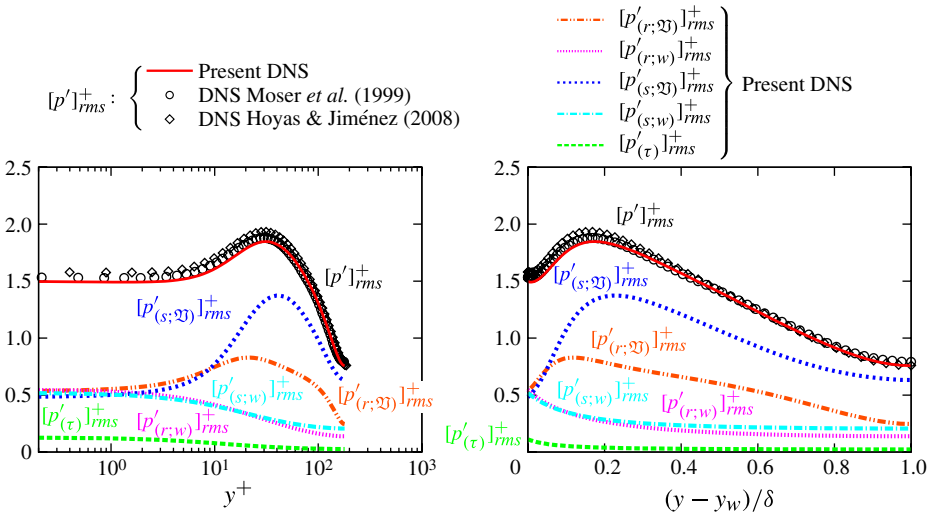


FIGURE 9. (Colour online) R.m.s. values of the five fluctuating pressure fields in the decomposition $p' = p'_{(r;\mathfrak{V})} + p'_{(r;w)} + p'_{(s;\mathfrak{V})} + p'_{(s;w)} + p'_{(\tau)}$ (2.11), from the present DNS computations ($Re_{\tau_w} = 179$; $\bar{M}_{CL} = 0.34$; $193 \times 129 \times 169$ grid; table 1), plotted against the non-dimensional distance from the wall in inner (y^+) and outer ($\delta^{-1}(y - y_w)$) scaling, and p'_{rms} from various DNS databases (Moser *et al.* 1999; Hoyas & Jiménez 2008; Gerolymos *et al.* 2010).

shows that both mechanisms of generation of p' (2.3*a*) are of the same magnitude at the wall (lower wall; figure 10), while $p'_{(s)}$ is the main mechanism (Chang *et al.* 1999) further away from the wall ($z = \text{const.}$ plane; figure 10). The same observations apply to the corresponding volume terms, $p'_{(r;\mathfrak{V})}$ and $p'_{(s;\mathfrak{V})}$ (figure 10). The wall-echo terms, $p'_{(r;w)}$ and $p'_{(s;w)}$, at the wall (lower wall; figure 10) are approximately equal to the corresponding volume terms, $p'_{(r;\mathfrak{V})}$ and $p'_{(s;\mathfrak{V})}$, but rapidly decay away from the wall ($z = \text{const.}$ plane; figure 10). Finally, the Stokes pressure $p'_{(\tau)}$ is substantially lower than the other terms and rapidly decays away from the wall (figure 10).

The results (figures 7–10) on the p' fields (2.11) provide guidance on the relative importance of each of the five p' fields. Nonetheless, the transposition of these results to the decomposition of correlations containing p' is not always straightforward, especially in the near-wall region ($y^+ \lessapprox 10$). For this reason we study in detail (§§ 3.3, 3.4 and 3.5) the correlations containing p' that appear in the transport equations for the Reynolds stresses (§ 3.2).

3.2. *Reynolds stress transport*

The equations governing the Reynolds stress tensor are central in single-point closure turbulence modelling (Lumley 1978; Hanjalić 1994). The exact transport equations for the Reynolds stresses in incompressible flow (Pope 2000, pp. 315–320)

https://doi.org/10.1017/jfm.2012.633 Published online by Cambridge University Press

Re_{τ_w}	$\bar{M}_{CL}$	$N_x \times N_y \times N_z$	L_x	L_y	L_z	Δx^+	Δy^+_w	$N_{y^+\leqslant 10}$	Δy^+_{CL}	Δz^+	Δt^+	$t^+_{obs_{GF}}$	$\Delta t^+_{s_{GF}}$
179	0.34	$193\times129\times169$	$4\pi\delta$	2δ	$4\pi\delta/3$	11.7	0.22	20	4.9	4.4	6.47×10^{-3}	1648	6.47×10^{-2}

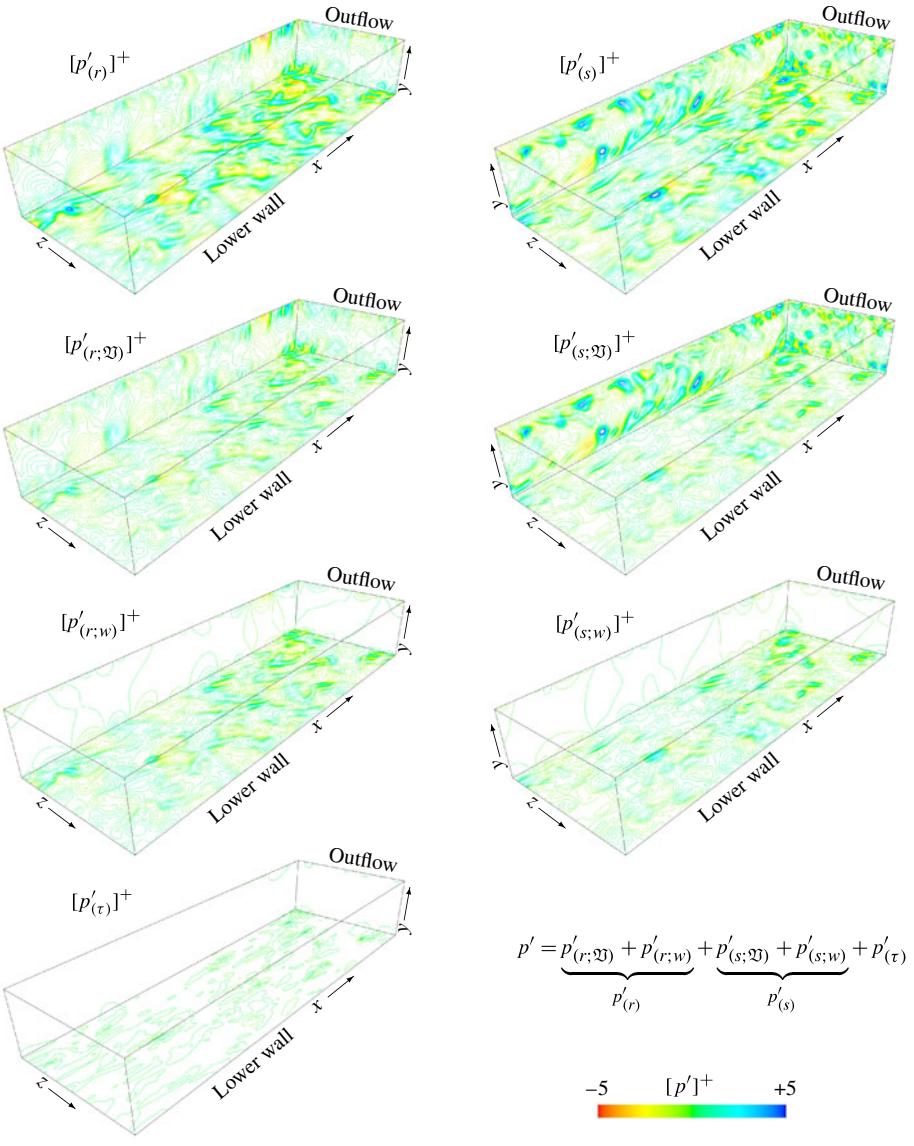


FIGURE 10. Instantaneous fluctuating pressure fields (2.11) from DNS computations ($Re_{\tau_w} = 179$; $\bar{M}_{CL} = 0.34$; $193\times129\times169$ grid; table 1), Stokes $[p'_{(\tau)}]^+$ (2.8), and rapid $[p'_{(r)}]^+$ and slow $[p'_{(s)}]^+$ (2.7), and their decomposition into weakly inhomogeneous volume fields, $[p'_{(r;\mathfrak{V})}]^+$ and $[p'_{(s;\mathfrak{V})}]^+$ (2.13), and strongly inhomogeneous wall-echo fields, $[p'_{(r;w)}]^+$ and $[p'_{(s;w)}]^+$ (2.16), in wall units (50 contours in the range $[-5, +5]$ on the lower wall, the outflow x periodic interface, and the z periodic interface).

https://doi.org/10.1017/jfm.2012.633 Published online by Cambridge University Press

read

$$\underbrace{\frac{\partial \rho \overline{u_i' u_j'}}{\partial t} + \frac{\partial}{\partial x_\ell}(\rho \overline{u_i' u_j'} \bar{u}_\ell)}_{\text{convection } C_{ij}} = \underbrace{\frac{\partial}{\partial x_\ell}\left(-\rho \overline{u_i' u_j' u_\ell'} - \overline{p' u_j'}\delta_{i\ell} - \overline{p' u_i'}\delta_{j\ell} + \mu \frac{\partial \overline{u_i' u_j'}}{\partial x_\ell}\right)}_{\text{diffusion } d_{ij}^{(u)} + d_{ij}^{(p)} + d_{ij}^{(\mu)}} + \underbrace{\overline{p'\left(\frac{\partial u_i'}{\partial x_j} + \frac{\partial u_j'}{\partial x_i}\right)}}_{\text{redistribution } \phi_{ij}} + \underbrace{\left(-\rho \overline{u_i' u_\ell'} \frac{\partial \tilde{u}_j}{\partial x_\ell} - \rho \overline{u_j' u_\ell'} \frac{\partial \tilde{u}_i}{\partial x_\ell}\right)}_{\text{production } P_{ij}} - \underbrace{\left(\frac{\partial}{\partial x_\ell}\left(\overline{\mu \frac{\partial u_i' u_j'}{\partial x_\ell}}\right) - \left(\overline{u_i' \frac{\partial \tau_{j\ell}'}{\partial x_\ell} + u_j' \frac{\partial \tau_{i\ell}'}{\partial x_\ell}}\right)\right)}_{\text{dissipation } \bar{\rho}\varepsilon_{ij}^{(\mu)} := 2\mu \overline{\partial_{x_\ell} u_i' \partial_{x_\ell} u_j'}} . \quad (3.1)$$

Convection C_{ij}, production P_{ij} and viscous diffusion $d_{ij}^{(\mu)}$ are exact terms, while all the other terms ($d_{ij}^{(u)}$, $d_{ij}^{(p)}$, ϕ_{ij} and $\varepsilon_{ij}^{(\mu)}$) require modelling. Pressure diffusion $d_{ij}^{(p)}$ and redistribution ϕ_{ij} can be grouped together into the velocity pressure-gradient correlation tensor Π_{ij},

$$\Pi_{ij} := -\overline{u_i' \frac{\partial p'}{\partial x_j}} - \overline{u_j' \frac{\partial p'}{\partial x_i}} = \underbrace{\overline{p'\left(\frac{\partial u_i'}{\partial x_j} + \frac{\partial u_j'}{\partial x_i}\right)}}_{\overline{2p'S_{ij}'}} \underbrace{- \left(\overline{\frac{\partial p' u_i'}{\partial x_j} + \frac{\partial p' u_j'}{\partial x_i}}\right)}_{d_{ij}^{(p)}} \overset{(3.1)}{=} \phi_{ij} + d_{ij}^{(p)}. \quad (3.2)$$

The velocity pressure-gradient tensor Π_{ij}, which is the term that appears in most of the original early developments (Chou 1945), tends to 0 as $y \to 0$ (in the viscous sublayer, where $d_{ij}^{(p)}$ and ϕ_{ij} cancel one another). In homogeneous turbulence (HT) $d_{ij}^{(p)} = 0 \overset{HT}{\iff} \phi_{ij} = \Pi_{ij}$.

3.3. *Pressure transport $\overline{p'u_i'}$ and pressure diffusion $d_{ij}^{(p)}$*

The p' splitting (2.11) applied to pressure transport $\overline{p'u_i'}$ and pressure diffusion $d_{ij}^{(p)}$ ((3.1) and (3.2)) indicates (figure 11) that the slow volume term $\overline{p'_{(s;\mathfrak{V})} v'}$ is the principal contribution to the wall-normal transport $\overline{p'v'}$, and even more to $d_{yy}^{(p)}$ (for fully developed plane channel flow $d_{yy}^{(p)} \overset{(3.1),\,(3.2)}{=} -2\partial_y \overline{p'v'}$), except in the near-wall region ($y^+ \lessapprox 5$) where all terms are of comparable importance (figure 11). Concerning $d_{xy}^{(p)}$ (for fully developed plane channel flow $d_{xy}^{(p)} \overset{(3.1),\,(3.2)}{=} -\partial_y \overline{p'u'}$), again the slow volume term $d_{xy}^{(p;s;\mathfrak{V})}$ is the most important contribution in the buffer and outer regions, whereas in the near-wall region ($y^+ \lessapprox 5$) all terms are of comparable importance (figure 11).

For modelling purposes it is important to note that, although the slow volume term $d_{ij}^{(p;s;\mathfrak{V})}$ is the main contribution (and a reasonable approximation) to $d_{ij}^{(p)}$ (figure 11), in the buffer and outer regions ($y^+ \gtrapprox 5$), this is not the case for pressure transport $\overline{p'u_i'}$, especially for $\overline{p'u'}$ (figure 11), where, for $5 \lessapprox y^+ \lessapprox 30$, $\overline{p'_{(s;\mathfrak{V})} u'}$ is of the opposite sign with respect to $\overline{p'u'}$.

https://doi.org/10.1017/jfm.2012.633 Published online by Cambridge University Press

Re_{τ_w}	$\bar{M}_{CL}$	$N_x \times N_y \times N_z$	L_x	L_y	L_z	Δx^+	Δy^+_w	$N_{y^+\leqslant 10}$	Δy^+_{CL}	Δz^+	Δt^+	$t^+_{obs_{GF}}$	$\Delta t^+_{s_{GF}}$
179	0.34	$193 \times 129 \times 169$	$4\pi\delta$	2δ	$4\pi\delta/3$	11.7	0.22	20	4.9	4.4	6.47×10^{-3}	1648	6.47×10^{-2}
178	0.00	$128 \times 129 \times 128$	$4\pi\delta$	2δ	$4\pi\delta/3$	17.7	0.05	14	4.4	5.9	Moser *et al.* (1999)		
186	0.00	$768 \times 97 \times 340$	$12\pi\delta$	2δ	$4\pi\delta$	8.9	0.10	11	6.1	6.7	Hoyas & Jiménez (2008)		

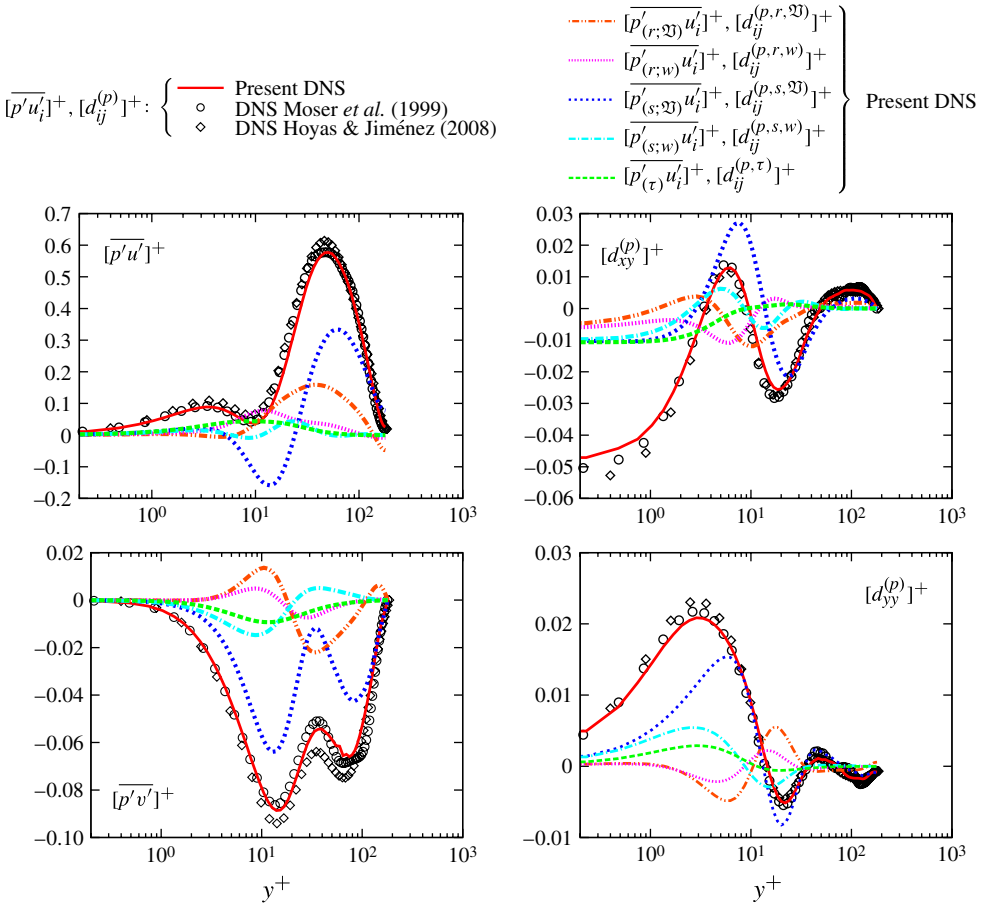


FIGURE 11. (Colour online) Distributions of the five terms in the incompressible p' splitting (2.11) of pressure transport, $\overline{p'_{(r;\mathfrak{V})}u'_i}$, $\overline{p'_{(r;w)}u'_i}$, $\overline{p'_{(s;\mathfrak{V})}u'_i}$, $\overline{p'_{(s;w)}u'_i}$ and $\overline{p'_{(\tau)}u'_i}$, from the present DNS computations ($Re_{\tau_w} = 179$; $\bar{M}_{CL} = 0.34$; $193 \times 129 \times 169$ grid; table 1), distributions of pressure transport $\overline{p'u'_i}$ from various DNS databases (Moser *et al.* 1999; Hoyas & Jiménez 2008; Gerolymos *et al.* 2010), and corresponding contributions to the pressure–diffusion tensor $d^{(p)}_{ij}$, in wall units, plotted against the non-dimensional distance from the wall y^+ (in fully developed incompressible plane channel flow $d^{(p)}_{xx} = d^{(p)}_{yz} = d^{(p)}_{zz} = d^{(p)}_{zx} = 0$).

These remarks imply that a consistent model for pressure diffusion $d^{(p)}_{ij}$, in the buffer and outer regions ($y^+ \gtrapprox 5$), can be built using only slow volume terms. However, such a model for $d^{(p)}_{ij}$ ($y^+ \gtrapprox 5$), based on $d^{(p;s;\mathfrak{V})}_{ij}$ only, cannot correspond to (or be built from) a satisfactory model for pressure transport $\overline{p'u'_i}$ (figure 11). The near-wall modelling of pressure diffusion $d^{(p)}_{ij}$ ($y^+ \lessapprox 5$) is more complex, since (figure 11) it must contain rapid terms and wall-echo terms (figure 11). To the authors' knowledge (Gerolymos *et al.* 2012*b*), no single-point closure for $d^{(p)}_{ij}$ takes into account the

https://doi.org/10.1017/jfm.2012.633 Published online by Cambridge University Press

Re_{τ_w}	$\bar{M}_{CL}$	$N_x \times N_y \times N_z$	L_x	L_y	L_z	Δx^+	Δy_w^+	$N_{y^+\leqslant 10}$	Δy_{CL}^+	Δz^+	Δt^+	$t^+_{obs_{GF}}$	$\Delta t^+_{s_{GF}}$
179	0.34	$193 \times 129 \times 169$	$4\pi\delta$	2δ	$4\pi\delta/3$	11.7	0.22	20	4.9	4.4	6.47×10^{-3}	1648	6.47×10^{-2}
178	0.00	$128 \times 129 \times 128$	$4\pi\delta$	2δ	$4\pi\delta/3$	17.7	0.05	14	4.4	5.9	Moser *et al.* (1999)		
186	0.00	$768 \times 97 \times 340$	$12\pi\delta$	2δ	$4\pi\delta$	8.9	0.10	11	6.1	6.7	Hoyas & Jiménez (2008)		

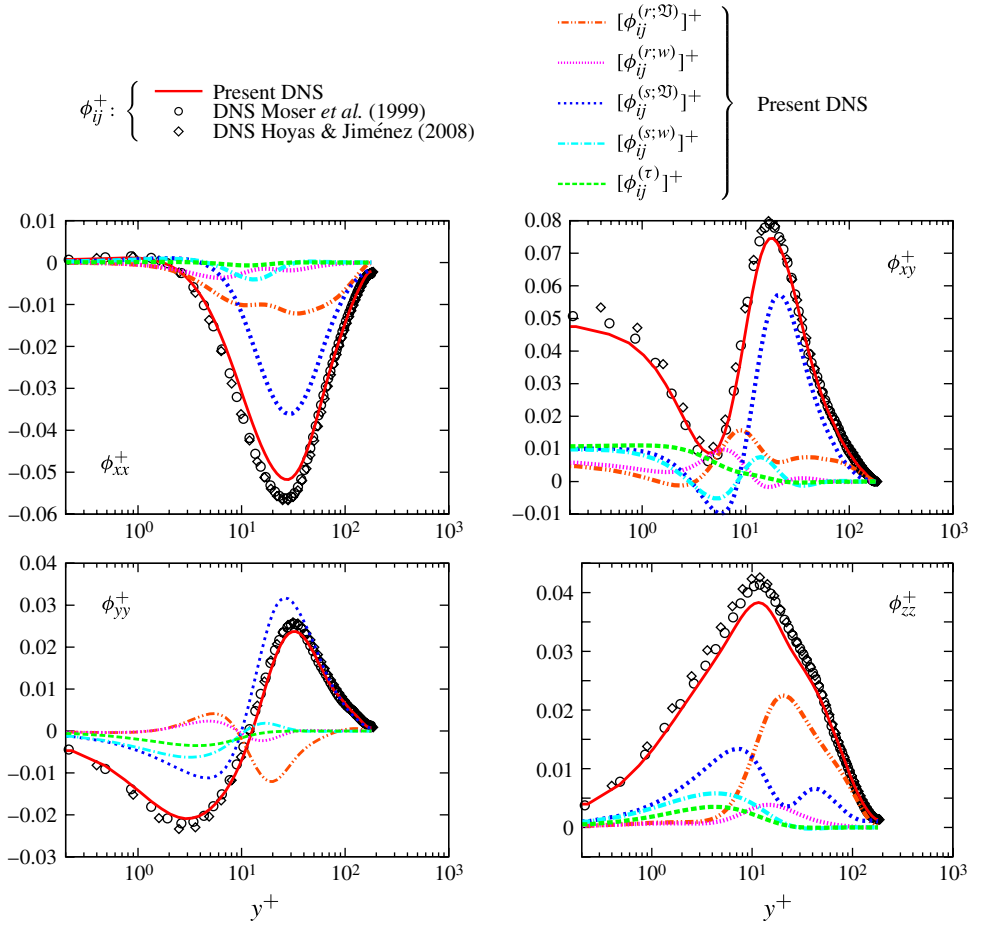


FIGURE 12. (Colour online) Distributions of the five terms in the incompressible p' splitting (2.11) of pressure–strain redistribution, $\phi_{ij}^{(r;\mathfrak{V})}$, $\phi_{ij}^{(r;w)}$, $\phi_{ij}^{(s;\mathfrak{V})}$, $\phi_{ij}^{(s;w)}$ and $\phi_{ij}^{(\tau)}$, from the present DNS computations ($Re_{\tau_w} = 179$; $\bar{M}_{CL} = 0.34$; $193 \times 129 \times 169$ grid; table 1), and distributions of pressure–strain redistribution ϕ_{ij} from various DNS databases (Moser *et al.* 1999; Hoyas & Jiménez 2008; Gerolymos *et al.* 2010), in wall units, plotted against the non-dimensional distance from the wall y^+ (in statistically two-dimensional plane flow $\phi_{zx} = \phi_{yz} = 0$).

wall-echo terms (Donaldson 1969; Hirt 1969; Daly & Harlow 1970; Lumley 1978; Fu 1993; Sauret & Vallet 2007; Vallet 2007).

3.4. *Pressure–strain redistribution* ϕ_{ij}

The application of the p' splitting (2.11) to pressure–strain redistribution ϕ_{ij} ((3.1) and (3.2)) shows again that the volume terms ($\phi_{ij}^{(r;\mathfrak{V})}$ and $\phi_{ij}^{(s;\mathfrak{V})}$) are the dominant contributions to ϕ_{ij} in the buffer and outer regions ($y^+ \gtrapprox 10$; figure 12). Note that $\phi_{zz}^{(r;\mathfrak{V})} > \phi_{zz}^{(s;\mathfrak{V})}$ for $y^+ \gtrapprox 10$ (figure 12), in contrast to the other components for which

https://doi.org/10.1017/jfm.2012.633 Published online by Cambridge University Press

the slow volume terms are the more important contributions to ϕ_{ij} in the buffer and outer regions ($y^+ \gtrapprox 15$; figure 12).

In the near-wall region ($y^+ \lessapprox 10$), the wall-echo terms ($\phi_{ij}^{(r;w)}$ and $\phi_{ij}^{(s;w)}$) are of the same order of magnitude as the corresponding volume terms ($\phi_{ij}^{(r;\mathfrak{V})}$ and $\phi_{ij}^{(s;\mathfrak{V})}$, respectively), satisfying an approximate equality at the wall, which (cf. § 2.2.5) implies that the energy-containing non-dimensional wavenumbers of the source terms (2.3*a*), (2.5*b*) and (2.6*a*) are sufficiently high for the interaction between the upper and lower walls to be negligible (figure 6). Furthermore, for the low-Reynolds-number case studied in the present work ($Re_{\tau_w} \cong 180$), the Stokes pressure term $\phi_{ij}^{(\tau)}$ is of the same order of magnitude, in the near-wall region ($y^+ \lessapprox 10$; figure 12), as the other terms of the p' splitting (2.11), and is particularly important for the shear component ϕ_{xy} (figure 12). At the wall ($y^+ = 0$; figure 12), $[\phi_{xy}^{(\tau)}]_{y^+=0}$ accounts for $\sim 25\,\%$ of $[\phi_{xy}]_{y^+=0}$. For a plane wall perpendicular to $\boldsymbol{e}_y$, at the wall ($y^+ = 0$), $[\phi_{xy}]_{y^+=0} \overset{(3.1),\,(3.2)}{=} [\overline{p'\partial_y u'}]_{y^+=0}$ (because $v'_{y^+=0} = 0 \implies [\partial_x v']_{y^+=0} = 0$). Therefore, the high level of $[\phi_{xy}^{(\tau)}]_{y^+=0}$ relative to the other terms of the p' splitting (2.11) implies that, at the wall, the fluctuating Stokes pressure $[p'_{(\tau)}]_{y^+=0}$ is well correlated with the fluctuating wall shear stress $[\tau'_{xy}]_{y^+=0} = \mu\,[\partial_y u']_{y^+=0}$. Note that none of the known models for ϕ_{ij} (Craft & Launder 1996; Gerolymos & Vallet 2001; Jakirlić & Hanjalić 2002; Suga 2004) gives the correct viscous sublayer behaviour of ϕ_{xy} and ϕ_{yy} ($y^+ \lessapprox 5$; figure 12). In fact, all known second-moment closures actually model $\Pi_{ij} = \phi_{ij} + d_{ij}^{(p)}$ in the viscous sublayer (Mansour *et al.* 1988), where ϕ_{ij} (figure 12) and $d_{ij}^{(p)}$ (figure 11) cancel one another, since $[\Pi_{ij}]_w = 0$, even when they separately model ϕ_{ij} and $d_{ij}^{(p)}$ (Gerolymos *et al.* 2012*b*) further away from the wall ($y^+ \lessapprox 5$).

3.5. *Velocity pressure-gradient* Π_{ij}

The velocity pressure-gradient correlation Π_{ij} (3.2) is exactly the sum of pressure diffusion $d_{ij}^{(p)}$ (§ 3.3) and pressure–strain redistribution ϕ_{ij} (§ 3.4). By definition (3.2) $[\Pi_{ij}]_{y^+=0}$ because of the no-slip wall boundary condition for the fluctuating velocity $[u'_i]_{y^+=0} = 0$, implying that $[\phi_{ij}]_{y^+=0} = -\,[d_{ij}^{(p)}]_{y^+=0}$, so that very near the wall we expect that $\Pi_{ij} := \phi_{ij} + d_{ij}^{(p)}$ will approach 0 asymptotically. Observation of DNS data ($y^+ \lessapprox 5$; figure 13) indicates that the rate at which Π_{zz} approaches 0 as $y^+ \to 0$ is much slower compared to the other components (Π_{xx}, Π_{xy} and Π_{yy}).

In fully developed incompressible plane channel flow, $d_{xx}^{(p)} = d_{zz}^{(p)} = 0$ by (3.2), implying not only that $\Pi_{xx} = \phi_{xx}$ and $\Pi_{zz} = \phi_{zz}$, but also that $\Pi_{\ell\ell} = d_{yy}^{(p)}$ (since $\phi_{\ell\ell} \overset{(3.2)}{=} 0$ by the incompressible fluctuating continuity equation $\partial_{x_\ell} u'_\ell = 0$). For the three components, Π_{xx}, Π_{xy} and Π_{yy}, the dominant contribution from the mechanisms of the p' splitting (2.11) comes from the slow volume terms ($\Pi_{xx}^{(s;\mathfrak{V})}$, $\Pi_{xy}^{(s;\mathfrak{V})}$ and $\Pi_{yy}^{(s;\mathfrak{V})}$), the rapid volume terms ($\Pi_{xx}^{(r;\mathfrak{V})}$, $\Pi_{xy}^{(r;\mathfrak{V})}$ and $\Pi_{yy}^{(r;\mathfrak{V})}$) being the main remaining contribution (figure 13). In contrast, all five mechanisms of p' generation in (2.11) contribute with the same order of magnitude in the near-wall region ($y^+ \lessapprox 10$; figure 13) to Π_{zz} (=ϕ_{zz} in fully developed incompressible plane channel flow), this difference between Π_{zz} and the other components being related to the slower rate at which Π_{zz} goes to 0 as $y^+ \to 0$ ($y^+ \lessapprox 5$; figure 13). Furthermore, in contrast to ϕ_{ij} (figure 12) and $d_{ij}^{(p)}$ (figure 11), for which the volume and wall-echo terms of each field (rapid or slow) are of the same sign, almost everywhere, and exhibit the same

https://doi.org/10.1017/jfm.2012.633 Published online by Cambridge University Press

Re_{τ_w}	$\bar{M}_{CL}$	$N_x \times N_y \times N_z$	L_x	L_y	L_z	Δx^+	Δy_w^+	$N_{y^+\leqslant 10}$	Δy_{CL}^+	Δz^+	Δt^+	$t^+_{obs_{GF}}$	$\Delta t^+_{s_{GF}}$
179	0.34	$193 \times 129 \times 169$	$4\pi\delta$	2δ	$4\pi\delta/3$	11.7	0.22	20	4.9	4.4	6.47×10^{-3}	1648	6.47×10^{-2}
178	0.00	$128 \times 129 \times 128$	$4\pi\delta$	2δ	$4\pi\delta/3$	17.7	0.05	14	4.4	5.9	Moser *et al.* (1999)		
186	0.00	$768 \times 97 \times 340$	$12\pi\delta$	2δ	$4\pi\delta$	8.9	0.10	11	6.1	6.7	Hoyas & Jiménez (2008)		

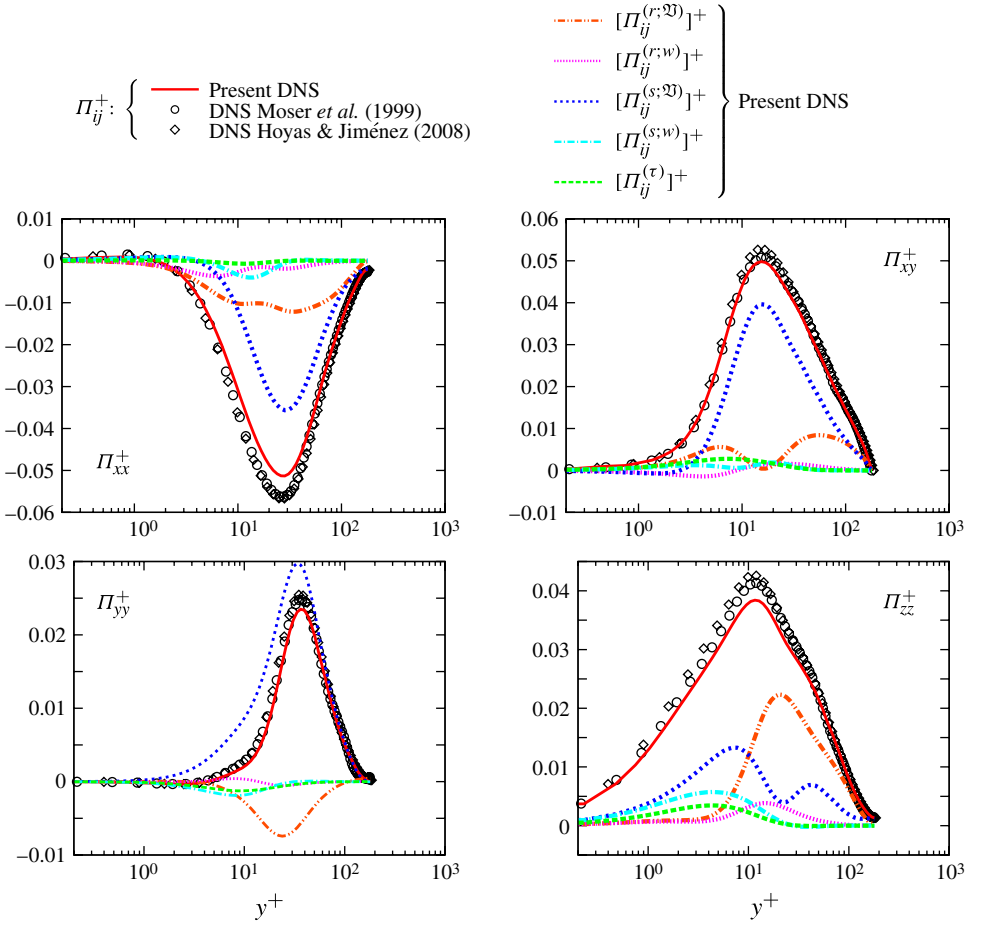


FIGURE 13. (Colour online) Distributions of the five terms in the incompressible p' splitting (2.11) of velocity pressure-gradient correlation, $\Pi_{ij}^{(r;\mathfrak{V})}$, $\Pi_{ij}^{(r;w)}$, $\Pi_{ij}^{(s;\mathfrak{V})}$, $\Pi_{ij}^{(s;w)}$ and $\Pi_{ij}^{(\tau)}$, from the present DNS computations ($Re_{\tau_w} = 179$; $\bar{M}_{CL} = 0.34$; $193 \times 129 \times 169$ grid; table 1), and distributions of velocity pressure-gradient correlation Π_{ij} from various DNS databases (Moser *et al.* 1999; Hoyas & Jiménez 2008; Gerolymos *et al.* 2010), in wall units, plotted against the non-dimensional distance from the wall y^+ (in fully developed incompressible plane channel flow $\Pi_{zx} = \Pi_{yz} = 0$, $\Pi_{xx} = \phi_{xx}$ and $\Pi_{zz} = \phi_{zz}$).

variation with y^+, this behaviour applies only to Π_{xx} and Π_{zz}. For the wall-normal Π_{yy} and the shear Π_{xy} components, the wall-echo and volume terms of each field (rapid or slow) are of opposite sign. In fact, in agreement with Manceau *et al.* (2001), all components of ϕ_{ij} (figure 12) are increased in absolute value by wall echo, and so are the components of $d_{ij}^{(p)}$ (figure 11). This observation is true for both the rapid and slow fields (figures 11 and 12), but with different factors depending on the particular component and y^+. Therefore, when these ϕ_{ij} and $d_{ij}^{(p)}$ are combined together, their

https://doi.org/10.1017/jfm.2012.633 Published online by Cambridge University Press

sum $\Pi_{ij} \overset{(3.2)}{:=} \phi_{ij} + d_{ij}^{(p)}$ behaves differently. This is not incompatible with their near-equality at the wall, where all components of Π_{ij} vanish, because their y gradients can be different. This observation is significant for near-wall modelling, because the term that appears in the Reynolds stress transport equation is Π_{ij}, and, whether ϕ_{ij} or $d_{ij}^{(p)}$ are modelled separately (Gerolymos *et al.* 2012*b*) or together (Mansour *et al.* 1988), it is the modelled sum that defines the quality of the model.

In order to explain the different behaviours of the various parts of the p' splitting ($p'_{(r;\mathfrak{V})}$, $p'_{(r;w)}$, $p'_{(s;\mathfrak{V})}$, $p'_{(s;w)}$) between Π_{xx} and Π_{zz}, on the one hand, and Π_{yy} and Π_{xy}, on the other (§ 3.5), consider the analytical expression (hence transfer function) relating different parts of the p' splitting (2.11) to the rapid and slow sources (2.3*a*). Let $m \in \{s, r\}$ denote the rapid or slow fields, and $n \in \{\mathfrak{V}, w\}$ denote the corresponding volume or wall parts. Then, combining the xz Fourier transform representation of $p'_{(m;n)}$ (2.5*a*) and $Q'_{(m)}$ (2.5*b*) with the Green's function solution of the corresponding field ((2.13) and (2.16)),

$$p'_{(m;n)}(x,y,z,t) \overset{(2.5),\ (2.13),\ (2.16)}{=} \int_{-\infty}^{+\infty}\int_{-\infty}^{+\infty}\left(\int_{-Ly/2}^{+Ly/2} G_n(y,Y;\kappa)\hat{Q}'_{(m)}(\kappa_x,Y,\kappa_z,t)\,\mathrm{d}Y\right)\mathrm{e}^{\mathrm{i}\kappa_x x+\mathrm{i}\kappa_z z}\,\mathrm{d}\kappa_x\,\mathrm{d}\kappa_z \tag{3.3a}$$

and, by direct differentiation and averaging of (3.3*a*), we have

$$[\Pi_{xx}]_{(m;n)} \overset{(3.2)}{:=} -2\overline{u'\frac{\partial p'}{\partial x}} \overset{(3.3a)}{=} -2u'\int_{-\infty}^{+\infty}\int_{-\infty}^{+\infty}\int_{-Ly/2}^{+Ly/2} G_n(y,Y;\kappa)\hat{Q}'_{(m)}(\kappa_x,Y,\kappa_z,t)\mathrm{i}\kappa_x\mathrm{e}^{\mathrm{i}\kappa_x x+\mathrm{i}\kappa_z z}\,\mathrm{d}\kappa_x\,\mathrm{d}\kappa_z\,\mathrm{d}Y, \tag{3.3b}$$

$$[\Pi_{yy}]_{(m;n)} \overset{(3.2)}{:=} -2\overline{v'\frac{\partial p'}{\partial y}} \overset{(3.3a)}{=} -2v'\int_{-\infty}^{+\infty}\int_{-\infty}^{+\infty}\int_{-Ly/2}^{+Ly/2} \frac{\partial G_n}{\partial y}(y,Y;\kappa)\hat{Q}'_{(m)}(\kappa_x,Y,\kappa_z,t)\mathrm{e}^{\mathrm{i}\kappa_x x+\mathrm{i}\kappa_z z}\,\mathrm{d}\kappa_x\,\mathrm{d}\kappa_z\,\mathrm{d}Y, \tag{3.3c}$$

$$[\Pi_{zz}]_{(m;n)} \overset{(3.2)}{:=} -2\overline{w'\frac{\partial p'}{\partial z}} \overset{(3.3a)}{=} -2w'\int_{-\infty}^{+\infty}\int_{-\infty}^{+\infty}\int_{-Ly/2}^{+Ly/2} G_n(y,Y;\kappa)\hat{Q}'_{(m)}(\kappa_x,Y,\kappa_z,t)\mathrm{i}\kappa_z\mathrm{e}^{\mathrm{i}\kappa_x x+\mathrm{i}\kappa_z z}\,\mathrm{d}\kappa_x\,\mathrm{d}\kappa_z\,\mathrm{d}Y, \tag{3.3d}$$

$$\begin{aligned}[\Pi_{xy}]_{(m;n)} &\overset{(3.2)}{:=} -\overline{u'\frac{\partial p'}{\partial y}} - \overline{v'\frac{\partial p'}{\partial x}} \\ &\overset{(3.3a)}{=} -v'\int_{-\infty}^{+\infty}\int_{-\infty}^{+\infty}\int_{-Ly/2}^{+Ly/2} G_n(y,Y;\kappa)\hat{Q}'_{(m)}(\kappa_x,Y,\kappa_z,t)\mathrm{i}\kappa_x\mathrm{e}^{\mathrm{i}\kappa_x x+\mathrm{i}\kappa_z z}\,\mathrm{d}\kappa_x\,\mathrm{d}\kappa_z\,\mathrm{d}Y \\ &\quad -u'\int_{-\infty}^{+\infty}\int_{-\infty}^{+\infty}\int_{-Ly/2}^{+Ly/2} \frac{\partial G_n}{\partial y}(y,Y;\kappa)\hat{Q}'_{(m)}(\kappa_x,Y,\kappa_z,t)\mathrm{e}^{\mathrm{i}\kappa_x x+\mathrm{i}\kappa_z z}\,\mathrm{d}\kappa_x\,\mathrm{d}\kappa_z\,\mathrm{d}Y. \end{aligned} \tag{3.3e}$$

https://doi.org/10.1017/jfm.2012.633 Published online by Cambridge University Press

It is obvious from (3.3) that there is a fundamental difference in the way the xz Fourier components of the sources interact with u_i' to build the components of Π_{ij}. For $[\Pi_{xx}]_{(m;n)}$ (3.3*b*) and $[\Pi_{zz}]_{(m;n)}$ (3.3*d*), the contribution of each wavenumber is weighted by $\mathrm{i}\kappa_x$ or $\mathrm{i}\kappa_z$ (this includes not only modulus weighting but also phase shift) and by the appropriate Green's function. This is no longer the case for $[\Pi_{yy}]_{(m;n)}$ (3.3*c*), where there is no wavenumber weighting and the y gradient of the Green's function appears. Therefore, contributions of the sources from different Y locations and different wavenumbers are weighted differently for $[\Pi_{yy}]_{(m;n)}$ compared to the other normal components, $[\Pi_{xx}]_{(m;n)}$ and $[\Pi_{zz}]_{(m;n)}$. This explains why the behaviour of the different fields in Π_{yy} (figure 13) is so profoundly different compared to Π_{xx} or Π_{zz}. Finally, Π_{xy} (3.3*e*) contains both types of integrals, and is arguably more complex to analyse. Similar analysis, based on (2.5*c*) and (2.8), applies to the Stokes field $p'_{(\tau)}$.

The above analysis hints at the reasons for the different relative behaviours of the contributions of different pressure fluctuation fields ($p'_{(r;\mathfrak{V})}$, $p'_{(r;w)}$, $p'_{(s;\mathfrak{V})}$, $p'_{(s;w)}$) in the various components of Π_{ij}. On the other hand, (3.3) suggests that further research is required, studying specifically the spectral behaviour of $\hat{Q}'_{(m)}$ and its convolution with the xz Fourier components of u_i', continuing the analysis of Chang *et al.* (1999), which focused on p' alone.

4. Conclusions

In the present paper, we consider fully developed (x-wise invariant in the mean) turbulent plane channel flow. Examination of the DNS data of Hoyas & Jiménez (2008), in the range $Re_{\tau_w} \in [180, 2000]$, indicates that, despite the pronounced dependence of $[p'_w]^+_{rms}$ on Re_{τ_w}, the y distribution of the ratio of slow to rapid pressure fluctuations, $[p'_{(r)}]^{-1}_{rms}[p'_{(s)}]_{rms}$, is reasonably independent of Re_{τ_w}, particularly in the near-wall region ($y^+ \lessapprox 50$), but also in the outer region ($\frac{2}{10}\delta \leqslant y - y_w \leqslant \frac{7}{10}\delta$), where it takes a nearly constant value (~ 1.6).

The Green's function (G_{Kim}) approach of Kim (1989), for the solution of the one-dimensional modified Helmholtz equation for each wall-parallel wavenumber, used in DNS computations to separate instantaneous pressure fluctuations p' into rapid, slow and Stokes terms ($p' = p'_{(r)} + p'_{(s)} + p'_{(\tau)}$), was extended so as to separate volume ($G_{\mathfrak{V}}$) and wall-echo (G_w) terms ($p' = p'_{(r;\mathfrak{V})} + p'_{(r;w)} + p'_{(s;\mathfrak{V})} + p'_{(s;w)} + p'_{(\tau)}$), corresponding to volume and surface integrals in the formal solution of the Poisson equation for p' (Chou 1945). The algorithm is based on appropriate Green's functions for the volume and wall-echo terms ($G_{Kim} = G_{\mathfrak{V}} + G_w$; appendix B), and is directly applicable to existing DNS databases containing flow fields sampled at different instants.

The method of images can be represented by an equivalent Green's function (G_{MWL}) whose expression proves that this method is the superposition (the modified Helmholtz equation for each wavenumber is linear) of the volume terms ($G_{\mathfrak{V}}$) and of the wall-echo effect ($G_{w_\pm}$) that each wall would induce in the absence of the other ($G_{MWL} = G_{\mathfrak{V}} + G_{w_+} + G_{w_-}$). The approximation of the method of images consists in neglecting the interaction between the upper and lower walls, whose effect is shown by the present exact theory to amplify wall echo, increasingly so as the non-dimensional wavenumber $\kappa\delta$ increases. Theoretical analysis indicates that the method of images is a high-wavenumber approximation, the approximation error growing exponentially with $(\kappa\delta)^{-1}$, but remaining reasonable for the usual wavenumbers of energy-containing structures (error $\lessapprox 1\,\%$ for $\ell_\kappa := 2\pi\kappa^{-1} \leqslant 4\delta$),

https://doi.org/10.1017/jfm.2012.633 Published online by Cambridge University Press

consistent with the generally accepted similarity between the near-wall structure of boundary layer and plane channel flows. These results are obtained by studying the Green's functions, and as such are independent of the particular distribution of the source terms (hence independent of Re_{τ_w} or $\bar{M}_{CL}$), depending only on the wavenumber. Nonetheless, although the error estimate qualifies the method of images as a good engineering approximation, the present exact theory is preferable for the fine analysis of wall-echo effects, to avoid distortion of the large-structures part of the spectrum, especially as it introduces no computational cost overhead.

Analysis of the p' splitting for low $Re_{\tau_w} = 180$ flow indicates the following points:

(*a*) At the wall, the instantaneous volume ($p'_{(r;\mathfrak{V})}$ and $p'_{(s;\mathfrak{V})}$) and wall-echo ($p'_{(r;w)}$ and $p'_{(s;w)}$) terms of the same field (rapid or slow) are approximately equal ($[p'_{(r;\mathfrak{V})}]_w \cong [p'_{(r;w)}]_w$ and $[p'_{(s;\mathfrak{V})}]_w \cong [p'_{(s;w)}]_w$), but this approximate equality only holds very near the wall ($y^+ \lessapprox 3$).

(*b*) Although this approximate equality between corresponding volume and wall-echo terms and similar near-wall behaviour ($y^+ \lessapprox 20$) hold for ϕ_{ij}, $\overline{p'u'_i}$ and $d^{(p)}_{ij}$, this does not apply to the velocity pressure-gradient correlation Π_{ij}. For the Π_{yy} and Π_{xy} components, wall echo opposes (opposite sign) the corresponding volume terms in the range $y^+ \lessapprox 20$, contrary to Π_{xx} and Π_{zz}. An explanation of this new finding can be sought in the way the xz Fourier components of the sources are weighted by wavenumber and Green's function or its y gradient in the integrals representing the gradients $\partial_x p'$, $\partial_y p'$ and $\partial_z p'$.

Theoretical analysis (appendix A) of compressibility effects in low-Mach-number flow of air shows that the additional compressible terms in the Poisson equation for p' scale with density fluctuations and spatial variations. DNS-based assessment of the order of magnitude of the extra compressible terms indicates that they can be reasonably neglected for centreline Mach number $\bar{M}_{CL} \lessapprox 0.35$, and that Morkovin's hypothesis stating that the leading-order effect of compressibility on turbulence is related to mean density variation ($\lessapprox 1.5\,\%$ for $\bar{M}_{CL} \cong 0.35$) applies to the fluctuating pressure field structure.

The main perspectives of this work are: (i) the application of the algorithm to higher-Re_{τ_w} flows; (ii) the detailed spectral analysis of Π_{ij} and the use of the data to improve near-wall modelling of pressure correlations; and (iii) the application of the algorithm to the compressible Poisson equation for p' at higher-$\bar{M}_{CL}$ (supersonic) flows.

Acknowledgements

The authors are listed alphabetically. We are particularly grateful to Professor B. A. Younis for many enlightening discussions. The computations were performed using HPC resources from GENCI–IDRIS (Grant 2010–022139). The source files of the code used and computer routines for the splitting are available as part of the freeware project 'aerodynamics' (Gerolymos & Vallet 2009; http://sourceforge.net/projects/aerodynamics). Tabulated data are available at http://www.aerodynamics.fr/DNS_database/CT_chnnl. The present work was partly supported by the EU-funded research project ProBand (STREP–FP6 AST4–CT–2005–012222).

https://doi.org/10.1017/jfm.2012.633 Published online by Cambridge University Press

Appendix A. Compressibility effects at the low-Mach-number limit

Since the present DNS database was obtained using a compressible solver (Gerolymos *et al.* 2010) at $\bar{M}_{CL} \approxeq 0.34$, we examine here in more detail the effects of compressibility on fluctuating pressure p', and discuss in particular the parameter that should be used in the scaling of the compressibility effects. This is also important in assessing how the incompressible flow limit is approached for low-Mach-number aerodynamic flows (Durran 1989), as far as correlations containing the fluctuating pressure are concerned.

A.1. *Compressible flow Poisson equation for p'*

The flow is modelled by the compressible Navier–Stokes equations (Gerolymos *et al.* 2010, (34)–(37), pp. 785–786). Taking the divergence of the momentum equation (Gerolymos *et al.* 2010, (34b), p. 785) readily yields

$$\frac{\partial^2}{\partial x_i \partial t}(\rho u_i) + \frac{\partial^2}{\partial x_i \partial x_j}(\rho u_i u_j) = -\nabla^2 p + \frac{\partial^2 \tau_{ij}}{\partial x_i \partial x_j} + \frac{\partial}{\partial x_i}(\rho f_{V_i}), \tag{A 1a}$$

where f_{V_i} is the body acceleration.

Pantano & Sarkar (2002) used the inviscid form of (A 1a), considering only acoustic pressure ($\mathrm{d}p_a = a^2 \mathrm{d}\rho$, where a is the speed of sound), to study compressibility effects in high-speed shear layers. Foysi *et al.* (2004) further developed (A 1a) using the Garrick operator $[D_{c_t}]^2$ (Garrick 1957) of theoretical compressible unsteady aerodynamics and aeroacoustics (Miles 1959; Bisplinghoff & Ashley 1962), which highlights a wavelike influence of the fluctuating density, and Mahle *et al.* (2007) applied it to high-speed compressible mixing layers. All these high-Mach-number studies used Favre decomposition (Favre 1965*a*,*b*), and the form $\partial^2_{x_i x_j}(u_i'' u_j'' - \overline{u_i'' u_j''})$ for the slow terms. Since we are interested here in establishing the order of magnitude of compressibility effects in comparison with the incompressible flow equation (1.1), we recast the fluctuating part of (A 1a) in a form containing (1.1) plus compressible terms. Furthermore, the point can be made that the most general scaling of compressibility effects are density fluctuations $\rho'_{rms} := \sqrt{\overline{\rho'^2}}$; therefore, all compressible terms are rewritten in terms of ρ gradients and fluctuations. This is in particular the case for correlations related to the dilatation (Ristorcelli 1997), which can be expressed using the continuity equation

$$\frac{\partial \rho}{\partial t} + \frac{\partial \rho u_\ell}{\partial x_\ell} = 0 \quad \overset{\Theta := \mathrm{div} \boldsymbol{V} = \partial_{x_\ell} u_\ell}{\Longrightarrow} \quad \Theta = -\frac{1}{\rho}\frac{\mathrm{D}\rho}{\mathrm{D}t}, \tag{A 1b}$$

where $D_t(\cdot) := \partial_t(\cdot) + u_\ell \partial_{x_\ell}(\cdot)$ is the substantial derivative (Pope 2000, p. 13). Then (A 1a) reads

$$\nabla^2 p \overset{\text{(A 1}a\text{), (A 1}b\text{)}}{=} \frac{\partial^2 \tau_{ij}}{\partial x_i \partial x_j} + \frac{\partial}{\partial x_i}(\rho f_{V_i}) - \rho \frac{\partial u_i}{\partial x_j}\frac{\partial u_j}{\partial x_i} + \underbrace{\rho \frac{\mathrm{D}}{\mathrm{D}t}\left(\frac{1}{\rho}\frac{\mathrm{D}\rho}{\mathrm{D}t}\right)}_{\overset{\text{(A 1}b\text{)}}{=} -\rho \frac{\mathrm{D}\Theta}{\mathrm{D}t}} - \frac{\mathrm{D}\boldsymbol{V}}{\mathrm{D}t} \cdot \mathrm{grad}\rho \tag{A 1c}$$

https://doi.org/10.1017/jfm.2012.633 Published online by Cambridge University Press

by straightforward computation, using the continuity equation (A 1*b*),

$$\begin{aligned}
&\frac{\partial^2}{\partial x_i\partial t}(\rho u_i)+\frac{\partial^2}{\partial x_i\partial x_j}(\rho u_iu_j)\\
&\quad=\frac{\partial}{\partial t}\left(\rho\Theta+u_i\frac{\partial\rho}{\partial x_i}\right)+\frac{\partial}{\partial x_i}\left(u_i\frac{\partial\rho u_j}{\partial x_j}+\rho u_j\frac{\partial u_i}{\partial x_j}\right)\\
&\quad\overset{(A\,1b)}{=}\frac{\partial}{\partial t}\left(\rho\Theta+u_i\frac{\partial\rho}{\partial x_i}\right)+\left(\Theta\frac{\partial\rho u_j}{\partial x_j}+u_i\frac{\partial}{\partial x_i}\left(\frac{\partial\rho u_j}{\partial x_j}\right)+\frac{\partial\rho u_j}{\partial x_i}\frac{\partial u_i}{\partial x_j}+\rho u_j\frac{\partial\Theta}{\partial x_j}\right)\\
&\quad=\left(\rho\overset{①}{\frac{\partial\Theta}{\partial t}}+\Theta\overset{②}{\frac{\partial\rho}{\partial t}}+\overset{③}{\frac{\partial u_i}{\partial t}}\overset{③}{\frac{\partial\rho}{\partial x_i}}+u_i\frac{\partial}{\partial x_i}\overset{④}{\left(\frac{\partial\rho}{\partial t}\right)}\right)\\
&\qquad+\left(\Theta\overset{⑤}{\frac{\partial\rho u_j}{\partial x_j}}+u_i\frac{\partial}{\partial x_i}\overset{⑥}{\left(\frac{\partial\rho u_j}{\partial x_j}\right)}+\rho\overset{⑦}{\frac{\partial u_i}{\partial x_j}}\frac{\partial u_j}{\partial x_i}+u_j\overset{⑧}{\frac{\partial u_i}{\partial x_j}}\frac{\partial\rho}{\partial x_i}+\rho u_j\overset{⑨}{\frac{\partial\Theta}{\partial x_j}}\right)\\
&\quad=\rho\underbrace{\left(\overset{①}{\frac{\partial\Theta}{\partial t}}+u_j\overset{⑨}{\frac{\partial\Theta}{\partial x_j}}\right)}_{=:\frac{D\Theta}{Dt}}+\Theta\underbrace{\left(\overset{②}{\frac{\partial\rho}{\partial t}}+\overset{⑤}{\frac{\partial\rho u_j}{\partial x_j}}\right)}_{\overset{(A\,1b)}{=}0}+\underbrace{\left(\overset{③}{\frac{\partial u_i}{\partial t}}+u_j\overset{⑧}{\frac{\partial u_i}{\partial x_j}}\right)}_{=:\frac{Du_i}{Dt}}\frac{\partial\rho}{\partial x_i}\\
&\qquad+u_i\frac{\partial}{\partial x_i}\underbrace{\left(\overset{④}{\frac{\partial\rho}{\partial t}}+\overset{⑥}{\frac{\partial\rho u_j}{\partial x_j}}\right)}_{\overset{(A\,1b)}{=}0}+\rho\overset{⑦}{\frac{\partial u_i}{\partial x_j}}\frac{\partial u_j}{\partial x_i}.
\end{aligned}\tag{A 1d}$$

Subtracting its Reynolds average from (A 1*c*) readily yields the working form of the compressible flow Poisson equation for the fluctuating static pressure p',

$$\begin{aligned}
\nabla^2p'=&\underbrace{\left[-\bar\rho\left(\frac{\partial u_i'}{\partial x_j}\frac{\partial u_j'}{\partial x_i}-\overline{\frac{\partial u_i'}{\partial x_j}\frac{\partial u_j'}{\partial x_i}}\right)\right]}_{\mathcal{Q}'_{(s)}}+\underbrace{\left[-\left(\rho'\frac{\partial u_i'}{\partial x_j}\frac{\partial u_j'}{\partial x_i}-\overline{\rho'\frac{\partial u_i'}{\partial x_j}\frac{\partial u_j'}{\partial x_i}}\right)\right]}_{\mathcal{Q}'_{(\rho';s)}}\\
&+\underbrace{\left[-2\bar\rho\left(\frac{\partial u_i'}{\partial x_j}\frac{\partial\bar u_j}{\partial x_i}\right)\right]}_{\mathcal{Q}'_{(r)}}+\underbrace{\left[-2\left(\rho'\frac{\partial u_i'}{\partial x_j}-\overline{\rho'\frac{\partial u_i'}{\partial x_j}}\right)\frac{\partial\bar u_j}{\partial x_i}\right]}_{\mathcal{Q}'_{(\rho';r)}}+\underbrace{\left[-\rho'\frac{\partial\bar u_i}{\partial x_j}\frac{\partial\bar u_j}{\partial x_i}\right]}_{\mathcal{Q}'_{(\rho')}}\\
&+\underbrace{\frac{\partial^2\tau_{ij'}}{\partial x_i\partial x_j}}_{\mathcal{Q}'_{(\tau)}}+\underbrace{\frac{\partial}{\partial x_i}(\rho f_{V_i}-\overline{\rho f_{V_i}})}_{\mathcal{Q}'_{(\mathrm{BF})}}+\underbrace{\left[\rho\frac{\mathrm{D}}{\mathrm{D}t}\left(\frac{1}{\rho}\frac{\mathrm{D}\rho}{\mathrm{D}t}\right)\right]'}_{\mathcal{Q}'_{(\Theta)}}+\underbrace{\left[-\frac{\mathrm{D}\boldsymbol{V}}{\mathrm{D}t}\cdot\mathrm{grad}\rho\right]'}_{\mathcal{Q}'_{(\dot V\nabla\rho)}},
\end{aligned}\tag{A 1e}$$

where

$$\overline{\frac{\mathrm{D}(\cdot)}{\mathrm{D}t}}:=\overline{\frac{\partial(\cdot)}{\partial t}+u_j\frac{\partial(\cdot)}{\partial x_j}}=\frac{\partial\overline{(\cdot)}}{\partial t}+\bar u_j\frac{\partial\overline{(\cdot)}}{\partial x_j}+\overline{u_j'\frac{\partial(\cdot)'}{\partial x_j}},\tag{A 1f}$$

$$\left[\frac{\mathrm{D}(\cdot)}{\mathrm{D}t}\right]':=\frac{\mathrm{D}(\cdot)}{\mathrm{D}t}-\overline{\frac{\mathrm{D}(\cdot)}{\mathrm{D}t}}=\frac{\partial(\cdot)'}{\partial t}+\bar u_j\frac{\partial(\cdot)'}{\partial x_j}+u_j'\frac{\partial\overline{(\cdot)}}{\partial x_j}+u_j'\frac{\partial(\cdot)'}{\partial x_j}-\overline{u_j'\frac{\partial(\cdot)'}{\partial x_j}}.\tag{A 1g}$$

https://doi.org/10.1017/jfm.2012.633 Published online by Cambridge University Press

Obviously,

$$Q'_{(\rho';s)} \overset{(A\,1e)}{=} \frac{\rho'}{\bar{\rho}} Q'_{(s)}, \tag{A 1h}$$

$$Q'_{(\rho';r)} \overset{(A\,1e)}{=} \frac{\rho'}{\bar{\rho}} Q'_{(r)} + 2\overline{\rho' \frac{\partial u'_i}{\partial x_j}} \frac{\partial \bar{u}_j}{\partial x_i}. \tag{A 1i}$$

A.2. *Quasi-incompressible flow approximations*

We start by summarizing some basic approximations for flows with very small mean density gradients and density fluctuations, which can be termed quasi-incompressible, and include most low-Mach-number flows without important heat transfer effects. We assume that for the class of flows under consideration

$$\frac{\rho'}{\bar{\rho}} \ll 1, \tag{A 2a}$$

$$\left|\overline{\frac{\mathrm{D}\rho}{\mathrm{D}t}}\right| \ll \left(\frac{\mathrm{D}\rho}{\mathrm{D}t}\right)'_{rms} =: \frac{\rho'_{rms}}{\mathscr{T}_{(D_t\rho)'}} \overset{(A\,2a)}{\ll} \frac{\bar{\rho}}{\mathscr{T}_{(D_t\rho)'}}, \tag{A 2b}$$

where $\mathscr{T}_{(D_t\rho)'} := \rho'_{rms}[(D_t\rho)'_{rms}]^{-1}$ is an appropriate time scale (it will be shown in § A.3 that, for plane channel flow, this time scale, made non-dimensional in wall units, satisfies $[\mathscr{T}_{(D_t\rho)'}]^+ = O(1)$), i.e. density fluctuations are very small compared to mean density (A 2*a*), and furthermore the Reynolds-averaged substantial derivative (A 1*f*) of ρ is negligible compared to its fluctuating part (A 1*g*), which is itself very small (A 2*b*). From (A 2*a*) we readily have the usual weakly compressible (Taulbee & VanOsdol 1991) approximation ($x \to 0 \implies (1+x)^{-1} = 1 - x + x^2 - x^3 + x^4 + \cdots$)

$$\frac{1}{\rho} \overset{(A\,2a)}{=} \frac{1}{\bar{\rho}} - \frac{\rho'}{\bar{\rho}^2} + O\left(\frac{\rho'^2}{\bar{\rho}^2}\right) \overset{(A\,2a)}{\approx} \frac{1}{\bar{\rho}} - \frac{\rho'}{\bar{\rho}^2}. \tag{A 3a}$$

Furthermore, (A 2*a*) and (A 2*b*) imply that

$$-\Theta \overset{(A\,1b)}{=} \frac{1}{\rho}\frac{\mathrm{D}\rho}{\mathrm{D}t} \overset{(A\,3a)}{\approx} \frac{1}{\bar{\rho}}\frac{\mathrm{D}\rho}{\mathrm{D}t} - \frac{\rho'}{\bar{\rho}^2}\frac{\mathrm{D}\rho}{\mathrm{D}t} \overset{(A\,2b)}{\approx} \frac{1}{\bar{\rho}}\frac{\mathrm{D}\rho}{\mathrm{D}t} + O\left(\frac{\rho'^2}{\bar{\rho}^2}\frac{1}{\mathscr{T}_{(D_t\rho)'}}\right) \overset{(A\,2)}{\approx} \frac{1}{\bar{\rho}}\frac{\mathrm{D}\rho}{\mathrm{D}t} \tag{A 3b}$$

and

$$-\left(\rho\frac{\mathrm{D}\Theta}{\mathrm{D}t}\right)' \overset{(A\,1b)}{=} \left(\rho\frac{\mathrm{D}}{\mathrm{D}t}\left(\frac{1}{\rho}\frac{\mathrm{D}\rho}{\mathrm{D}t}\right)\right)' = \left(\frac{\mathrm{D}^2\rho}{\mathrm{D}t^2} - \frac{1}{\rho}\left(\frac{\mathrm{D}\rho}{\mathrm{D}t}\right)^2\right)'$$
$$\overset{(A\,2),\,(A\,3a)}{=} \left(\frac{\mathrm{D}^2\rho}{\mathrm{D}t^2}\right)' + O\left(\frac{\rho'^2}{\bar{\rho}}\frac{1}{\mathscr{T}^2_{(D_t\rho)'}}\right) \overset{(A\,2)}{\approx} \left(\frac{\mathrm{D}^2\rho}{\mathrm{D}t^2}\right)', \tag{A 3c}$$

where (A 2*b*) was used to establish the leading term of the error.

It was preferred to use density fluctuations and variations to establish order-of-magnitude relations, and to calculate correlations and orders of magnitude related to dilatation Θ via (A 1*b*), both because they are easier to understand physically than dilatation (indeed, the transport equation for the dilatation variance $D_t\overline{\Theta'^2}$ is actually obtained by multiplying (A 1*e*) by Θ') and because they are more reliable numerically (in terms of required grid resolution and associated numerical error), the more so as $\bar{M}_{CL}$ decreases.

https://doi.org/10.1017/jfm.2012.633 Published online by Cambridge University Press

A.3. *Low-Mach-number fully developed plane channel flow*

For the flow studied here (plane channel flow, $Re_{\tau_w}=180$, $\bar{M}_{CL}=0.34$), conditions (A 2) leading to the approximations (A 3) are satisfied. Making all quantities non-dimensional in wall units ($\bar{\rho}_w$, $\bar{\nu}_w$, $\bar{u}_\tau$), we obtain density variance $[\rho']^+_{rms}\lessapprox 2.5\times10^{-3}$ (figure 14d) and variance of the substantial derivative of density $[D_t\rho']^+_{rms}\lessapprox 3\times10^{-4}$ (figure 14d), with mean $\left[\left|\overline{D_t\rho}\right|\right]^+\lessapprox 4\times10^{-5}$ (figure 14c). Taking into account that $\bar{\rho}^+\approxeq 1$ with an accuracy of 1.5 % (figure 14a), condition (A 2*a*) is verified as $\rho'\sim(3/1000)\bar{\rho}$, and the separation in (A 2*b*) is of one order of magnitude. Therefore (A 3) are expected to hold. Verification of (A 3*a*) comes from comparing $[\rho']^+_{rms}$ and $[(\rho^{-1})']^+_{rms}$, which are almost equal to within excellent accuracy (the two curves are indistinguishable; figure 14d) – although not plotted here, the same applies to skewness (opposite) and flatness (equal) of ρ' and $(\rho^{-1})'$. Furthermore, because of the very small variation of $\bar{\rho}(y)$, we have $[\left|d_y\bar{\rho}\right|]^+\lessapprox 2\times10^{-3}=O([\rho']^+_{rms})$ (figure 14d) – the order-of-magnitude relation between $[d_y\bar{\rho}]^+$ and $[\rho']^+_{rms}$ can also be justified by considering the production term in the transport equation for density variance $\overline{\rho'^2}$ (Taulbee & VanOsdol 1991, (17), p. 4), which, for the flow under consideration, is $-\overline{\rho'v'}d_y\bar{\rho}$. The approximation (A 3*b*) is corroborated by the excellent superposition of the DNS data for $[\overline{D_t\rho}]^+$ and $[\overline{\rho^{-1}D_t\rho}]^+\overset{\text{(A 1}b\text{)}}{=}-\bar{\Theta}^+$ (figure 14c).

In the case of two dimensions in the mean fully developed (x-wise invariant in the mean) compressible channel flow with $\boldsymbol{f}_V=f_{V_x}(t)\boldsymbol{e}_x$ (Coleman, Kim & Moser 1995; Huang, Coleman & Bradshaw 1995; Gerolymos *et al.* 2010) and using (A 1*h*) and (A 1*i*), (A 1*e*) made non-dimensional in wall units reads

$$[\nabla^2p']^+=\underbrace{\left(1+\frac{[\rho']^+}{\bar{\rho}^+}\right)[\mathcal{Q}'_{(s)}+\mathcal{Q}'_{(r)}]^+ +2\left[\overline{\rho'\frac{\partial v'}{\partial x}}\frac{\mathrm{d}\bar{u}}{\mathrm{d}y}\right]^+}_{[\mathcal{Q}'_{(s)}+\mathcal{Q}'_{(\rho';s)}+\mathcal{Q}'_{(r)}+\mathcal{Q}'_{(\rho';r)}]^+}+\underbrace{0}_{[\mathcal{Q}'_{(\rho')}]^+=0}$$
$$+\underbrace{f^+_{V_x}\left[\frac{\partial\rho'}{\partial x}\right]^+}_{[\mathcal{Q}'_{(\mathrm{BF})}]^+}+[\mathcal{Q}'_{(\Theta)}]^+ +[\mathcal{Q}'_{(\dot{\nu}\nabla\rho)}]^+ +[\mathcal{Q}'_{(\tau)}]^+ \tag{A 4}$$

exactly. Statistics of the individual source terms in (A 4) were not available, but it is possible to make order-of-magnitude estimates, by relating them to available DNS data.

(i) $[\mathcal{Q}'_{(s)}+\mathcal{Q}'_{(r)}]^+$: Observation of instantaneous values indicates that $[\mathcal{Q}'_{(s)}+\mathcal{Q}'_{(r)}]^+\in[-1,1]$, implying that the terms that were retained in the incompressible analysis (1.1) are $[\mathcal{Q}'_{(s)}+\mathcal{Q}'_{(r)}]^+\sim O(1/10)$ for the present flow conditions (plane channel flow, $Re_{\tau_w}=180$, $\bar{M}_{CL}=0.34$).

(ii) $[\mathcal{Q}'_{(\rho';s)}]^+$, $[\mathcal{Q}'_{(\rho';r)}]^+$, $[\mathcal{Q}'_{(\rho')}]^+$: The term $\mathcal{Q}'_{(\rho')}$ (A 1*e*) is identically equal to 0 for this flow. Obviously, the term $2\overline{\rho'\partial_xv'}d_y\bar{u}=O(2c_{(\rho',\partial_xv')}\rho'_{rms}(\partial_xv')_{rms}d_y\bar{u})$ and, using the definition of $\mathcal{Q}'_{(r)}$ (A 1*e*), we have $2\overline{\rho'\partial_xv'}d_y\bar{u}=O(c_{(\rho',\partial_xv')}\bar{\rho}^{-1}\rho'_{rms}(\mathcal{Q}'_{(r)})_{rms})$. In the present flow $[\left|\overline{\rho'\partial_xv'}\right|d_y\bar{u}]^+\lessapprox 3\times10^{-6}$ is negligibly small (figure 14b) – the present DNS data indicate that the correlation coefficient $c_{(\rho',\partial_xv')}\approxeq 0.3\pm0.05$ in the range $y^+\in[1,100]$, falling to 0 at the wall and at the channel centreline.

(iii) $[\mathcal{Q}'_{(\mathrm{BF})}]^+$: Concerning the body force term $[\mathcal{Q}'_{(\mathrm{BF})}]^+$ (A 4), it obviously scales with $[\rho']^+_{rms}$. It also scales with $Re^{-1}_{\tau_w}$ (decreases with increasing Re_{τ_w}), because volume

https://doi.org/10.1017/jfm.2012.633 Published online by Cambridge University Press

Re_{τ_w}	$\bar{M}_{CL}$	$N_x \times N_y \times N_z$	L_x	L_y	L_z	Δx^+	Δy^+_w	$N_{y^+\leqslant 10}$	Δy^+_{CL}	Δz^+	Δt^+	$t^+_{obs_{GF}}$	$\Delta t^+_{s_{GF}}$
179	0.34	$193 \times 129 \times 169$	$4\pi\delta$	2δ	$4\pi\delta/3$	11.7	0.22	20	4.9	4.4	6.47×10^{-3}	1648	6.47×10^{-2}

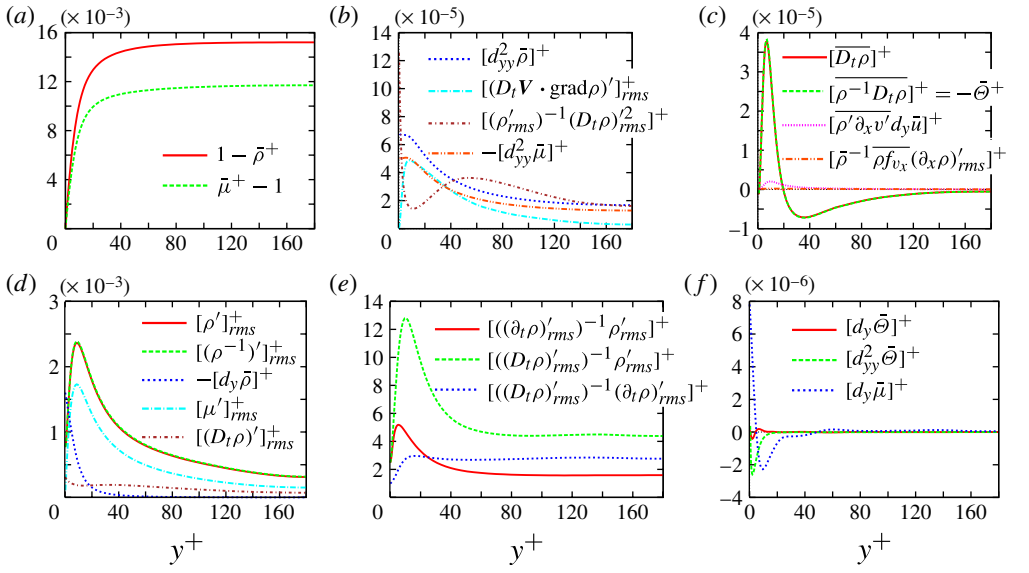


FIGURE 14. (Colour online) Present DNS-computed data ($Re_{\tau_w} = 180$; $\bar{M}_{CL} = 0.34$; $257 \times 129 \times 385$ grid; table 1) related to density variation and fluctuation: (*a*) $\bar{\rho}$, $\bar{\mu}$; (*b*) $d^2_{yy}\bar{\rho}$, $[(D_t \boldsymbol{V} \cdot \mathrm{grad}\,\rho)']_{rms}$, $((\partial_t\rho)'_{rms})^{-1}\,((D_t\rho)'_{rms})^2$, $-d^2_{yy}\bar{\mu}$; (*c*) $\overline{D_t\rho}$, $\overline{\rho^{-1}D_t\rho} = -\bar{\Theta}$, $\overline{\rho'\partial_x v'}\,d_y\bar{u}$, $\bar{\rho}^{-1}\overline{\rho f_{V_x}}\,(\partial_x\rho)'_{rms}$; (*d*) ρ'_{rms}, $(\rho^{-1})'_{rms}$, $-d_y\bar{\rho}$, μ'_{rms}, $(D_t\rho)'_{rms}$; (*e*) $((\partial_t\rho)'_{rms})^{-1}\,\rho'_{rms}$, $((D_t\rho)'_{rms})^{-1}\,\rho'_{rms}$, $((D_t\rho)'_{rms})^{-1}\,(\partial_t\rho)'_{rms}$; (*f*) $d_y\bar{\Theta}$, $d^2_{yy}\bar{\Theta}$, $d_y\bar{\mu}$, in wall units, relevant to the order-of-magnitude analysis of compressibility effects in (A 1*e*).

integration and subsequent averaging of the momentum equation (Gerolymos *et al.* 2010, (34b), p. 785) yields the exact relation $\overline{\rho_B f_{V_x}} = Re^{-1}_{\tau_w}$, where, because of the small variation and fluctuation of density, the bulk density (Gerolymos *et al.* 2010, (46a), p. 791) $\rho^+_B \approxeq \bar{\rho}^+ \approxeq 1$. Present DNS data indicate that $[\bar{\rho}^{-1}\overline{\rho f_{V_x}}\,(\partial_x\rho)'_{rms}]^+ \lessapprox 2 \times 10^{-7}$ (figure 14c).

(iv) $[Q'_{(\dot{\mathcal{V}}\nabla_\rho)}]^+$: It is easy to show that the acceleration density-gradient source term $[(D_t \boldsymbol{V} \cdot \mathrm{grad}\,\rho)']^+$ (A 1*e*) should scale with $[\rho']^+_{rms}$ (figure 14d) and $\left[\left|d_y\bar{\rho}\right|\right]^+$ (figure 14d), weighted by acceleration statistics. The DNS data indicate that $[(D_t \boldsymbol{V} \cdot \mathrm{grad}\,\rho)']^+_{rms} \lessapprox 5 \times 10^{-5}$ (figure 14b).

(v) $[Q'_{(\Theta)}]^+$: By (A 3*c*), we have $Q'_{(\Theta)} \overset{\text{(A 1}e\text{)}}{:=} -(\rho D_t\Theta)' \overset{\text{(A 1}b\text{)}}{=} \rho(D_t\,(\rho^{-1}D_t\rho)' \overset{\text{(A 3}c\text{)}}{\approxeq} (D^2_{tt}\rho)'$. Statistics for $\rho D_t(\rho^{-1}D_t\rho)$ or $D^2_{tt}\rho$ were not available. We can make a rough estimate of its order of magnitude. From the available statistics for $(D_t\rho)'_{rms}$ (figure 14d) and $(\partial_t\rho)'_{rms}$ (not plotted), we can define associated time scales, $\mathscr{T}_{(D_t\rho)'} := \rho'_{rms}\,[(D_t\rho)'_{rms}]^{-1}$ and $\mathscr{T}_{(\partial_t\rho)'} := \rho'_{rms}\,[(\partial_t\rho)'_{rms}]^{-1}$. These specific time scales (figure 14e), associated with the fluctuation of the Eulerian and Lagrangian time derivatives, are practically constant in the major part of the channel ($y^+ \gtrapprox 15$), and their ratio (figure 14e) is ~ 1 near the wall where convection is small, and grows to ~ 3 for $y^+ \gtrapprox 15$, which is also a typical value for the ratio of Lagrangian to Eulerian time scales (Dosio *et al.* 2005), although

https://doi.org/10.1017/jfm.2012.633 Published online by Cambridge University Press

these are not the time scales defined here. Then, by analogy, we assume that the same time scale $\mathscr{T}_{(D_t\rho)'}$ relates the fluctuation of the time derivative of $D_t\rho$ to $(D_t\rho)'_{rms}$, namely

$$\left[\rho\frac{\mathrm{D}}{\mathrm{D}t}\left(\rho^{-1}\frac{\mathrm{D}\rho}{\mathrm{D}t}\right)\right]'_{rms}\overset{(\mathrm{A}\,3c)}{\approxeq}\left(\frac{\mathrm{D}(D_t\rho)}{\mathrm{D}t}\right)'_{rms}\sim\frac{(D_t\rho)'_{rms}}{\mathscr{T}_{(D_t\rho)'}}=O\left(\frac{[(D_t\rho)']^2_{rms}}{\rho'_{rms}}\right),\quad(\mathrm{A}\,5)$$

which suggests that this term is not expected to be important in the present flow, where $[(\rho'_{rms})^{-1}[(D_t\rho)']^2_{rms}]^+\lessapprox 4\times10^{-5}$ (figure 14b). Note that the term associated with $\bar\rho$ in D^2_{tt} is of the same order of magnitude as the estimate (A 5), namely $[|d^2_{yy}\bar\rho|]^+\lessapprox 6\times10^{-5}$ (figure 14b).

(vi) $[Q'_{(\tau)}]^+$: The present calculations used a Newtonian constitutive relation (Gerolymos *et al.* 2010, (36a), p. 786), with $\mu_b=0$ and $\mu=\mu(T)$ (Gerolymos *et al.* 2010, (37), p. 786). The exact expression of $Q'_{(\tau)}$,

$$\begin{aligned}
Q'_{(\tau)}&\overset{(\mathrm{A}\,1e)}{:=}\frac{\partial^2\tau_{ij'}}{\partial x_i\partial x_j}\\
&=\left((\tfrac43\mu+\mu_b)\nabla^2\Theta+4\frac{\partial\mu}{\partial x_i}\frac{\partial S_{ij}}{\partial x_j}+2S_{ij}\frac{\partial^2\mu}{\partial x_i\partial x_j}+\Theta\nabla^2(\mu_b-\tfrac23\mu)+2\frac{\partial(\mu_b-\frac23\mu)}{\partial x_j}\frac{\partial\Theta}{\partial x_j}\right)'\\
&=\left((\tfrac43\mu'+\mu'_b)\nabla^2\bar\Theta+4\frac{\partial\mu'}{\partial x_i}\frac{\partial\bar S_{ij}}{\partial x_j}+2S'_{ij}\frac{\partial^2\bar\mu}{\partial x_i\partial x_j}+\Theta'\nabla^2(\bar\mu_b-\tfrac23\bar\mu)+2\frac{\partial(\mu'_b-\frac23\mu')}{\partial x_j}\frac{\partial\bar\Theta}{\partial x_j}\right)\\
&\quad+\left((\tfrac43\bar\mu+\bar\mu_b)\nabla^2\Theta'+4\frac{\partial\bar\mu}{\partial x_i}\frac{\partial S'_{ij}}{\partial x_j}+2\bar S_{ij}\frac{\partial^2\mu'}{\partial x_i\partial x_j}+\bar\Theta\nabla^2(\mu'_b-\tfrac23\mu')+2\frac{\partial(\bar\mu_b-\frac23\bar\mu)}{\partial x_j}\frac{\partial\Theta'}{\partial x_j}\right)\\
&\quad+\left((\tfrac43\mu'+\mu'_b)\nabla^2\Theta'+4\frac{\partial\mu'}{\partial x_i}\frac{\partial S'_{ij}}{\partial x_j}+2S'_{ij}\frac{\partial^2\mu'}{\partial x_i\partial x_j}+\Theta'\nabla^2(\mu'_b-\tfrac23\mu')+2\frac{\partial(\mu'_b-\frac23\mu')}{\partial x_j}\frac{\partial\Theta'}{\partial x_j}\right)\\
&\quad-\overline{\left((\tfrac43\mu'+\mu'_b)\nabla^2\Theta'+4\frac{\partial\mu'}{\partial x_i}\frac{\partial S'_{ij}}{\partial x_j}+2S'_{ij}\frac{\partial^2\mu'}{\partial x_i\partial x_j}+\Theta'\nabla^2(\mu'_b-\tfrac23\mu')+2\frac{\partial(\mu'_b-\frac23\mu')}{\partial x_j}\frac{\partial\Theta'}{\partial x_j}\right)}
\end{aligned}\quad(\mathrm{A}\,6)$$

involves terms depending on the variation and fluctuation of μ and Θ. For this reason, in strictly incompressible flow, $Q'_{(\tau)}=0$. In the present flow (plane channel flow, $Re_{\tau_w}=180$, $\bar M_{CL}=0.34$), mean viscosity varies in a way very similar to ρ, $\bar\mu^+\approxeq 1$ with an accuracy of 1.2 % (figure 14a), and the same similarity with density applies to spatial variations, $[|d_y\bar\mu|]^+\lessapprox 8\times10^{-6}$ (figure 14f) and $[|d^2_{yy}\bar\mu|]^+\lessapprox 5\times10^{-5}$ (figure 14b), and fluctuation, $[\mu']^+_{rms}\lessapprox 2\times10^{-3}$ (figure 14d). As already stated, mean dilatation $|\bar\Theta^+|\overset{(\mathrm{A}\,1b)}{=}\left[\left|\overline{\rho^{-1}D_t\rho}\right|\right]^+\lessapprox 4\times10^{-5}$, with gradients $\left[|d_y\bar\Theta|\right]^+\lessapprox 4\times10^{-7}$ (figure 14f) and $\left[|d^2_{yy}\bar\Theta|\right]^+\lessapprox 2\times10^{-6}$ (figure 14f), and fluctuation $[\Theta']^+_{rms}\overset{(\mathrm{A}\,3b)}{\approxeq}\left[D_t\rho'\right]^+_{rms}\lessapprox 3\times10^{-4}$ (figure 14d). Therefore, terms containing products of the small (in wall units) quantities $d_y\bar\mu$, $d^2_{yy}\bar\mu$, $\bar\Theta$, $d_y\bar\Theta$, $d^2_{yy}\bar\Theta$, μ' (and its space derivatives) and Θ' (and its space derivatives) can be considered negligible compared to other terms, and we have ($\mu_b=0$)

$$Q'_{(\tau)}=\frac43\bar\mu\nabla^2\Theta'+4\frac{\partial S'_{yj}}{\partial x_j}\frac{\mathrm{d}\bar\mu}{\mathrm{d}y}+2\frac{\partial v'}{\partial y}\frac{\mathrm{d}^2\bar\mu}{\mathrm{d}y^2}+2\frac{\partial\mu'}{\partial x}\frac{\mathrm{d}^2\bar u}{\mathrm{d}y^2}+2\frac{\mathrm{d}\bar u}{\mathrm{d}y}\frac{\partial^2\mu'}{\partial x\partial y}+o(Q'_{(\tau)}),\quad(\mathrm{A}\,7)$$

where $S_{ij}:=(\partial_{x_j}u_i+\partial_{x_i}u_j)/2$ is the rate-of-strain tensor.

https://doi.org/10.1017/jfm.2012.633 Published online by Cambridge University Press

Using the above estimates in (A 1*e*) and (A 4), we may write

$$[\nabla^2 p']^+ = [Q'_{(s)} + Q'_{(r)}]^+ + \overbrace{[Q'_{(\rho';s)} + Q'_{(\rho';r)}]^+}^{\frac{[\rho']^+}{\bar{\rho}^+}[Q'_{(s)}+Q'_{(r)}]^+ + O([\rho']^+_{rms}[Q'_{(r)}]^+_{rms})} + \overbrace{[Q'_{(\rho')}]^+}^{=0} + \underbrace{[Q'_{(\mathrm{BF})}]^+}_{O\left(\frac{[\rho']^+_{rms}}{Re_{\tau_w}}\right)} + \underbrace{[Q'_{(\Theta)}]^+}_{O\left(\frac{[(D_t\rho)']^+_{rms}{}^2}{[\rho']^+_{rms}}\right)} + \underbrace{[Q'_{(\dot{V}\nabla\rho)}]^+}_{O([\rho']^+_{rms},[d_y\bar{\rho}]^+)} + \underbrace{[Q'_{(\tau)}]^+}_{O([(D_t\rho)']^+_{rms},[\mu']^+_{rms},[d_y\bar{\mu}]^+,[d^2_{yy}\bar{\mu}]^+)} . \tag{A 8}$$

By (A 8) it is clear that all extra compressible terms in (A 1*e*), compared to (1.1), scale with $[\rho']^+_{rms}$ or $[(D_t\rho)']^+_{rms}$ and $[d_y\bar{\rho}]^+$ (μ gradients and fluctuations, in wall units, being of the same order of magnitude as corresponding gradients and fluctuations of ρ; figure 14). The order-of-magnitude analysis of different terms indicates that they can be reasonably neglected for the flow studied in the present work (plane channel flow, $Re_{\tau_w} = 180$, $\bar{M}_{CL} = 0.34$). As a consequence, the main influence of compressibility appears in the retained quasi-incompressible terms $Q'_{(s)} + Q'_{(r)}$ (A 1*e*) and (1.1), through the variation of $\bar{\rho}(y)$, indicating the validity of Morkovin's hypothesis (So *et al.* 1998), which states that, for low-Mach-number flow, the effects of compressibility on turbulence are due to the mean density gradient, the influence of ρ' being a higher-order effect.

Appendix B. Green's functions

We analyse the mathematical tools for the solution of the modified Helmholtz equation (2.6), which provides the terms of the p' splitting (2.2) and (2.11) for each xz Fourier component of p' (2.5*a*). The Green's functions approach for the solution of (2.6) is briefly summarized in § B.1. In § B.2 we study the case of spatially xz varying Fourier components ($\kappa := \sqrt{\kappa_x^2 + \kappa_z^2} \neq 0$), for which the Green's function has the general form (B 9), parametrized by two functions, $A_1(Y;\kappa)$ and $A_2(Y;\kappa)$, which are determined by the boundary conditions. The homogeneous Neumann boundary conditions (2.6*b*) yield (§ B.2.1) the well-known solution of Kim (1989), $G_{Kim}(y, Y; \kappa \neq 0)$ (B 10*c*), providing the solution (2.7) for the rapid $p'_{(r)}$ and slow $p'_{(s)}$ parts (2.2). The solution (Chang *et al.* 1999; Moser *et al.* 1999) for the Stokes part $p'_{(\tau)}$ (2.2), with $Q'_{(\tau)} = 0$ in strictly incompressible flow equations (2.3*a*) and (2.6*a*), which is driven by the inhomogeneous Neumann boundary conditions (2.3*b*), (2.4) and (2.6*b*), given by $q_{BC}(y; \kappa \neq 0, B_\pm)$ (B 12), is calculated in § B.2.2. The free-space Green's function $G_{\mathfrak{V}}(y, Y; \kappa \neq 0)$ (B 14), which provides the solution (2.13) for the rapid $p'_{(r;\mathfrak{V})}$ and slow $p'_{(s;\mathfrak{V})}$ volume parts of the p' splitting (2.11), is calculated in § B.2.3. Finally, for use in the analysis (§ 2.2.4) of the method-of-images approach (Manceau *et al.* 2001), we calculate in § B.2.4 the Green's functions $G_\pm(y, Y; \kappa \neq 0)$ (B 18) and in § B.2.5 the boundary-condition functions $q_{BC_\pm}(y; \kappa \neq 0, B_\pm)$ (B 22) for the half-space problems with only one (upper or lower) of the walls present. In § B.3 we discuss the singular case $\kappa := \sqrt{\kappa_x^2 + \kappa_z^2} = 0 \implies \kappa = \kappa_x = \kappa_z = 0$, for which the modified Helmholtz equation (2.6) can be solved if and only if the compatibility conditions (B 24) hold. We revisit in §§ B.3.1–B.3.5 the same problems as for the $\kappa \neq 0$ case, and calculate the corresponding Green's functions $G_{Kim}(y, Y; \kappa = 0)$

https://doi.org/10.1017/jfm.2012.633 Published online by Cambridge University Press

and $G_{\mathfrak{V}}(y, Y; \kappa = 0) = G_{\pm}(y, Y; \kappa = 0)$ ((B 27), (B 34) and (B 36)) and boundary-condition functions $q_{BC}(y; \kappa = 0, B_-, B_+)$ (B 33) and $q_{BC_\pm}(y; \kappa = 0, B_\pm)$ (B 38), for the $\kappa = 0$ case. Finally, in § B.4 we calculate the Green's function $G_{MWL}(y, Y; \kappa)$ (B 42*a*), which corresponds to the method-of-images evaluation (2.17) of the rapid $p'_{(r;MWL)}$ and slow $p'_{(s;MWL)}$ parts, and evaluate the error of the method-of-images approximation as a function of the wavenumber (B 46). The application of these mathematical results to the calculation of the p' splitting is described in the main paper (§ 2.2).

B.1. *Green's function solution of the modified Helmholtz equation*

As discussed in § 2.2, we have to solve the generic modified Helmholtz equation (Cheng, Huang & Leiterman 2006)

$$\frac{\mathrm{d}^2 q(y;\kappa)}{\mathrm{d}y^2} - \kappa^2 q(y;\kappa) = Q(y;\kappa), \quad y \in (L_-, L_+), \tag{B 1}$$

with associated boundary conditions at $y \in \{L_-, L_+\}$, for the complex-valued function $q : \mathbb{R} \longrightarrow \mathbb{C}$, $Q(y)$ being a given complex-valued function $Q : \mathbb{R} \longrightarrow \mathbb{C}$, and $\kappa \in \mathbb{R}_{\geqslant 0}$. Note that there is no loss of generality in assuming $\kappa \in \mathbb{R}_{\geqslant 0}$ because (B 1) depends on κ^2 and is therefore independent of the sign of κ. The general method of solution (Bender & Orszag 1978) of the linear ODE (B 1) is based on the determination of the appropriate Green's function $G(y, Y; \kappa)$, the solution of

$$\frac{\partial^2 G(y, Y; \kappa)}{\partial y^2} - \kappa^2 G(y, Y; \kappa) = \delta(y - Y), \quad \forall\ y, Y \in [L_-, L_+], \tag{B 2a}$$

$$\lim_{\epsilon \to 0^+} \left[\frac{\partial G}{\partial y}(y = Y + \epsilon, Y; \kappa) - \frac{\partial G}{\partial y}(y = Y - \epsilon, Y; \kappa) \right] = 1, \quad \forall\ Y \in [L_-, L_+], \tag{B 2b}$$

$$G(y, Y; \kappa) \in C^0(L_-, L_+), \tag{B 2c}$$

$$G(y, Y; \kappa) \in C^1(L_-, L_+) \setminus \{Y\}, \tag{B 2d}$$

so that

$$q(y;\kappa) := \int_{L_-}^{L_+} G(y, Y; \kappa) Q(Y; \kappa)\, \mathrm{d}Y \tag{B 3}$$

satisfies (B 1) because of (B 2), as can be verified by substituting (B 3) into (B 1). The Green's function satisfies the symmetry (reciprocity) condition

$$G(y, Y; \kappa) = G(Y, y; \kappa), \quad \forall\ y, Y \in (L_-, L_+),\ \forall\ \kappa \in \mathbb{R}_{\geqslant 0}, \tag{B 4}$$

because the modified Helmholtz operator $[d^2_{yy}(\cdot) - \kappa^2(\cdot)]$ is a self-adjoint linear differential operator (Ince 1926; Courant & Hilbert 1953). As shown in Bender & Orszag (1978), the general solution of (B 2) is

$$G(y, Y; \kappa) = \begin{cases} A_1(Y;\kappa) q_1(y;\kappa) + A_2(Y;\kappa) q_2(y;\kappa), & y \leqslant Y, \\ \left(A_1(Y;\kappa) - \dfrac{q_2(Y;\kappa)}{[W(q_1, q_2)](Y;\kappa)} \right) q_1(y;\kappa) \\ \quad + \left(A_2(Y;\kappa) + \dfrac{q_1(Y;\kappa)}{[W(q_1, q_2)](Y;\kappa)} \right) q_2(y;\kappa) & y \geqslant Y, \end{cases} \tag{B 5}$$

https://doi.org/10.1017/jfm.2012.633 Published online by Cambridge University Press

where $q_1(y;\kappa)$ and $q_2(y;\kappa)$ are two linearly independent solutions of the corresponding homogeneous equation $q''(y;\kappa)-\kappa^2 q(y;\kappa)=0$,

$$[W(q_1,q_2)](y;\kappa):=\det\begin{bmatrix} q_1(y;\kappa) & q_2(y;\kappa) \\ q_1'(y;\kappa) & q_2'(y;\kappa)\end{bmatrix}\neq 0 \tag{B 6}$$

is the Wronskian (the prime in (B 6) denotes differentiation with respect to y, κ being a parameter), which is $\neq 0$ if and only if the two solutions are linearly independent. The functions $A_1(Y;\kappa)$ and $A_2(Y;\kappa)$ are determined by the boundary conditions. It is straightforward to verify that $G(y,Y;\kappa)$ (B 5) is continuous at $y=Y$. Note that by straightforward differentiation of (B 3), we obtain

$$q'(y;\kappa)=\int_{L_-}^{L_+}\frac{\partial G}{\partial y}(y,Y;\kappa)Q(Y;\kappa)\,\mathrm{d}Y. \tag{B 7}$$

The cases $\kappa\neq 0$ and $\kappa=0$ are fundamentally different, not only because the two linearly independent solutions of the homogeneous equation $q''(y;\kappa)-\kappa^2 q(y;\kappa)=0$ differ, but principally because $\kappa=0$ is a characteristic number (eigenvalue) of (B 1), namely, $q''(y;\kappa)-\kappa^2 q(y;\kappa)\overset{\kappa=0}{=}q''(y;\kappa=0)=0$ with homogeneous Neumann boundary conditions admits the constant function as an eigensolution (Ince 1926; Courant & Hilbert 1953).

B.2. *Case $\kappa\neq 0$ (xz varying components)*

When $\kappa\neq 0$ the two linearly independent solutions of the homogeneous equation $q''(y;\kappa\neq 0)-\kappa^2 q(y;\kappa\neq 0)=0$ are

$$q_1(y;\kappa\neq 0)=\mathrm{e}^{+\kappa y}, \tag{B 8a}$$

$$q_2(y;\kappa\neq 0)=\mathrm{e}^{-\kappa y}, \tag{B 8b}$$

with Wronskian

$$[W(q_1,q_2)](y;\kappa\neq 0)=\det\begin{bmatrix} \mathrm{e}^{+\kappa y} & \mathrm{e}^{-\kappa y} \\ +\kappa\mathrm{e}^{+\kappa y} & -\kappa\mathrm{e}^{-\kappa y}\end{bmatrix}=-2\kappa\neq 0, \tag{B 8c}$$

so that solution (B 5) reads

$$G(y,Y;\kappa\neq 0)=\begin{cases} A_1(Y;\kappa)\mathrm{e}^{+\kappa y}+A_2(Y;\kappa)\mathrm{e}^{-\kappa y}, & y\leqslant Y, \\ A_1(Y;\kappa)\mathrm{e}^{+\kappa y}+A_2(Y;\kappa)\mathrm{e}^{-\kappa y}+\dfrac{1}{\kappa}\sinh[\kappa(y-Y)], & y\geqslant Y.\end{cases} \tag{B 9}$$

The functions $A_1(Y;\kappa)$ and $A_2(Y;\kappa)$ are determined so as to satisfy the boundary conditions.

B.2.1. $G_{Kim}(y,Y;\kappa\neq 0)$

Kim (1989) solves for the homogeneous Neumann boundary conditions (2.6*b*),

$$\frac{\partial G_{Kim}}{\partial y}\left(y=\pm\frac{L_y}{2},Y;\kappa\right)=0 \overset{\text{(B 3)}}{\Longleftrightarrow} \frac{\partial q_{Kim}}{\partial y}\left(y=\pm\frac{L_y}{2};\kappa\right)=0. \tag{B 10a}$$

Straightforward calculations yield the functions $A_1(Y;\kappa)$ and $A_2(Y;\kappa)$ in (B 9), which satisfy (B 10*a*), giving

$$G_{Kim}(y,Y;\kappa\neq 0)=-\frac{\cosh[\kappa(L_y-|y-Y|)]+\cosh[\kappa(y+Y)]}{2\kappa\sinh\kappa L_y}. \tag{B 10b}$$

https://doi.org/10.1017/jfm.2012.633 Published online by Cambridge University Press

This 'if-less' expression, which highlights the symmetry (reciprocity) condition (B 4), is equivalent to the form in Kim (1989, (8), p. 440), written here using dimensional variables,

$$G_{Kim}(y,Y;\kappa\neq0)=\begin{cases}-\dfrac{\cosh[\kappa(\frac{1}{2}L_y-Y)]\cosh[\kappa(\frac{1}{2}L_y+y)]}{\kappa\sinh\kappa L_y}, & y\leqslant Y,\\ -\dfrac{\cosh[\kappa(\frac{1}{2}L_y-y)]\cosh[\kappa(\frac{1}{2}L_y+Y)]}{\kappa\sinh\kappa L_y}, & y\geqslant Y,\end{cases}\tag{B 10c}$$

because using well-known identities (Harris & Stocker (1998, p. 249) $\cosh(a+b)=\cosh a\cosh b+\sinh a\sinh b$ and $\cosh(a-b)=\cosh a\cosh b-\sinh a\sinh b$)

$$\begin{aligned}2\cosh[\kappa(\tfrac{1}{2}L_y-Y)]\cosh[\kappa(\tfrac{1}{2}L_y+y)]&=\cosh[\kappa(L_y-Y+y)]+\cosh[\kappa(-Y-y)]\\&=\cosh[\kappa(L_y-|y-Y|)]+\cosh[\kappa(y+Y)],\\&\qquad\forall\ y\leqslant Y,\end{aligned}\tag{B 10d}$$

$$\begin{aligned}2\cosh[\kappa(\tfrac{1}{2}L_y-y)]\cosh[\kappa(\tfrac{1}{2}L_y+Y)]&=\cosh[\kappa(L_y-y+Y)]+\cosh[\kappa(-y-Y)]\\&=\cosh[\kappa(L_y-|y-Y|)]+\cosh[\kappa(y+Y)],\\&\qquad\forall\ y\geqslant Y.\end{aligned}\tag{B 10e}$$

B.2.2. *Accommodating the boundary conditions ($\kappa\neq0$)*

To take into account normal gradients $d_yq(y=\pm L_y/2;\kappa\neq0)=B_\pm(\kappa\neq0)\neq0$ at the channel walls, corresponding to the Stokes pressure (2.3) and (2.6), Chang *et al.* (1999) superpose a boundary condition q_{BC} term onto the solution of Kim (1989),

$$q(y;\kappa\neq0,B_\pm)=\int_{-L_y/2}^{+L_y/2}G_{Kim}(y,Y;\kappa\neq0)Q(Y;\kappa\neq0)\,\mathrm{d}Y+q_{BC}(y;\kappa\neq0,B_\pm),\tag{B 11a}$$

$$\frac{\mathrm{d}^2q(y;\kappa\neq0,B_\pm)}{\mathrm{d}y^2}-\kappa^2q(y;\kappa\neq0,B_\pm)=Q(y;\kappa\neq0),\quad y\in(-\tfrac{1}{2}L_y,+\tfrac{1}{2}L_y),\tag{B 11b}$$

$$\frac{\mathrm{d}^2q_{BC}(y;\kappa\neq0,B_\pm)}{\mathrm{d}y^2}-\kappa^2q_{BC}(y;\kappa\neq0,B_\pm)=0,\quad y\in(-\tfrac{1}{2}L_y,+\tfrac{1}{2}L_y),\tag{B 11c}$$

$$\frac{\mathrm{d}q}{\mathrm{d}y}(y=\pm L_y/2;\kappa\neq0,B_\pm)\overset{(B\,10a)}{=}\frac{\mathrm{d}q_{BC}}{\mathrm{d}y}(y=\pm L_y/2;\kappa\neq0,B_\pm)=B_\pm(\kappa\neq0).\tag{B 11d}$$

By (B 3) and (B 10), the superposition (B 11*a*) is the solution to (B 11*b*), with boundary conditions (B 11*d*). The solution of (B 11*c*) with boundary conditions (B 11*d*) is readily obtained by direct integration (Chang *et al.* 1999; Foysi *et al.* 2004), and reads

$$q_{BC}(y;\kappa\neq0,B_\pm)=\frac{B_+\cosh[\kappa(\frac{1}{2}L_y+y)]-B_-\cosh[\kappa(\frac{1}{2}L_y-y)]}{\kappa\sinh\kappa L_y}.\tag{B 12}$$

B.2.3. *Free-space Green's function $G_{\mathfrak{V}}(y,Y;\kappa\neq0)$*

The free-space Green's function is directly obtained from the general solution (B 9) by requiring that the solution should tend to 0 as $y\to\pm\infty$, for any finite distribution of sources $Q(y;\kappa\neq0)$ with compact support, which is equivalent to

$$\lim_{y\to\pm\infty}q_{\mathfrak{V}}(y;\kappa\neq0)=0\overset{(B\,3)}{\iff}\lim_{y\to\pm\infty}G_{\mathfrak{V}}(y,Y;\kappa\neq0)=0,\quad\forall\ Y\in\mathbb{R}\setminus\{y\}.\tag{B 13}$$

https://doi.org/10.1017/jfm.2012.633 Published online by Cambridge University Press

Using (B 13) to determine the functions $A_1(Y;\kappa)$ and $A_2(Y;\kappa)$ in (B 9) readily gives

$$G_{\mathfrak{V}}(y,Y;\kappa\neq 0)=-\frac{\mathrm{e}^{-\kappa|y-Y|}}{2\kappa}. \tag{B 14}$$

B.2.4. *Upper/lower wall Green's functions* $G_{\pm}(y,Y;\kappa\neq 0)$

These Green's functions correspond to the problems where the domain of interest is $(-\infty,L_y/2)$ (isolated upper-wall influence; G_+) or $(-L_y/2,+\infty)$ (isolated lower-wall influence; G_-), i.e. they are half-space problems ($\pm y\in(-\infty,L_y/2)$). For each of these problems, only one of the walls is present. The associated boundary conditions are zero gradient at the wall of the problem ($y=\pm L_y/2$), and bounded influence at infinity of the problem ($y\to\mp\infty$), i.e. in terms of Green's functions

$$G_+(y,Y;\kappa\neq 0)\text{ satisfies (B 2)}\implies\text{(B 3) and (B 7)}, \tag{B 15a}$$

$$\frac{\partial G_+}{\partial y}(y=+\tfrac{1}{2}L_y,Y;\kappa\neq 0)=0, \tag{B 15b}$$

$$\lim_{y\to-\infty}G_+(y,Y;\kappa\neq 0)=0,\quad\forall\ Y\in\mathbb{R}\setminus\{y\}, \tag{B 15c}$$

to study the virtual influence of the upper wall, and

$$G_-(y,Y;\kappa\neq 0)\text{ satisfies (B 2)}\implies\text{(B 3) and (B 7)}, \tag{B 16a}$$

$$\frac{\partial G_-}{\partial y}(y=-\tfrac{1}{2}L_y,Y;\kappa\neq 0)=0, \tag{B 16b}$$

$$\lim_{y\to+\infty}G_-(y,Y;\kappa\neq 0)=0,\quad\forall\ Y\in\mathbb{R}\setminus\{y\}, \tag{B 16c}$$

to study the virtual influence of the lower wall. By (B 3), boundary conditions (B 15*b*) and (B 16*b*) imply zero gradient at the wall of the problem (upper for G_+ and lower for G_-). Boundary conditions (B 15*c*) and (B 16*c*) ensure boundedness at infinity for the half-space corresponding to each problem. Straightforward computation of the functions $A_1(Y;\kappa)$ and $A_2(Y;\kappa)$ in (B 9) yields

$$G_-(y,Y;\kappa\neq 0)=-\frac{\mathrm{e}^{-\kappa|y-Y|}}{2\kappa}-\frac{\mathrm{e}^{-\kappa(L_y+y+Y)}}{2\kappa},\quad y,Y\in[-\tfrac{1}{2}L_y,+\infty), \tag{B 17a}$$

$$G_+(y,Y;\kappa\neq 0)=-\frac{\mathrm{e}^{-\kappa|y-Y|}}{2\kappa}-\frac{\mathrm{e}^{-\kappa(L_y-y-Y)}}{2\kappa},\quad y,Y\in(-\infty,+\tfrac{1}{2}L_y], \tag{B 17b}$$

which by (B 14) read

$$G_-(y,Y;\kappa\neq 0)=G_{\mathfrak{V}}(y,Y;\kappa\neq 0)-\frac{\mathrm{e}^{-\kappa(L_y+y+Y)}}{2\kappa},\quad y,Y\in[-\tfrac{1}{2}L_y,+\infty), \tag{B 18a}$$

$$G_+(y,Y;\kappa\neq 0)=G_{\mathfrak{V}}(y,Y;\kappa\neq 0)-\frac{\mathrm{e}^{-\kappa(L_y-y-Y)}}{2\kappa},\quad y,Y\in(-\infty,+\tfrac{1}{2}L_y], \tag{B 18b}$$

i.e. the presence of a single wall in any of the two half-space problems induces an additive correction to the free-space Green's function, the wall echo $G_{w_\pm}(y,Y;\kappa\neq 0)$,

$$G_{w_\pm}(y,Y;\kappa\neq 0):=G_{\pm}(y,Y;\kappa\neq 0)-G_{\mathfrak{V}}(y,Y;\kappa\neq 0). \tag{B 19}$$

B.2.5. *Accommodating the boundary conditions for the half-space problems* ($\kappa\neq 0$)

To take into account normal gradients $d_y q(y=\pm L_y/2;\kappa\neq 0)=B_\pm(\kappa\neq 0)\neq 0$ at the wall for each of the half-space problems of § B.2.4, we may proceed exactly as in § B.2.2, by superposing a boundary condition $q_{BC_\pm}$ term onto the corresponding

https://doi.org/10.1017/jfm.2012.633 Published online by Cambridge University Press

solution (B 16) with zero gradient condition, namely,

$$q(y;\kappa\neq 0,B_-)=\int_{-L_y/2}^{+L_y/2}G_-(y,Y;\kappa\neq 0)Q(Y;\kappa\neq 0)\,\mathrm{d}Y+q_{BC_-}(y;\kappa\neq 0,B_-),\quad\text{(B 20}a\text{)}$$

$$\frac{\mathrm{d}^2q(y;\kappa\neq 0,B_-)}{\mathrm{d}y^2}-\kappa^2q(y;\kappa\neq 0,B_-)=Q(y;\kappa\neq 0),\quad y\in(-\tfrac{1}{2}L_y,+\infty),\quad\text{(B 20}b\text{)}$$

$$\frac{\mathrm{d}^2q_{BC_-}(y;\kappa\neq 0,B_-)}{\mathrm{d}y^2}-\kappa^2q_{BC_-}(y;\kappa,B_-)=0,\quad y\in(-\tfrac{1}{2}L_y,+\infty),\quad\text{(B 20}c\text{)}$$

$$\frac{\mathrm{d}q}{\mathrm{d}y}(y=-\tfrac{1}{2}L_y;\kappa\neq 0,B_-)\overset{\text{(B 16}b\text{)}}{=}\frac{\mathrm{d}q_{BC_-}}{\mathrm{d}y}(y=-\tfrac{1}{2}L_y;\kappa\neq 0,B_-)=B_-(\kappa\neq 0),\quad\text{(B 20}d\text{)}$$

$$\lim_{y\to+\infty}q_{BC_-}(y;\kappa\neq 0,B_-)=0,\quad\text{(B 20}e\text{)}$$

to study the virtual influence of the lower wall boundary condition on the solution, and

$$q(y;\kappa\neq 0,B_+)=\int_{-L_y/2}^{+L_y/2}G_+(y,Y;\kappa\neq 0)Q(Y;\kappa\neq 0)\,\mathrm{d}Y+q_{BC_+}(y;\kappa\neq 0,B_+),\quad\text{(B 21}a\text{)}$$

$$\frac{\mathrm{d}^2q(y;\kappa\neq 0,B_+)}{\mathrm{d}y^2}-\kappa^2q(y;\kappa\neq 0,B_+)=Q(y;\kappa\neq 0),\quad y\in(-\infty,+\tfrac{1}{2}L_y),\quad\text{(B 21}b\text{)}$$

$$\frac{\mathrm{d}^2q_{BC_+}(y;\kappa\neq 0,B_+)}{\mathrm{d}y^2}-\kappa^2q_{BC_+}(y;\kappa\neq 0,B_+)=0,\quad y\in(-\infty,+\tfrac{1}{2}L_y),\quad\text{(B 21}c\text{)}$$

$$\frac{\mathrm{d}q}{\mathrm{d}y}(y=+\tfrac{1}{2}L_y;\kappa\neq 0,B_+)\overset{\text{(B 15}b\text{)}}{=}\frac{\mathrm{d}q_{BC_+}}{\mathrm{d}y}(y=+\tfrac{1}{2}L_y;\kappa\neq 0,B_+)=B_+(\kappa\neq 0),\quad\text{(B 21}d\text{)}$$

$$\lim_{y\to-\infty}q_{BC_+}(y;\kappa\neq 0,B_+)=0,\quad\text{(B 21}e\text{)}$$

to study the virtual influence of the upper wall boundary condition on the solution. By (B 16), the superposition (B 20*a*) is the solution to (B 20*b*), with boundary conditions (B 20*d*) and (B 20*e*). By (B 15), the superposition (B 21*a*) is the solution to (B 21*b*), with boundary conditions (B 21*d*) and (B 21*e*). Straightforward computation yields

$$q_{BC_\pm}(y;\kappa\neq 0,B_\pm)=\pm\frac{B_\pm}{\kappa}\mathrm{e}^{-\kappa((L_y/2)\mp y)}.\quad\text{(B 22)}$$

B.3. *Case* $\kappa=0$ *(xz constant component)*

When $\kappa=0$, (B 1) becomes a Poisson equation (Katz & Plotkin 1991),

$$\frac{\mathrm{d}^2q(y;\kappa=0)}{\mathrm{d}y^2}=Q(y;\kappa=0),\quad y\in(-\tfrac{1}{2}L_y,\tfrac{1}{2}L_y).\quad\text{(B 23)}$$

The limits as $\kappa\to 0$ of the solutions obtained in § B.2 for $\kappa\neq 0$ are all singular, as can be easily verified by straightforward computation, in contrast to the case of the same problem with Dirichlet boundary conditions (Zauderer 2006). This is related to the existence of solutions of (B 23) with Neumann boundary conditions at $y=\pm L_y/2$, because integrating (B 23) yields

$$\frac{\mathrm{d}q}{\mathrm{d}y}(y=+\tfrac{1}{2}L_y;\kappa=0)-\frac{\mathrm{d}q}{\mathrm{d}y}(y=-\tfrac{1}{2}L_y;\kappa=0)=\int_{-L_y/2}^{+L_y/2}Q(Y;\kappa=0)\,\mathrm{d}Y,\quad\text{(B 24)}$$

https://doi.org/10.1017/jfm.2012.633 Published online by Cambridge University Press

implying that (B 23) with gradient boundary conditions $q'(y = \pm L_y/2; \kappa = 0) = B_\pm(\kappa = 0)$ can only be solved if and only if the compatibility condition (B 24) is satisfied by the integral of the source term and the boundary conditions.

In the particular case of homogeneous Neumann boundary conditions $B_\pm(\kappa = 0) = 0$, which is the most important since $B_\pm(\kappa = 0) \neq 0$ is only concerned with the Stokes pressure ((2.3) and (2.6)), the homogeneous equivalent of (B 23), $q''(y; \kappa = 0) = 0$, admits any constant function as solution, i.e. any constant function is an eigenfunction (Ince 1926; Courant & Hilbert 1953; Myint-U & Debnath 2007) of the homogeneous equivalent of (B 23), $q''(y; \kappa = 0) = 0$, with boundary conditions $q'(y = \pm L_y/2; \kappa = 0) = 0$, and $\kappa = 0$ is a characteristic number of the homogeneous equivalent of (B 1), $q''(y; \kappa) - \kappa^2 q(y; \kappa) = 0$ with boundary conditions $q'(y = \pm L_y/2; \kappa) = 0$. Therefore, a solution only exists provided the corresponding compatibility relation (Ince 1926; Courant & Hilbert 1953) holds, i.e. the integral in (B 24) is equal to zero. This is analogous to the three-dimensional compatibility relation for the Poisson equation with Neumann boundary conditions (Ockendon *et al.* 2003; Zauderer 2006).

B.3.1. $G_{Kim}(y, Y; \kappa = 0)$

In this case ((2.3*b*) and (2.6*b*)) zero gradient boundary conditions apply on both walls ($y = \pm L_y/2$). Assuming that the compatibility relation

$$\int_{-L_y/2}^{+L_y/2} Q(Y; \kappa = 0)\, \mathrm{d}Y = 0 \tag{B 25}$$

holds, there are two different ways for constructing a modified Green's function (Courant & Hilbert 1953; Zauderer 2006) for solving (B 23) with homogeneous Neumann boundary conditions. The first method described in Courant & Hilbert (1953) makes explicit use of the eigensolution of (B 23) in a modified definition of the problem (B 2) for calculating the modified Green's function which satisfies the boundary conditions, but has also to modify (B 3). The second method (Zauderer 2006), which leads to the Green's function used by Kim (1989), uses the standard definition of the Green's function (B 2) along with the standard integral solution (B 3). In this latter case, however, the boundary conditions are not explicitly included in the solution but are enforced by the compatibility relation (B 25).

Hence, assuming that the compatibility relation (B 25) holds, so that (B 10*a*) for $\kappa = 0$ may be satisfied, the Green's function corresponding to (B 23) satisfies

$$\frac{\partial^2 G_{Kim}(y, Y; \kappa = 0)}{\partial y^2} = \delta(y - Y), \tag{B 26a}$$

$$\lim_{\epsilon \to 0^+} \left[\frac{\partial G_{Kim}}{\partial y}(Y + \epsilon, Y; \kappa = 0) - \frac{\partial G_{Kim}}{\partial y}(Y - \epsilon, Y; \kappa = 0) \right] = 1, \tag{B 26b}$$

$$G_{Kim}(y, Y; \kappa = 0) \in C^0(-\tfrac{1}{2}L_y, +\tfrac{1}{2}L_y), \tag{B 26c}$$

$$G_{Kim}(y, Y; \kappa) \in C^1(-\tfrac{1}{2}L_y, +\tfrac{1}{2}L_y) \setminus \{Y\}. \tag{B 26d}$$

It is therefore made up by two straight lines joined together at Y, since, by (B 26*a*), we have $\partial^2_{yy} G(y, Y; \kappa = 0) = 0$ for all $y \neq Y$. If we further admit that $G_{Kim}(y, Y; \kappa = 0) = G_{Kim}(Y, y; \kappa = 0)$ (B 4), as expected because of the self-adjointedness of the operator $[d^2_{yy}(\cdot)]$ (Ince 1926; Courant & Hilbert 1953), we must have (Katz & Plotkin 1991) $G_{Kim}(y, Y; \kappa = 0) = G_{Kim}(|y - Y|; \kappa = 0)$, so that

$$G_{Kim}(y, Y; \kappa = 0) = \frac{|y - Y|}{2} + c. \tag{B 27}$$

https://doi.org/10.1017/jfm.2012.633 Published online by Cambridge University Press

The factor $1/2$ is required to satisfy (B 26*b*), and $c \in \mathbb{R}$ is a constant. The value of c has no influence whatsoever on the solution (B 3) because of the compatibility condition (B 25),

$$\begin{aligned}\int_{-L_y/2}^{+L_y/2} \left(\frac{|y-Y|}{2}+c\right) Q(Y;\kappa=0)\,\mathrm{d}Y &= \int_{-L_y/2}^{+L_y/2} \frac{|y-Y|}{2} Q(Y;\kappa=0)\,\mathrm{d}Y + c\int_{-L_y/2}^{+L_y/2} Q(Y;\kappa=0)\,\mathrm{d}Y \\ &\overset{(\mathrm{B}\,25)}{=} \int_{-L_y/2}^{+L_y/2} \frac{|y-Y|}{2} Q(Y;\kappa=0)\,\mathrm{d}Y. \end{aligned} \tag{B 28}$$

The simplest choice $c=0$ corresponding to the reasonable situation $G_{Kim}(y,y;\kappa=0)=0$ is made,

$$G_{Kim}(y,Y;\kappa=0)=\frac{|y-Y|}{2}, \tag{B 29}$$

and we have

$$\begin{aligned}\frac{\mathrm{d}q_{Kim}}{\mathrm{d}y}(y=\pm\tfrac{1}{2}L_y;\kappa=0) &\overset{(\mathrm{B}\,3)}{=} \int_{-L_y/2}^{+L_y/2} \frac{\partial G_{Kim}}{\partial y}(y,Y;\kappa=0) Q(Y;\kappa=0)\,\mathrm{d}Y \\ &\overset{(\mathrm{B}\,29)}{=} \pm\frac{1}{2}\int_{-L_y/2}^{+L_y/2} Q(Y;\kappa=0)\,\mathrm{d}Y \overset{(\mathrm{B}\,25)}{=} 0. \end{aligned} \tag{B 30}$$

Note that in this case it is the compatibility relation (B 25), and not the Green's function alone, that is responsible for satisfying the boundary conditions.

B.3.2. *Accommodating the boundary conditions ($\kappa=0$)*

Finally, the solution of the boundary-condition problem (required for $p'_{(\tau)}$) can be obtained directly by integrating

$$\frac{\mathrm{d}^2 q_{BC}(y;\kappa=0,B_\pm)}{\mathrm{d}y^2}=0, \quad y\in(-\tfrac{1}{2}L_y,+\tfrac{1}{2}L_y), \tag{B 31a}$$

$$\frac{\mathrm{d}q_{BC}}{\mathrm{d}y}(y=\pm\tfrac{1}{2}L_y;\kappa=0,B_\pm)=B_\pm(\kappa=0). \tag{B 31b}$$

The solution exists if and only if

$$B_-(\kappa=0)=B_+(\kappa=0) \tag{B 32}$$

and is obviously a straight line, defined up to an additive constant,

$$q_{BC}(y;\kappa=0,B_\pm)=\tfrac{1}{2}B_- y+\tfrac{1}{2}B_+ y+q_{BC_0}, \tag{B 33}$$

where, by (B 33), $q_{BC}(y=0;\kappa=0)=q_{BC_0}$ is the solution at the centreline.

B.3.3. *Free-space Green's function $G_{\mathfrak{V}}(y,Y;\kappa=0)$*

The solution for the free-space Green's function $G_{\mathfrak{V}}(y,Y;\kappa=0)$ is obtained in exactly the same way as for $G_{Kim}(y,Y;\kappa=0)$ (§ B.3.1), yielding, by (B 29),

$$G_{\mathfrak{V}}(y,Y;\kappa=0)=G_{Kim}(y,Y;\kappa=0)=\frac{|y-Y|}{2}. \tag{B 34}$$

https://doi.org/10.1017/jfm.2012.633 Published online by Cambridge University Press

Again, the sources $Q(y;\kappa=0)$ must satisfy the compatibility condition (B 25) to ensure boundedness as $|y|\to\infty$,

$$\lim_{|y|\to\infty}\int_{-L_y/2}^{+L_y/2} G_{\mathfrak{V}}(y,Y\kappa=0)Q(Y;\kappa=0)\,\mathrm{d}Y$$
$$\overset{\text{(B 34)}}{=}\lim_{|y|\to\infty}\left\{\left(\int_{-L_y/2}^{+L_y/2}Q(Y;\kappa=0)\,\mathrm{d}Y\right)\frac{|y|}{2}\right\}\overset{\text{(B 25)}}{=}0,\quad\forall\ Y\in\mathbb{R}\setminus\{y\},\ \text{(B 35)}$$

which is zero if and only if (B 25) holds.

B.3.4. *Upper/lower wall Green's functions* $G_{\pm}(y,Y;\kappa=0)$

The solution for $G_{\pm}(y,Y;\kappa=0)$ is again obtained in exactly the same way as for $G_{Kim}(y,Y;\kappa=0)$ (§ B.3.1), yielding, by (B 34),

$$G_{\pm}(y,Y;\kappa=0)=G_{\mathfrak{V}}(y,Y;\kappa=0)=G_{Kim}(y,Y;\kappa=0)=\frac{|y-Y|}{2}.\qquad\text{(B 36)}$$

The boundary conditions for the gradient at the wall ($y=\mp L_y/2$), and for boundedness at $\pm\infty$, are again satisfied by relations analogous to (B 30) and (B 35), if and only if the compatibility relation (B 25) holds.

B.3.5. *Accommodating the boundary conditions for the half-space problems* ($\kappa=0$)

Finally, the solution of the boundary conditions (required for $p'_{(\tau)}$), in the case of the half-space problems, can be obtained directly by integrating

$$\frac{\mathrm{d}^2 q_{BC_\pm}(y;\kappa=0,B_\pm)}{\mathrm{d}y^2}=0,\quad \mp y\in(-\tfrac{1}{2}L_y,+\infty),\qquad\text{(B 37}a\text{)}$$

$$\frac{\mathrm{d}q_{BC_\pm}}{\mathrm{d}y}(y=\pm\tfrac{1}{2}L_y;\kappa=0,B_\pm)=B_\pm(\kappa=0).\qquad\text{(B 37}b\text{)}$$

The solution is obviously a straight line of slope $B_\pm(\kappa=0)$, and is bounded as $|y|\to\infty$ if and only if the compatibility condition

$$B_\pm(\kappa=0)=0\implies q_{BC_\pm}(y;\kappa=0,B_\pm)=0\qquad\text{(B 38)}$$

holds.

B.4. *Approximation error in the method of images*

One interesting application of the half-space problems is that, by superposition, they give the solution obtained by the method of images (Manceau *et al.* 2001). Indeed, the method of images corresponds to applying the free-space Green's function on the domain $y\in(-\frac{1}{2}L_y,+\frac{1}{2}L_y)$, and on two ghost domains $y\in(-\frac{3}{2}L_y,-\frac{L_y}{2})\cup(+\frac{1}{2}L_y,+\frac{3}{2}L_y)$, with appropriately reflected source terms (figure 4),

$$Q_{MWL}(y;\kappa)=Q(-L_y-y;\kappa),\quad y\in(-\tfrac{3}{2}L_y,-\tfrac{1}{2}L_y),\qquad\text{(B 39}a\text{)}$$

$$Q_{MWL}(y;\kappa)=Q(y;\kappa),\quad y\in(-\tfrac{1}{2}L_y,+\tfrac{1}{2}L_y),\qquad\text{(B 39}b\text{)}$$

$$Q_{MWL}(y;\kappa)=Q(+L_y-y;\kappa),\quad y\in(+\tfrac{1}{2}L_y,+\tfrac{3}{2}L_y),\qquad\text{(B 39}c\text{)}$$

and the approximation to the solution obtained by the method of images used by Manceau *et al.* (2001) (although Manceau *et al.* (2001) neglect $q_{BC}(y;\kappa,B_\pm)$, this can be added to $q_{MWL}(y;\kappa)$ (B 40) to obtain the approximation of the complete solution

https://doi.org/10.1017/jfm.2012.633 Published online by Cambridge University Press

(B 11*a*)) is

$$q_{MWL}(y;\kappa) := \int_{-(3/2)L_y}^{+(3/2)L_y} G_{\mathfrak{V}}(y,Y;\kappa) Q_{MWL}(Y;\kappa)\,\mathrm{d}Y. \tag{B 40}$$

It is straightforward to construct a kernel $G_{MWL}(y,Y;\kappa)$, which, applied on the source terms in the actual computational domain $y\in(-L_y/2,-L_y/2)$, will return the method-of-images approximation (B 40), because, defining $Y_\pm := \pm L_y - Y$, we have

$$\begin{aligned}
q_{MWL}(y;\kappa) &= \int_{-(3/2)L_y}^{+(3/2)L_y} G_{\mathfrak{V}}(y,Y;\kappa) Q_{MWL}(Y;\kappa)\,\mathrm{d}Y \\
&\overset{(B\,39),\,(B\,40)}{=} \int_{-(3/2)L_y}^{-L_y/2} G_{\mathfrak{V}}(y,Y;\kappa) Q(-L_y-Y;\kappa)\,\mathrm{d}Y \\
&\quad + \int_{-L_y/2}^{+L_y/2} G_{\mathfrak{V}}(y,Y;\kappa) Q(Y;\kappa)\,\mathrm{d}Y \\
&\quad + \int_{+L_y/2}^{+(3/2)L_y} G_{\mathfrak{V}}(y,Y;\kappa) Q(+L_y-Y;\kappa)\,\mathrm{d}Y \\
&= -\int_{+L_y/2}^{-L_y/2} G_{\mathfrak{V}}(y,-L_y-Y_-;\kappa) Q(Y_-;\kappa)\,\mathrm{d}Y_- \\
&\quad + \int_{-L_y/2}^{+L_y/2} G_{\mathfrak{V}}(y,Y;\kappa) Q(Y;\kappa)\,\mathrm{d}Y \\
&\quad - \int_{+L_y/2}^{-L_y/2} G_{\mathfrak{V}}(y,L_y-Y_+;\kappa) Q(Y_+;\kappa)\,\mathrm{d}Y_+,
\end{aligned} \tag{B 41}$$

yielding

$$q_{MWL}(y;\kappa) = \int_{-L_y/2}^{+L_y/2} G_{MWL}(y,Y;\kappa) Q(Y;\kappa)\,\mathrm{d}Y, \tag{B 42a}$$

$$G_{MWL}(y,Y;\kappa) := G_{\mathfrak{V}}(y,Y;\kappa) + G_{\mathfrak{V}}(y,-L_y-Y;\kappa) + G_{\mathfrak{V}}(y,L_y-Y;\kappa), \tag{B 42b}$$

and by (B 14)

$$G_{MWL}(y,Y;\kappa\neq 0) \overset{(B\,14)}{=} -\frac{\mathrm{e}^{-\kappa|y-Y|}}{2\kappa} - \frac{\mathrm{e}^{-\kappa|L_y+y+Y|}}{2\kappa} - \frac{\mathrm{e}^{-\kappa|L_y-y-Y|}}{2\kappa}. \tag{B 42c}$$

Note that (B 42) (which is the one-dimensional equivalent of Manceau *et al.* (2001, (4.2), p. 314)) gives the solution by integrating the sources in the actual domain $Y\in[-L_y/2,+L_y/2]$ with an approximate Green's function $G_{MWL}(y,Y;\kappa)$ (B 42*b*). This representation (B 42) readily yields the approximation error of the method of images, by comparison with the exact solution (B 10*b*) obtained using $G_{Kim}(y,Y;\kappa)$. If we consider the actual domain $y,Y\in[-L_y/2,+L_y/2]$, we have

$$\left.\begin{aligned} -\tfrac{1}{2}L_y \leqslant y \leqslant +\tfrac{1}{2}L_y \\ -\tfrac{1}{2}L_y \leqslant Y \leqslant +\tfrac{1}{2}L_y \end{aligned}\right\} \Longrightarrow \begin{cases} L_y+(y+Y)\geqslant 0 \\ L_y-(y+Y)\geqslant 0 \end{cases} \tag{B 43a}$$

https://doi.org/10.1017/jfm.2012.633 Published online by Cambridge University Press

so that

$$G_{MWL}(y,Y;\kappa\neq 0) \overset{(\text{B }42c),\ (\text{B }43)}{=} -\frac{\mathrm{e}^{-\kappa|y-Y|}}{2\kappa}-\frac{\mathrm{e}^{-\kappa(L_y+y+Y)}}{2\kappa} - \frac{\mathrm{e}^{-\kappa(L_y-y-Y)}}{2\kappa}, \quad \forall\ y,Y\in[-\tfrac{1}{2}L_y,+\tfrac{1}{2}L_y] \quad (\text{B }43b)$$

$$\overset{(\text{B }14),\ (\text{B }18)}{=} G_{\mathfrak{V}}(y,Y;\kappa\neq 0) + \underbrace{G_{-}(y,Y;\kappa\neq 0)-G_{\mathfrak{V}}(y,Y;\kappa\neq 0)}_{G_{w_-}(y,Y;\kappa\neq 0)\quad(\text{B }19)} + \underbrace{G_{+}(y,Y;\kappa\neq 0)-G_{\mathfrak{V}}(y,Y;\kappa\neq 0)}_{G_{w_+}(y,Y;\kappa\neq 0)\quad(\text{B }19)} \quad \forall\ y,Y\in[-\tfrac{1}{2}L_y,+\tfrac{1}{2}L_y], \quad (\text{B }43c)$$

i.e. the images problem (Manceau *et al.* 2001) is equivalent to adding to the free-space Green's function an independent wall-echo correction for each wall, the wall-echo correction for the upper (lower) wall being exactly the wall echo of the half-space problem with only the upper (lower) wall present (§ B.2.4). Note that by (B 36) we have $G_{w_-}(y,Y;\kappa=0)=G_{w_+}(y,Y;\kappa=0)=0$ so that (B 43*c*) holds for all $\kappa\in\mathbb{R}_{\geqslant 0}$.

By (B 10*b*) and (B 43*b*), we may directly compute the error made when approximating the Green's function by the method of images

$$\frac{1}{L_y}(G_{MWL}(y,Y;\kappa\neq 0)-G_{Kim}(y,Y;\kappa\neq 0)) \overset{(\text{B }10b),\ (\text{B }43b)}{=} \frac{\mathrm{e}^{-\kappa L_y}}{2\kappa L_y\sinh\kappa L_y}(\cosh\kappa\,|y-Y|+\mathrm{e}^{-\kappa L_y}\cosh\kappa(y+Y)) \quad \forall\ y,Y\in[-\tfrac{1}{2}L_y,+\tfrac{1}{2}L_y], \quad (\text{B }44)$$

where (B 44) was made non-dimensional by dividing the Green's functions by L_y. Obviously

$$y,Y\in[-\tfrac{1}{2}L_y,+\tfrac{1}{2}L_y] \implies \left.\begin{matrix}0\leqslant|y-Y|\leqslant L_y\\ 0\leqslant|y+Y|\leqslant L_y\end{matrix}\right\} \implies \begin{cases}0\leqslant\cosh\kappa\,|y-Y|\leqslant\cosh\kappa L_y\\ 0\leqslant\cosh\kappa\,|y+Y|\leqslant\cosh\kappa L_y\end{cases} \quad (\text{B }45)$$

since $\cosh x=\cosh|x|$ is positive and strictly increasing for all $|x|\in\mathbb{R}_{\geqslant 0}$. Hence (note also that, by (B 44), $G_{MWL}(y,Y;\kappa\neq 0)-G_{Kim}(y,Y;\kappa\neq 0)\geqslant 0$ for all $y,Y\in[-L_y/2,+L_y/2]$) we obtain

$$\frac{1}{L_y}\left(\max_{y,Y\in[-L_y/2,+L_y/2]}|G_{MWL}(y,Y;\kappa)-G_{Kim}(y,Y;\kappa)|\right) \leqslant \underbrace{\frac{\mathrm{e}^{-\kappa L_y}(1+\mathrm{e}^{-\kappa L_y})\cosh\kappa L_y}{2\kappa L_y\sinh\kappa L_y}}_{E_{MWL}(\kappa L_y)}, \quad (\text{B }46)$$

showing that the upper bound of approximation error made by the method of images is a function of the non-dimensional (outer scaling) wavenumber κL_y (figure 5).

https://doi.org/10.1017/jfm.2012.633 Published online by Cambridge University Press

REFERENCES

DEL ÁLAMO, J. C. & JIMÉNEZ, J. 2003 Spectra of the very large anisotropic scales in turbulent channels. *Phys. Fluids* **15** (6), L41–L44.

DEL ÁLAMO, J. C., JIMÉNEZ, J., ZANDONADE, P. & MOSER, R. D. 2004 Scaling of the energy spectra of turbulent channels. *J. Fluid Mech.* **500**, 135–144.

BALAKUMAR, B. J. & ADRIAN, R. J. 2007 Large- and very-large-scale motions in channel and boundary-layer flows. *Phil. Trans. R. Soc. Lond.* A **365**, 665–681.

BENDER, C. M. & ORSZAG, S. A. 1978 *Advanced Mathematical Methods for Scientists and Engineers*, pp. 16–19 Springer.

BISPLINGHOFF, R. L. & ASHLEY, H. 1962 *Principles of Aeroelasticity*, p. 76. Wiley.

BRIGGS, W. L. & HENSON, V. E. 1995 *The DFT: An Owner's Manual for the Discrete Fourier Transform*, pp. 144–150 SIAM.

CHANG, P. A. III, PIOMELLI, U. & BLAKE, W. K. 1999 Relations between wall-pressure and velocity-field sources. *Phys. Fluids* **11** (11), 3434–3448.

CHENG, H., HUANG, J. & LEITERMAN, T. J. 2006 An adaptive fast solver for the modified Helmholtz equation in 2-D. *J. Comput. Phys.* **211**, 616–637.

CHOU, P. Y. 1945 On velocity correlations and the solutions of the equations of turbulent fluctuations. *Q. Appl. Maths* **3**, 38–54.

COLEMAN, G. N., KIM, J. & MOSER, R. D. 1995 A numerical study of turbulent supersonic isothermal-wall channel flow. *J. Fluid Mech.* **305**, 159–183.

CORCOS, G. M. 1964 The structure of the turbulent pressure field in boundary-layer flows. *J. Fluid Mech.* **18**, 353–378.

CORMACK, D. E. 1975 Topics in geophysical fluid dynamics: I. Natural convection in shallow cavities. II. Studies of a phenomenological turbulence model. PhD thesis, California Institute of Technology, Pasadena.

COURANT, R. & HILBERT, D. 1953*Methods of Mathematical Physics*, vol. I, pp. 351–358, 371–377. Interscience.

CRAFT, T. J. & LAUNDER, B. 1996 A Reynolds-stress model designed for complex geometries. *Intl J. Heat Fluid Flow* **17**, 245–254.

DALY, B. J. & HARLOW, F. H. 1970 Transport equations in turbulence. *Phys. Fluids* **13**, 2634–2649.

DAVIDSON, P. A. 2004 *Turbulence*. Oxford University Press.

DONALDSON, C. DU P. 1969 A computer study of an analytical model of boundary-layer transition. *AIAA J.* **7** (2), 271–278.

DOSIO, A., VILÀ-GUERAU DE ARELLANO, J., HOLTSLAG, A. A. M. & BUILTJES, P. J. H. 2005 Relating Eulerian and Lagrangian statistics for the turbulent dispersion in the atmospheric convective boundary-layer. *J. Atmos. Sci.* **62** (4), 1175–1191.

DURBIN, P. A. 1993 A Reynolds-stress model for near-wall turbulence. *J. Fluid Mech.* **249**, 465–498.

DURBIN, P. A. 1995 Separated flow computation with the k–ε–v^2 model. *AIAA J.* **33** (4), 659–664.

DURRAN, D. R. 1989 Improving the anelastic approximation. *J. Atmos. Sci.* **46** (11), 1453–1461.

FAVRE, A. 1965*a* Equations des gaz turbulents compressibles – I – formes générales. *J. Méc.* **4**, 361–390.

FAVRE, A. 1965*b* Equations des gaz turbulents compressibles – II – méthode des vitesses moyennes; méthode des vitesses moyennes pondérées par la masse volumique. *J. Méc.* **4**, 391–421.

FOYSI, H., SARKAR, S. & FRIEDRICH, R. 2004 Compressibility effects and turbulence scalings in supersonic channel flow. *J. Fluid Mech.* **509**, 207–216.

FU, S. 1993 Modelling of the pressure–velocity correlation in turbulence diffusion. *Comput. Fluids* **22**, 199–205.

GARRICK, I. E. 1957 Nonsteady wing charactreristics. In *Aerodynamic Components of Aircraft at High Speeds* (ed. A. F. Donovan & H. R. Lawrence), High Speed Aerodynamics and Jet Propulsion, vol. VII, pp. 658–793. Princeton University Press.

GEROLYMOS, G. A., LO, C. & VALLET, I. 2012*a* Tensorial representations of Reynolds-stress pressure–strain redistribution. *Trans. ASME: J. Appl. Mech.* **79** (4), 044506.

https://doi.org/10.1017/jfm.2012.633 Published online by Cambridge University Press

GEROLYMOS, G. A., LO, C., VALLET, I. & YOUNIS, B. A. 2012*b* Term-by-term analysis of near-wall second moment closures. *AIAA J.* **50** (12), 2848–2864.

GEROLYMOS, G. A., SAURET, E. & VALLET, I. 2004 Contribution to the single-point-closure Reynolds-stress modelling of inhomogeneous flow. *Theor. Comput. Fluid Dyn.* **17** (5–6), 407–431.

GEROLYMOS, G. A., SÉNÉCHAL, D. & VALLET, I. 2009 Very-high-order WENO schemes. *J. Comput. Phys.* **228**, 8481–8524.

GEROLYMOS, G. A., SÉNÉCHAL, D. & VALLET, I. 2010 Performance of very-high-order upwind schemes for DNS of compressible wall-turbulence. *Intl J. Numer. Meth. Fluids* **63**, 769–810.

GEROLYMOS, G. A. & VALLET, I. 2001 Wall-normal-free near-wall Reynolds-stress closure for 3-D compressible separated flows. *AIAA J.* **39** (10), 1833–1842.

GEROLYMOS, G. A. & VALLET, I. 2009 SourceForge: aerodynamics. http://sourceforge.net/projects/aerodynamics.

GIBSON, M. M. & LAUNDER, B. E. 1978 Ground effects on pressure fluctuations in the atmospheric boundary-layer. *J. Fluid Mech.* **86**, 491–511.

GOODY, M. 2004 Empirical spectral model of surface pressure fluctuations. *AIAA J.* **42** (9), 1788–1794.

HAMBA, F. 1999 Effects of pressure fluctuations on turbulence growth in compressible homogeneous shear flow. *Phys. Fluids* **11** (6), 1623–1635.

HANJALIĆ, K. 1994 Advanced turbulence closure models: a view of current status and future prospects. *Intl J. Heat Fluid Flow* **15**, 178–203.

HARRIS, J. W. & STOCKER, H. 1998 *Handbook of Mathematics and Computational Science*. Springer.

HIRT, C. W. 1969 Generalized turbulence transport equations. *International Semuinar of the International Center for Heat and Mass Transfer, Herceg Novi, Yugoslavia.*

HOYAS, S. & JIMÉNEZ, J. 2006 Scaling of the velocity fluctuations in turbulent channels up to $Re_\tau = 2003$. *Phys. Fluids* **18**, 011702.

HOYAS, S. & JIMÉNEZ, J. 2008 Reynolds number effects on the Reynolds-stress budgets in turbulent channels. *Phys. Fluids* **20**, 101511.

HU, Z. W., MORFEY, C. L. & SANDHAM, N. D. 2002 Aeroacoustics of wall-bounded turbulent flow. *AIAA J.* **40** (3), 465–473.

HU, Z. W., MORFEY, C. L. & SANDHAM, N. D. 2006 Wall pressure and shear stress spectra from direct simulations of channel flow. *AIAA J.* **44** (7), 1541–1549.

HU, Z. W. & SANDHAM, N. D. 2001 DNS databases for turbulent Couette and Poiseuille flow. *Tech. Rep.* AFM-01-04. AFM Research Group, School of Engineering Sciences, University of Southampton.

HUANG, P. G., COLEMAN, G. N. & BRADSHAW, P. 1995 Compressible turbulent channel flows: DNS results and modelling. *J. Fluid Mech.* **305**, 185–218.

HUNT, J. C. R. & GRAHAM, J. M. R. 1978 Free-stream turbulence near plane boundaries. *J. Fluid Mech.* **84**, 209–235.

HUTCHINS, N. & MARUSIC, I. 2007 Evidence of very long meandering features in the logarithmic region of turbulent boundary-layers. *J. Fluid Mech.* **579**, 1–28.

INCE, I. L. 1926*Ordinary Differential Equations*, 1st edn, pp. 123–126, 254–263, 266–269. Dover.

JAKIRLIĆ, S. & HANJALIĆ, K. 2002 A new approach to modelling near-wall turbulence energy and stress dissipation. *J. Fluid Mech.* **459**, 139–166.

JOVANOVIĆ, J. 2004 *The Statistical Dynamics of Turbulence*. Springer.

KATZ, J. & PLOTKIN, A. 1991 *Low-Speed Aerodynamics: From Wing Theory to Panel Methods*, pp. 52–57 McGraw-Hill.

KIM, J. 1989 On the structure of pressure fluctuations in simulated turbulent channel-flow. *J. Fluid Mech.* **205**, 421–451.

KIM, J., MOIN, P. & MOSER, R. 1987 Turbulence statistics in fully developed channel flow at low-Reynolds-number. *J. Fluid Mech.* **177**, 133–166.

LAUNDER, B. E. & LI, S. P. 1994 On the elimination of wall-topography parameters from 2-moment closure. *Phys. Fluids* **6**, 999–1006.

https://doi.org/10.1017/jfm.2012.633 Published online by Cambridge University Press

LAUNDER, B. E., REECE, G. J. & RODI, W. 1975 Progress in the development of a Reynolds-stress turbulence closure. *J. Fluid Mech.* **68**, 537–566.

LUMLEY, J. L. 1978 Computational modelling of turbulent flows. *Adv. Appl. Mech.* **18**, 123–176.

MAHLE, I., FOYSI, H., SARKAR, S. & FRIEDRICH, R. 2007 On the turbulence structure of inert and reacting compressible mixing layers. *J. Fluid Mech.* **593**, 171–180.

MANCEAU, R. & HANJALIĆ, K. 2002 Elliptic blending model: a new near-wall Reynolds-stress turbulence closure. *Phys. Fluids* **14** (2), 744–754.

MANCEAU, R., WANG, M. & LAURENCE, D. 2001 Inhomogeneity and anisotropy effects on the redistribution term in Reynolds-averaged Navier–Stokes modelling. *J. Fluid Mech.* **438**, 307–338.

MANSOUR, N. N., KIM, J. & MOIN, P. 1988 Reynolds-stress and dissipation-rate budgets in a turbulent channel flow. *J. Fluid Mech.* **194**, 15–44.

MARMANIS, H. 1998 Analogy between the Navier–Stokes equations and Maxwell's equations: application to turbulence. *Phys. Fluids* **10** (6), 1428–1437.

MILES, J. W. 1959 *The Potential Theory of Unsteady Supersonic Flow*, p. 2ff. Cambridge University Press.

MONIN, A. S. & YAGLOM, A. M. 1971 *Statistical Fluid Mechanics: Mechanics of Turbulence*, vol. 1. MIT Press.

MOSER, R. D., KIM, J. & MANSOUR, N. N. 1999 Direct numerical simulation of turbulent channel flow up to $Re_\tau = 590$. *Phys. Fluids* **11** (4), 943–945.

MYINT-U, T. & DEBNATH, L. 2007 *Linear Partial Differential Equations for Scientists and Engineers,* 4th edn, pp. 310–317 Birkhäuser.

NAKA, Y., OMORI, T., OBI, S. & MASUDA, S. 2006 Simultaneous measurements of fluctuating velocity and pressure in a turbulent mixing layer. *Intl J. Heat Fluid Flow* **27**, 737–746.

OCKENDON, J., HOWISON, S., LACEY, A. & MOVCHAN, A. 2003 *Applied Partial Differential Equations*, rev. edn, pp. 163–166, 169–174. Oxford University Press.

PANTANO, C. & SARKAR, S. 2002 A study of compressibility effects in the high-speed turbulent shear layer using direct simulation. *J. Fluid Mech.* **451**, 329–371.

PANTON, R. L. & LINEBARGER, J. H. 1974 Wall pressure spectra calculations for equilibrium boundary-layers. *J. Fluid Mech.* **65**, 261–287.

PEROT, B. 1999 Turbulence modelling using body-force potentials. *Phys. Fluids* **11** (9), 2645–2656.

PIQUET, J. 1999 *Turbulent Flows – Models and Physics*. Springer.

POPE, S. B. 2000 *Turbulent Flows*. Cambridge University Press.

RISTORCELLI, J. R. 1997 A pseudosound constitutive relationship for the dilatational covariances in compressible turbulence. *J. Fluid Mech.* **347**, 37–70.

RISTORCELLI, J. R., LUMLEY, J. L. & ABID, R. 1995 A rapid-pressure covariance representation consistent with the Taylor–Proudman theorem materially frame indifferent in the 2-D limit. *J. Fluid Mech.* **292**, 111–152.

ROTTA, J. 1951*a* Statistische Theorie nichthomogener Turbulenz – 1. Mitteilung. *Z. Phys.* **129**, 547–572.

ROTTA, J. 1951*b* Statistische Theorie nichthomogener Turbulenz – 2. Mitteilung. *Z. Phys.* **131**, 51–77.

SAURET, E. & VALLET, I. 2007 Near-wall turbulent pressure diffusion modelling and influence in 3-D secondary flows. *Trans. ASME: J. Fluids Engng* **129** (5), 634–642.

SCHWARZ, W. R. & BRADSHAW, P. 1994 Term-by-term tests of stress-transport turbulence models in a 3-D boundary-layer. *Phys. Fluids* A **6** (2), 986–998.

SHIH, T. H. & LUMLEY, J. L. 1993 Critical comparison of 2-order closures with direct numerical simulations of homogeneous turbulence. *AIAA J.* **31** (4), 663–670.

SHIR, C. C. 1973 A preliminary numerical study of atmospheric turbulent flows in the idealized planetary boundary-layer. *J. Atmos. Sci.* **30**, 1327–1339.

SO, R. M. C., GATSKI, T. B. & SOMMER, T. P. 1998 Morkovin hypothesis and the modelling of wall-bounded compressible turbulent flows. *AIAA J.* **36** (9), 1583–1592.

SPEZIALE, C. G., SARKAR, S. & GATSKI, T. B. 1991 Modelling the pressure–strain correlation of turbulence: an invariant dynamical systems approach. *J. Fluid Mech.* **227**, 245–272.

https://doi.org/10.1017/jfm.2012.633 Published online by Cambridge University Press

SUGA, K. 2004 Modelling the rapid part of the pressure–diffusion process in the Reynolds stress transport equation. *Trans. ASME: J. Fluids Engng* **126**, 634–641.

TAULBEE, D. & VANOSDOL, J. 1991 Modelling turbulent compressible flows: the mass fluctuating velocity and squared density. *AIAA Paper* 1991-0524.

TSUJI, Y., FRANSSON, J. H. M., ALFREDSSON, P. H. & JOHANSSON, A. V. 2007 Pressure statistics and their scalings in high-Reynolds-number turbulent boundary-layers. *J. Fluid Mech.* **585**, 1–40.

TSUJI, Y. & ISHIHARA, T. 2003 Similarity scaling of pressure fluctuation in turbulence. *Phys. Rev.* E **68**, 026309.

VALLET, I. 2007 Reynolds-stress modelling of 3-D secondary flows with emphasis on turbulent diffusion closure. *Trans. ASME: J. Appl. Mech.* **74** (6), 1142–1156.

ZAUDERER, E. 2006 *Partial Differential Equations of Applied Mathematics*, pp. 446–447, 451–454. Wiley.

https://doi.org/10.1017/jfm.2012.633 Published online by Cambridge University Press